and analyzed by XRD. XRD patterns from this system are given in Fig. 1. The cubic pyrochlore-type structure of $Pb_{1.83}(Nb_{1.71}Zn_{0.29})O_{6.39}$[27] was identified in the x = 0.0, 0.1, and 0.3 compositions at the 900 °C calcination temperature. The pyrochlore formation reaction from PbO and the columbite precursors is an extremely fast process, which is completed within 2–3 min at temperatures as low as 750 °C.[28] With increased calcination temperatures the amount of perovskite phase increased sharply. In our work, it was observed that the primary phase in all of the compositions at 950 °C was well-crystallized perovskite. Within the detection limits of the XRD technique, the samples were essentially 100% perovskite and free of pyrochlore. The heat treatment and percent perovskite phase for all the compositions are listed in Table I. The first two rows listed are for the calcined powders, and the remaining data are derived from sintered samples using powders calcined at 950 °C.

In this study, the combination of using a double crucible, excess PbO (2 mol%), and a fast heating/cooling rate (20 °C/min) were shown to be effective in reducing the total amount of pyrochlore phase during calcination at 950 °C. The 2 mol% excess PbO was chosen because there were observations reported that compositions with excess PbO additions greater than 2.8 mol% resulted in degraded electrical properties. This was attributed to the presence of an excess PbO layer at the grain boundary.[29,30]

XRD patterns from a set of samples prepared at various sintering temperatures are given in Fig. 2. In this study, for the x = 0 composition single-phase perovskite was obtained for sintering temperatures below 1150 °C. Above 1150 °C, the cubic pyrochlore phase $Pb_{1.83}(Nb_{1.71}Zn_{0.29})O_{6.39}$[27] formed and the percentage of pyrochlore phase increased as the sintering temperature increased, as shown in Table I. This behavior also appeared in the x = 0.1 composition at sintering temperatures above 1200 °C. The behavior is believed to be due to the volatilization of PbO at high temperatures. Nevertheless, the XRD patterns for the x = 0.3 and 0.5 compositions do not show the formation of the

TABLE I. Perovskite phase development during calcinations and sintering process of 0.5PNN–(0.5 – x)PZN–xPZT system. (The first two rows indicate the data in calcined powders and the rest of the rows are data from sintering of powders calcined at 950 °C.)

Temperature (°C)	Perovskite phase (%)			
	x = 0.0	x = 0.1	x = 0.3	x = 0.5
900[a]	91.53	92.67	92.5	100
950[a]	100	100	100	100
1000	100	100	...	...
1050	100	100	100	...
1100	100	100	100	...
1150	100	100	100	100
1200	84.468	100	100	100
1225	76.249	76.79	100	100
1250	...	...	100	100
1275	...	...	100	100

[a]Calcination temperatures.

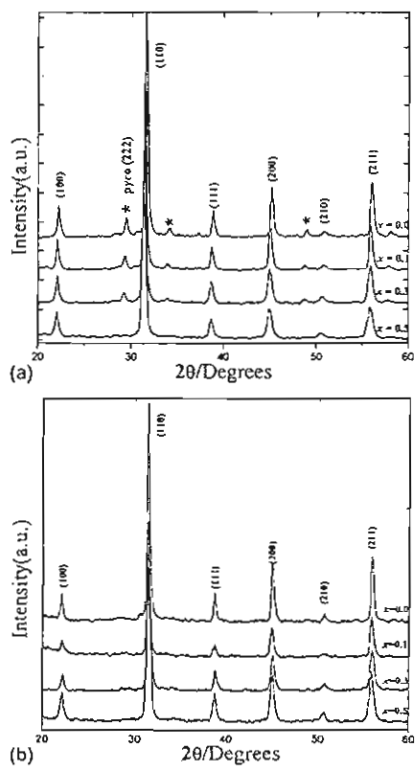

FIG. 1. Powder XRD patterns of a stoichiometric composition of 0.5PNN–(0.5 – x)PZN–xPZT ceramics: (a) calcined at 900 °C for 4 h with 20 °C/min heating rate, (b) calcined at 950 °C for 2 h with 20 °C/min heating rate; pyrochlore phase indicated with (*).

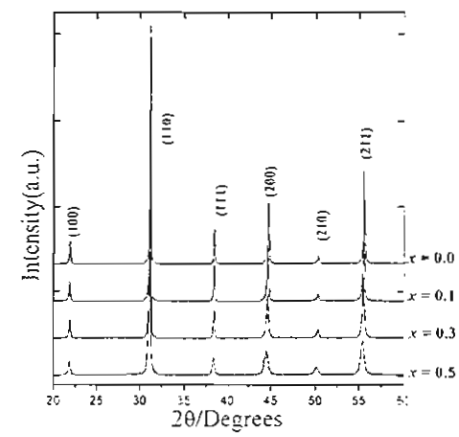

FIG. 2. XRD patterns of 0.5PNN–(0.5 – x)PZN–xPZT ceramics at the optimum sintering conditions.

pyrochlore phase. It is interesting to note that the intensity of (100) perovskite peak decreased at high temperatures for the $0.1 \leq x \leq 0.5$ composition.

In the PNN–PZN–PZT system, the A-site is occupied by Pb^{2+} (1.630 Å) ions, and the Ni^{2+}, Nb^{5+}, Zn^{2+}, Zr^{4+}, and Ti^{4+} ions occupy the B site of the ABO_3 perovskite crystal structure. The average ionic radius of B-site ions in the composition $0.5Pb(Ni_{1/3}Nb_{2/3})O_3$–$(0.5 - x)Pb(Zn_{1/3}Nb_{2/3})O_3$–$xPb(Zr_{1/2}Ti_{1/2})O_3$ can be calculated from the following equation:

$$r_{B\text{-site}} = 0.5\left[\tfrac{1}{3}r_{Ni^{2+}} + \tfrac{2}{3}r_{Nb^{5+}}\right] + (0.5 - x)\left[\tfrac{1}{3}r_{Zn^{2+}} + \tfrac{2}{3}r_{Nb^{5+}}\right] + x\left[\tfrac{1}{2}r_{Zr^{4+}} + \tfrac{1}{2}r_{Ti^{4+}}\right] \quad (2)$$

where the ionic radii of Ni^{2+}, Nb^{5+}, Zn^{2+}, Zr^{4+}, and Ti^{4+} are 0.830, 0.780, 0.880, 0.860 and 0.745 Å, respectively.[31] A simple description of the geometric packing within perovskite structure can be characterized by tolerance factor t, which is defined by the following equation:[5,8,13,32]

$$t = \frac{(r_A + r_O)}{\sqrt{2}(r_B + r_O)}, \quad (3)$$

where r_A, r_B, and r_O are the ionic radii of the A, B and O ions, respectively. The calculated average B-site ionic radii and tolerance factor of the PNN–PZN–PZT system is presented in Table II using 1.260 Å for the radius of O^{2-}.[31] The effective size of the B-site ion decreases with an increasing mol faction of PZT primarily due to the smaller ionic radii of Ti^{4+}. This results in a slight increase in the tolerance factor as it approaches 1.0. However, the lattice parameter is found to increase as the mol faction of PZT increases, and the symmetry changes from pseudocubic to rhombohedral.

The crystal symmetry of PNN at room temperature was determined to be pseudo-cubic perovskite with a cell parameter $a = 4.0308$ Å. The PZN composition at room temperature was determined to be the rhombohedral space group $R3m$. According to the $PbZrO_3$–$PbTiO_3$ phase diagram, at room temperature $Pb(Zr_{1/2}Ti_{1/2})O_3$ is within the tetragonal phase field near the MPB region.[33] In this work, the crystal structure and lattice parameters of the PNN–PZN–PZT compositions were determined through room temperature diffraction experiments. The indexing procedure of the perovskite phase in the $x = 0.0$ and $x = 0.1$ samples was performed based on cubic symmetry. For the $x = 0.3$ and 0.5 samples, however, no splitting of 002 and 200 peak was observed with increased PZT concentration, as shown in Fig. 2. However, the superposition was clearly observed for the (220) peak as shown in Fig. 3. This result indicates that the crystal structure was rhombohedral. In addition, from the data listed in Table II, it is evident that the lattice parameter a increased with increasing concentration of PZT due to the increase in B-site radius.

B. Dielectric properties

The permittivity at 1 kHz as a function of temperature for 0.5PNN–(0.5 – x)PZN–xPZT ceramics under different sintering conditions is shown in Fig. 4. The sintering temperature was found to have a significant effect on the

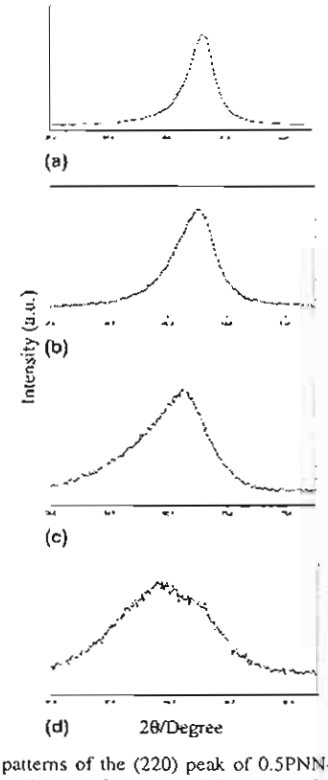

FIG. 3. XRD patterns of the (220) peak of 0.5PNN–(0.5 – x)PZN–xPZT ceramics: (a) $x = 0$, (b) $x = 0.1$, (c) $x = 0.3$, (d) $x = 0.5$.

TABLE II. Comparison of the calculated average B-site ionic radii, the crystal structure, and lattice parameters derived from XRD data.

Composition 0.5PNN–(0.5 – x)PZN–xPZT	Average B-site ionic radii (Å)	Tolerance factor, t	Lattice parameter, a (Å)	Crystal structure	Distortion angle, α
$x = 0.0$	0.8050	0.9896	4.049	Cubic	90.0
$x = 0.1$	0.8039	0.9901	4.054	Cubic	90.0
$x = 0.3$	0.8018	0.9912	4.057	Rhombohedral	89.88
$x = 0.5$	0.7996	0.9922	4.060	Rhombohedral	89.89

permittivity. All compositions exhibited an increase in the permittivity with increased sintering temperatures. However, at the highest sintering temperature the permittivity decreased due to the formation of a pyrochlore phase. The $x = 0$ composition showed an increase in permittivity up to a maximum of 10,000 at a sintering temperature of 1150 °C. At higher sintering temperatures there is both a decrease in permittivity and a shift in the temperature at which the permittivity is maximum (T_m) from −20 to −50 °C. This shift in T_m is likely to be the result of a change in the stoichiometry of the perovskite phase due to the effects of Zn volatilization and the formation of the pyrochlore phase $Pb_{1.83}(Nb_{1.71}Zn_{0.29})O_{6.39}$. This shifted the overall perovskite composition closer to PNN, with a lower T_m of −120 °C. In addition, the decrease in permittivity that was observed was the result of the low permittivity of $Pb_{1.83}(Nb_{1.71}Zn_{0.29})O_{6.39}$ ($\epsilon_r \sim 100$).

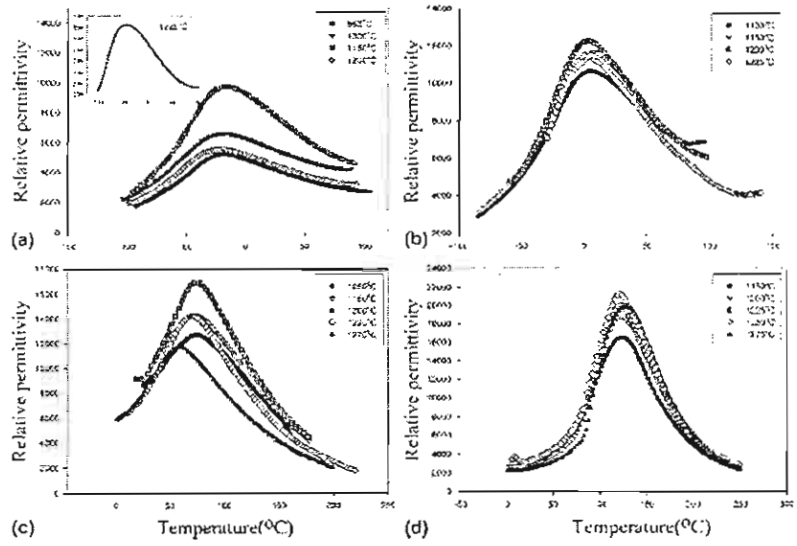

FIG. 4. Relative permittivity and dissipation factor at 1kHz for 0.5PNN–(0.5 − x)PZN –xPZT: (a) $x = 0$, (b) $x = 0.1$, (c) $x = 0.3$, (d) $x = 0.5$. Dielectric data for different sintering temperatures is shown.

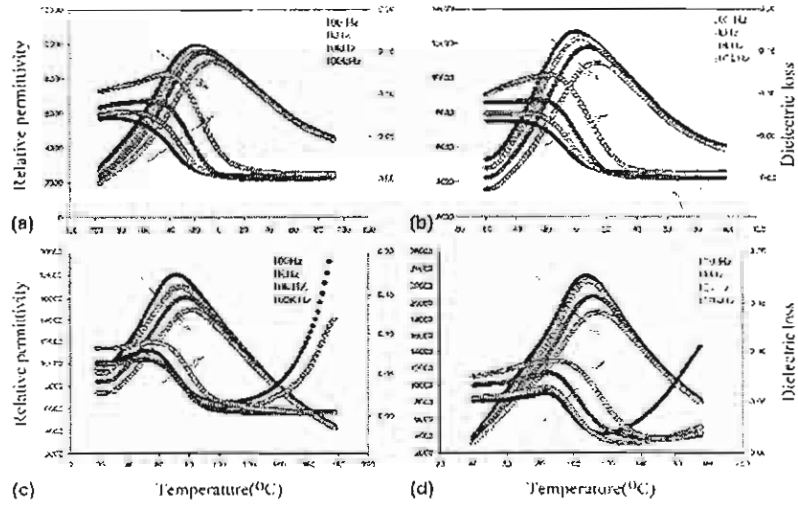

FIG. 5. Relative permittivity and dissipation factor of 0.5PNN–(0.5 − x)PZN–xPZT ceramics prepared at the optimum sintering conditions. (a) $x = 0$, ceramics sintered at 1150 °C for 2 h; (b) $x = 0.1$, ceramics sintered at 1200 °C for 2 h; (c) $x = 0.3$, ceramics sintered at 1200 °C for 2 h; (d) $x = 0.5$, ceramics sintered at 1250 °C for 2 h.

The $x = 0.1$ composition exhibited a maximum permittivity of approximately 12,000 with a $T_m \sim 0$ °C at a sintering temperature of 1200 °C. Higher sintering temperatures resulted in a decrease in the permittivity. Likewise the $x = 0.3$ composition exhibited a maximum permittivity of 17,000 at $T_m = 70$ °C at a sintering temperature of 1200 °C. Consistent with the other compositions, increased sintering temperatures resulted in a decrease in permittivity and a shift in T_m. Finally, the highest permittivities in this study were recorded for the $x = 0.5$ composition at a sintering temperature of 1250 °C with $\epsilon_{r,max} = 22{,}000$ at $T_m \sim 120$ °C. This is significantly larger than the previous value reported in the literature.[23]

In this work, the dielectric experiments showed that the optimum sintering conditions for 0.5PNN–(0.5 – x) PZN–xPZT were for 2 h at 1150, 1200, 1200, and 1250 °C, for the $x = 0$, $x = 0.1$, $x = 0.3$, and $x = 0.5$ compositions, respectively. Ceramics sintered under these conditions were used in the determination of the crystal structure and lattice parameters, which had been shown in Figs. 2 and 3, and Table II. The following characterization of the dielectric and ferroelectric properties of each composition was also carried out in sample sintered at their optimum conditions.

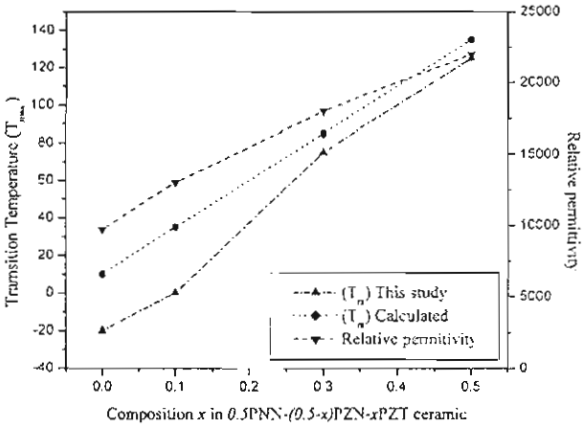

FIG. 6. T_m, calculated T_m, and maximum relative permittivity as a function of composition x at 1 kHz.

Figure 5 shows the dielectric properties for each composition at the optimum sintering conditions. All of compositions showed a broadening of the permittivity maxima and the T_m increased with increasing measurement frequency, as expected. Experimental results indicate that all of compositions show a diffuse phase transition with the strong frequency dispersion, which is characteristic of relaxor ferroelectrics.[1,3,12,34] From this result, it is clear from the sharpness of the permittivity peak that the compositions gradually approached normal ferroelectric behavior as the mol fraction of PZT increased. As x approached 0, the behavior was strongly relaxor in nature. This may be a function of the degree of B-site cation ordering or the influence of the macro-domains.

In general, the sintering temperature of this system increased with increased mol percent of PZT. Both the maximum permittivity, $\epsilon_{r,max}$ and T_m increased quasi-linearly as the molar fraction of PZT increased. The T_m of the constituent compounds PNN, PZN, and PZT are −120, 140, and 390 °C, respectively,[10,19,33] which can be used to calculate an empirical estimate of T_m via the equation:

$$T_m = 0.5 \times (-120\ °C) + (0.5 - x) \times (140\ °C) + x \times (390\ °C) \quad . \tag{4}$$

The variation of the measured T_m, the calculated T_m, and the measured $\epsilon_{r,max}$ with composition x is shown in Fig. 6. It is evident that Eq. (4) gives a reasonable indication of the transition temperature T_m. A summary of the dielectric properties for each of the compositions is shown in Table III. As Table III illustrates, the PNN–PZN–PZT ceramics in this study resulted in significantly higher permittivities than in previous studies. Through controlling PbO loss and preventing pyrochlore phase formation, single-phase perovskite ceramics can be processed with excellent electrical properties.

TABLE III. Comparisons of dielectric properties of ceramics in the 0.5PNN–(0.5 – x) PZN–xPZT system at the optimum sintering conditions.

	Composition 0.5PNN–(0.5 – x)PZN–xPZT	Percent perovskite	T_m (°C)	Relative permittivity (at 25 °C) at 1 kHz	Relative permittivity (at T_m) at 1 kHz	Dielectric loss (at 25 °C) at 1 kHz
Lee *et al.*[23]	$x = 0.0$	85	55	4000	6000	···
	$x = 0.1$	87	80	4700	8000	···
	$x = 0.3$	92	140	5500	13000	···
	$x = 0.5$	78	225	2500	7000	···
Vierheilig *et al.*[37]	$x = 0.0$	100	−10	6077	6980	0.010
This work	$x = 0.0$	100	−20	8500	9700	0.011
	$x = 0.1$	100	0	11500	13000	0.032
	$x = 0.3$	100	70	9000	18000	0.050
	$x = 0.5$	100	125	4000	22000	0.048

C. Ferroelectric properties

Polarization hysteresis measurements at room temperature were performed using a modified Sawyer–Tower circuit. The hysteresis loops as a function of x are shown in Fig 7. The $x = 0$ and $x = 0.1$ compositions exhibited slim loops characteristic of relaxor ferroelectrics. The saturation polarization P_s, remanent polarization P_r, and coercive field E_c were increased with increased mol percent of PZT as illustrated in Table IV. The loop area values were calculated by integrating the polarization with respect to the electric field. The maximum remanent polarization was observed for the $x = 0.5$ composition. The values of P_s, P_r, and E_c for the $x = 0.5$ composition are 31.9 $\mu C/cm^2$, 25.2 $\mu C/cm^2$, and 4.0 kV/cm, respectively.

These hysteresis data are consistent with the dielectric results in illustrating the gradual trend from relaxor to normal ferroelectric as the mol fraction of PZT is increased.[1,35,36] The hysteresis loops for the compositions $x = 0$ and $x = 0.3$ at various temperatures are shown in Fig. 8. The coercive field values for each composition were found to exhibit an increase with decreased temperature. This is due to the influence of the metastable macro-domain structure and the immobilizations of the domain walls.[1,35,36]

The $x = 0.3$ and 0.5 compositions exhibited square loop behavior at −66 °C. However, as the temperature increased the square loops transformed to slim loops and the remanent polarization and coercive filed values decreased significantly. The $x = 0$ and $x = 0.1$ compositions exhibited slim loop behavior near room temperature. All of compositions displayed a clear transition from square-loop behavior to slim-loop behavior in

TABLE IV. Polarization hysteresis data as a function of x in the 0.5PNN–(0.5 – x)PZN–xPZT system.

Composition	P_s ($\mu C/cm^2$)	P_r ($\mu C/cm^2$)	E_c (kV/cm)	Loop area (mC/cm^2)
$x = 0.0$	22.5	0.9	0.008	49.88
$x = 0.1$	23.8	1.8	0.010	72.81
$x = 0.3$	28.1	8.5	1.221	255.12
$x = 0.5$	31.9	25.2	4.024	628.47

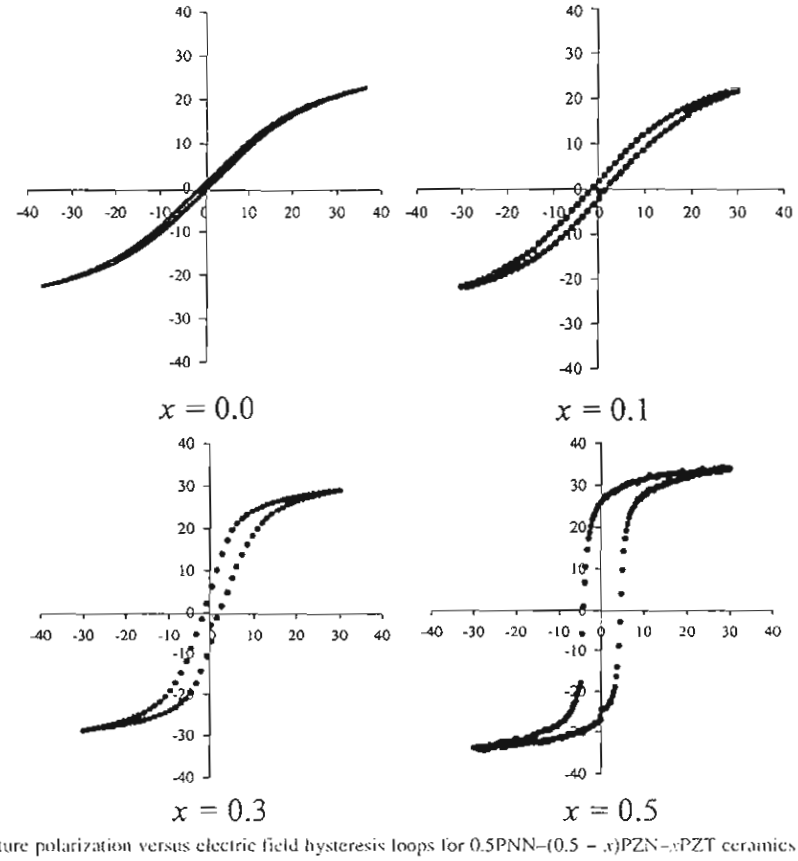

FIG. 7. Room-temperature polarization versus electric field hysteresis loops for 0.5PNN–(0.5 – x)PZN–xPZT ceramics at the optimum sintering conditions.

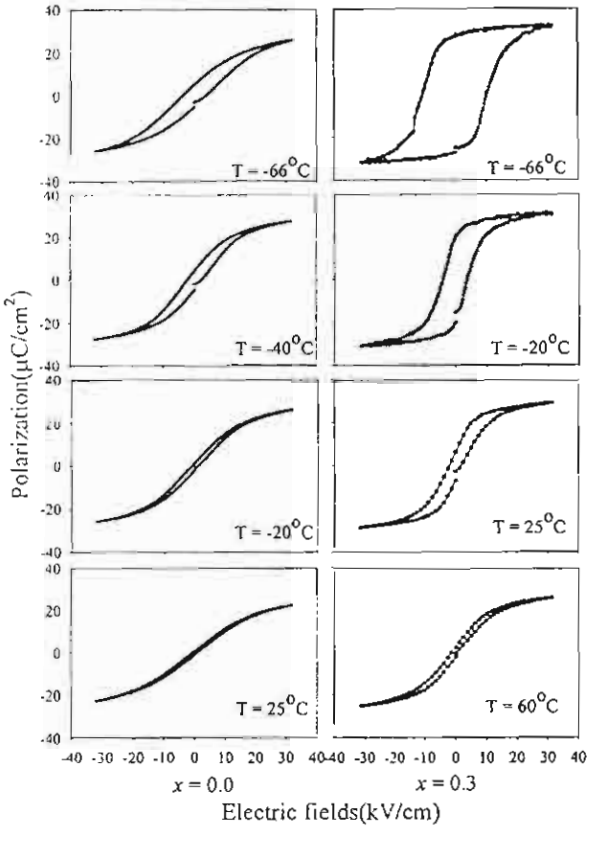

FIG. 8. Temperature dependence of the *P–E* hysteresis of 0.5PNN–(0.5 – *x*)PZN–*x*PZT ceramics at optimum sintering conditions, compositions $x = 0$ and $x = 0.3$ are shown

the vicinity of T_m. In addition, the hysteresis loops showed that the remanent polarization is nonzero at T_m but decays to zero at temperatures above T_m.

IV. CONCLUSIONS

In this work, it was shown that by controlling PbO loss and preventing pyrochlore formation high permittivity ceramics in the PNN–PZN–PZT system can be processed through high-temperature calcination. This can be accomplished by utilizing a double crucible during calcination, adding excess PbO (2mol%), and maintaining a fast heating/cooling rate (20 °C/min). The dielectric properties and the T_m of 0.5PNN–(0.5 – *x*)PZN–*x*PZT was found to increase with increasing PZT concentration. Furthermore, the transition from the normal ferroelectric to the relaxor ferroelectric state was clearly observed as the mol fraction of PZT decreased. The optimum dielectric properties were observed for the $x = 0.5$ composition with a permittivity of 22,000 and P_s, P_r and E_c values of 31.9 μC/cm², 25.2μC/cm², and 4.0 kV/cm, respectively.

ACKNOWLEDGMENTS

The authors are grateful to the Thailand Research Fund, Graduate School Chiang Mai University and Ministry of University Affairs for financial support.

REFERENCES

1. L.E. Cross, Ferroelectrics **76**, 241 (1987).
2. T.R. Shrout and A. Halliyal, Am. Ceram. Soc. Bull. **66**, 704 (1987).
3. K. Uchino, Ferroelectrics **151**, 321 (1994).
4. K. Uchino, Solid State Ionics **108**, 43 (1998).
5. K. Uchino, *Ferroelectric Devices* (Marcel Dekker, New York, 2000).
6. K. Uchino, *Piezoelectric Actuators and Ultrasonic Motors* (Kluwer Academic Publishers, Boston, MA, 1996).
7. V.A. Bokov and I.E. Mylnikova, Sov. Phys-Solid State **2**, 2428 (1960).
8. J. Kuwata, K. Uchino, and S. Nomura, Ferroelectrics **37**, 579 (1981).
9. K. Uchino, Ceram. Int. **21**, 309 (1995).
10. S.E. Park and T.R. Shrout, IEEE Tr. UFFC. **44**, 1140 (1997).
11. M.L. Mulvihill, L.E. Cross, W. Cao, and K. Uchino, J. Am. Ceram. Soc. **80**, 1462 (1997).
12. C.A. Randall and A.S. Bhalla, Jpn. J. Appl. Phys. **29**, 327 (1990).
13. A.S. Bhalla, R. Guo, and R. Roy, Mat. Res. Innovat. **4**, 3 (2000).
14. N. Mizutani, N. Wakiya, K. Shinozaki, and N. Ishizawa, Mater. Res. Bull. **30**, 1121 (1995).
15. A. Halliyal, U. Kumar, R.E. Newham, and L.E. Cross, Am. Ceram. Soc. Bull. **66**, 671 (1987).
16. J.R. Belsick, A. Halliyal, U. Kumar, and R.E. Newnham, Am. Ceram. Soc. Bull. **66**, 664 (1987).
17. H.Q. Fan and H.E. Kim, J. Appl. Phys. **91**, 317 (2002).
18. H.Q. Fan and H.E. Kim, J. Mater. Res. **17**, 180 (2002).
19. V.A. Bokov and I.E. Myl'nikova, Sov. Phys. Solid State **3**, 631 (1961).
20. L. Veitch, Thesis, Pennsylvania State University (1982).
21. D. Luff, R. Lane, K.R. Brown, and H.J. Marshallsay, Trans. J. Brit. Ceram. Soc. **73**, 251 (1974).
22. O. Babushkin, T. Lindback, J.C. Luc, and J. Leblais, J. Eur. Ceram. Soc. **18**, 737 (1998).
23. S.H. Lee, H.G. Kim, H.I. Choi, and G. Sa-Gong, IEEE Int. Conf. Prop. Appl. Dielectric Mater. **2**, 1062 (1997).
24. S.L. Swartz and T.R. Shrout, Mater. Res. Bull. **17**, 1245 (1982).
25. G. Robert, M.D. Maeder, D. Damjanovic, and N. Setter, J. Am. Ceram. Soc. **84**, 2869 (2001).
26. S. Ananta, R. Tipakontitikul, and T. Tunkasiri, Mater. Lett. **4214**, 1 (2002).
27. JCPDS No. 25-0446 (International Center for Diffraction Data, Newton Square, PA, 2000).
28. H.M. Jang, S.R. Cho, and K.M. Lee, J. Am. Ceram. Soc. **78**, 297 (1995).
29. F. Xia and X. Yao, J. Mater. Sci. **36**, 247 (2001).
30. S.L. Swartz, T.R. Shrout, W.A. Schulze, and L. E. Cross, J. Am. Ceram. Soc. **67**, 311 (1984).
31. R.D. Shannon, Acta. Crystallogr. A **32**, 751 (1976).
32. T.R. Shrout, R. Eitel, and C.A. Randall, IEEE Tr. UFFC. **44**, 1140 (2002).
33. A.J. Moulson and J.M. Herbert, *Electroceramics: Materials, Properties, Applications* (Chapman and Hall, New York, 1990).
34. L.E. Cross, Ferroelectrics **151**, 305 (1994).
35. H. Fan, L. Zhang, L. Zhang, and X. Yao, J. Phys. Condens. Matter **12**, 4381 (2000).
36. D. Pandey, Key Eng. Mater. **101–102**, 177 (1995).
37. A. Vierheilig, A. Safari, and A. Halliyal, Ceram. Trans. **8**, 75 (1990).

เอกสารหมายเลข 1.7

Available online at www.sciencedirect.com
SCIENCE DIRECT®
Current Applied Physics 4 (2004) 179–181
Current Applied Physics
Physics, Chemistry and Materials Science
www.elsevier.com/locate/cap

Effect of sintering temperatures on phase transition of lead zirconate ceramics

C. Puchmark *, S. Jiansirisomboon, G. Rujijanagul, T. Tunkasiri

Department of Physics, Faculty of Science, Chiang Mai University, Chiang Mai 50200, Thailand

Abstract

In this report, effect of sintering temperature on the phase transition temperature from antiferroelectric phase to paraelectric phase of $PbZrO_3$ is presented. $PbZrO_3$ ceramics were prepared via the solid state reaction route. Calcination and sintering were done at 750 °C for 2 h and 1150–1250 °C for 2 h respectively. The transition temperature increased with increasing sintering temperature up to 1200 °C then decreased with the temperature.

PACS: 77.80.–e
Keywords: Antiferroelectrics; Lead zirconate; Ceramics

1. Introduction

Lead zirconate ($PbZrO_3$) is an antiferroelectric ceramic. It is reported that $PbZrO_3$ has an orthorhombic crystal structure at room temperature with lattice parameters of $a = 5.87$ Å, $b = 11.74$ Å, $c = 8.20$ Å. The dielectric constant of $PbZrO_3$ shows a sharp maximum at the phase transition from orthorhombic to cubic at the Curie point near 230 °C [1]. It is reported that antiferroelectric to ferroelectric transition (under the application of a strong electric field to the ceramics in the antiferroelectric phase) leads to significant energy storage [2]. Thus, $PbZrO_3$ is a candidate material for energy storage applications. It is reported that the properties of $PbZrO_3$ can be improved by adding Ba ions into the Pb sites of $PbZrO_3$ [3–6]. The important modified $PbZrO_3$ compound is $(Pb_{1-x}Ba_x)ZrO_3$. Many authors have reported that as the Ba ions in $(Pb_{1-x}Ba_x)ZrO_3$ increase, the Curie temperature of the $(Pb_{1-x}Ba_x)ZrO_3$ shifts to a lower temperature [3,7]. However there is no report about effect of sintering temperature on the phase transition of $PbZrO_3$. In the present paper, experimental results of the preparation of $PbZrO_3$ by solid state reaction are presented. The effect of the sintering temperature on the phase transition was studied.

2. Experiment

In the present study, $PbZrO_3$ powders were prepared by the mixed-oxide method. Reagent-grade PbO and ZrO_2 powders were used as the starting materials. The starting powders were ball milled in ethyl alcohol for 24 h using zirconia balls as the grinding media. After mixing, the slurry was dried and the powder ground into a fine powder using an agate mortar and pestle. The mixed powder was calcined at various temperatures ranging from 500 to 900 °C for 3 h at a heating rate of 5 °C/min. In order to study the phase formation of the calcined powders, X-ray diffraction analysis (XRD) was performed using a diffractometer with Cu K_α radiation. It was found that powders calcined at ≥775 °C provide a single phase of $PbZrO_3$. To improve compaction, 0.3 wt% of PVA binder was blended with the powder before pressing at 40 MPa into cylindrical pellets 15 mm in diameter and 2 mm in thickness. The pellets were then sintered at 1100–1300 °C for 2 h at a heating rate of 5 °C/min. The density of the sintered samples was measured by the Archimedes method with distilled water as the fluid medium. (The phases present in the sintered samples after various sintering temperatures

* Corresponding author.
E-mail address: kungmic2002@yahoo.com (C. Puchmark).

1567-1739/$ - see front matter © 2003 Elsevier B.V. All rights reserved.
doi:10.1016/j.cap.2003.11.003

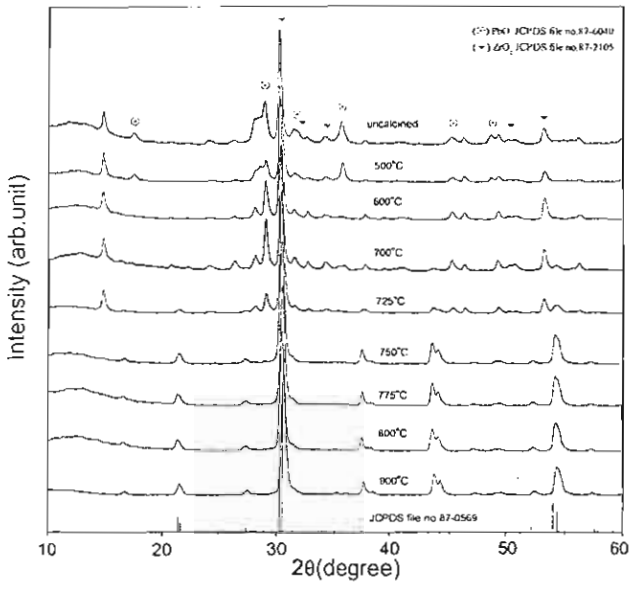

Fig. 1. X-ray diffraction patterns of $PbZrO_3$ calcined at different temperatures.

was investigated by XRD.) Microstructural evolution of the sintered samples was examined by using scanning electron microscopy (SEM). For dielectric measure-

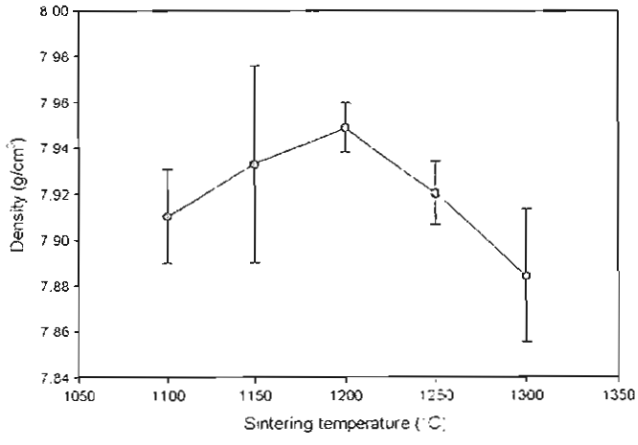

Fig. 2. Plot of density as a function of sintering temperature of $PbZrO_3$ ceramics.

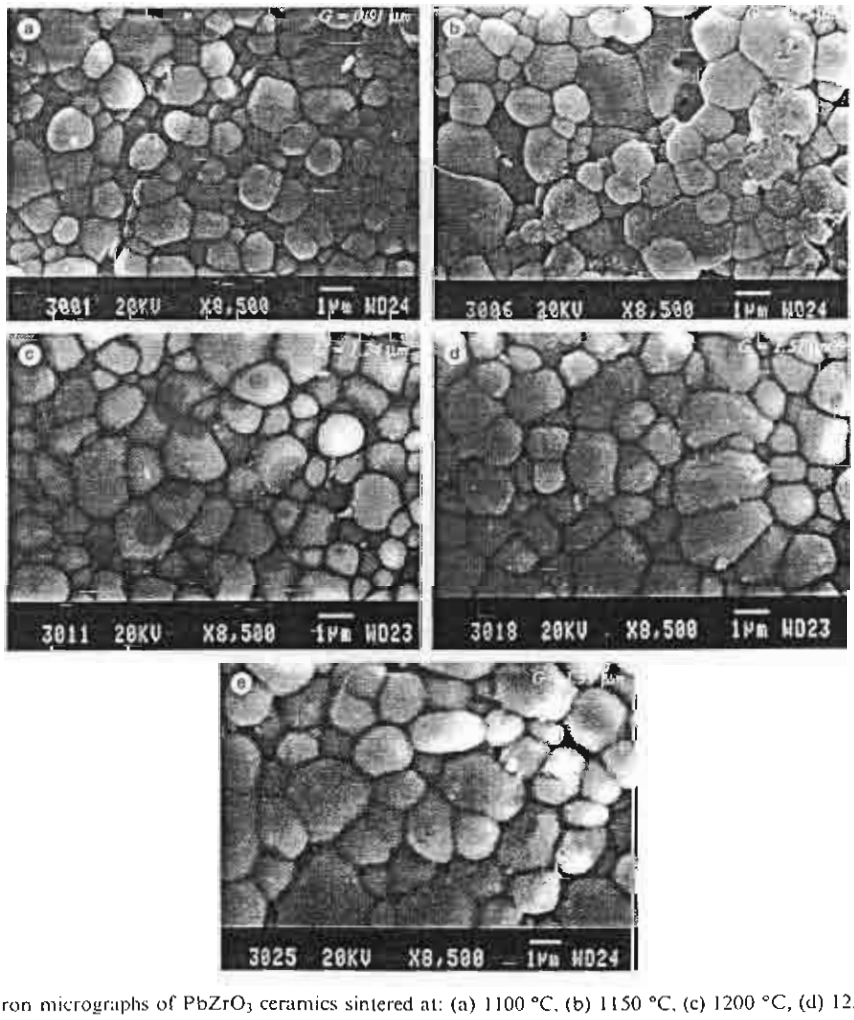

Fig. 3. Scanning electron micrographs of $PbZrO_3$ ceramics sintered at: (a) 1100 °C, (b) 1150 °C, (c) 1200 °C, (d) 1250 °C and (e) 1300 °C.

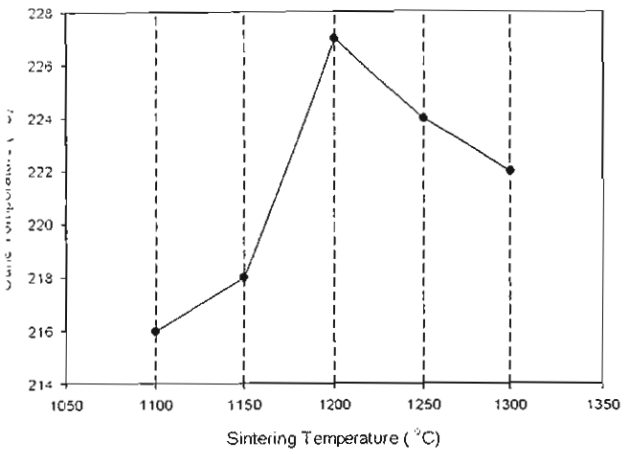

ig. 4. Plot of Curie-temperature as a function of sintering temperature f $PbZrO_3$ ceramics sintered at different temperatures.

ients. gold electrodes were sputtered on the samples hich were then subjected to an automated dielectric ystem measurement controlled by a computer. An mpedance analyzer was also used to measure the ielectric constant and dissipation factor. The dielectric onstant and dissipation factors were measured at kHz. as the samples were heated in the range of 5–250 °C at a rate of 3 °C/min. The phase transition of he samples was studied by measuring the dielectric– emperature curve.

3. Results and discussion

From the XRD pattern (Fig. 1), the second phase was bserved at calcination temperatures below 775 °C. The nalysis was carried out based on the Joint Committee n Powder Diffraction Standard (JCPDS) [8]. A plot of lensity as a function of calcination temperature is hown in Fig. 2. The density increases with increasing he calcination temperature up to 1200 °C and decreases vith further increase of the calcination temperature. Fig. shows SEM micrographs of the $PbZrO_3$ ceramics intered at various temperatures. The grain size increases slightly with increasing sintering temperature. ully dense grain packing was found in samples sintered t higher sintering temperatures.

The dielectric constants of $PbZrO_3$ at temperature bove the phase transition may be expressed by an approximation to the Curie–Weiss law. In the present work, the Curie temperature of the samples was normally obtained from the plot of ε_r^{-1} as a function of temperature. The variation of Curie temperature with sintering temperature is shown in Fig. 4. Many authors have reported that as the Ba ions added to $PbZrO_3$ increased, the Curie temperature of the materials is shifted to a lower temperature [3,7]. In this work, the Curie temperature increases with sintering temperature up to 1200 °C, then decreases with further increase of the sintering temperature. It can be noted that the dielectric results corresponded well with the density results.

4. Conclusion

In the present work, $PbZrO_3$ was prepared via the mixed oxide method. The single phase of $PbZrO_3$ was found in samples calcined at temperatures $\geqslant$ 775 °C. The sintering temperature affects the density, microstructure and phase transition.

Acknowledgements

We would like to thank the Thailand Research Fund, Graduate School, Chiang Mai University, Faculty of Science Chiang Mai University and Ministry of University Affairs for financial support throughout the project.

References

[1] B. Jaffe, W.R. Cook, H. Jaffe, Piezoelectric Ceramics, RAN Publishers, 1971, pp. 123–131.
[2] E.E. Oren, E. Taspinar, A.C. Tas, J. Am. Ceram. Soc. 80 (10) (1997) 2714.
[3] G. Shirane, Phys. Rev. 86 (2) (1952) 219.
[4] B.P. Pokharel, M.K. Datta, D. Pandey, J. Mater. Sci. 34 (1999) 691.
[5] B.P. Pokharel, D. Pandey, J. Appl. Phys. 88 (9) (2000) 5364.
[6] K.H. Yoon, S.C. Hwang, J. Mater. Sci. 32 (1997) 17.
[7] S. Roberts, J. Am. Ceram. Soc. 33 (2) (1950) 63, 64 (9) (1981) 533–538.
[8] Powder Diffraction File, Card No.80-0569. Joint Committee on Powder Diffraction Standards, Swarthmore, PA.

เอกสารหมายเลข 1.8

Ferroelectric Letters, 31:1–13, 2004

ISSN: 0731-5171 print / 1543-5288 online
DOI: 10.1080/07315170490449763

Taylor & Francis
Taylor & Francis Group

Effect of Sintering Temperature on Phase Transition and Mechanical Properties of Lead Zirconate Ceramics

C. PUCHMARK, G. RUJIJANAGUL, S. JIANSIRISOMBOON, and T. TUNKASIRI

Department of Physics, Faculty of Science, Chiang Mai University, Chiang Mai, Thailand 50200

Communicated by George W. Taylor

(Received July 1, 2003)

Phase transition and mechanical properties of $PbZrO_3$ (PZ) at different sintering temperatures were studied. The Curie temperature depends on the sintering temperature. Hardness and fracture toughness of the PZ were measured using Vickers and Knoop microhardness testers. The lower density at the higher sintering temperature resulting from the loss of lead oxide (PbO) causes the lower value of the Curie temperature, hardness and fracture toughness. The results were well corresponding to the microstructure of the PZ ceramics.

Keywords: lead zirconate ceramics; $PbZrO_3$; phase transition; mechanical properties

INTRODUCTION

$PbZrO_3$ (PZ) is an antiferroelectric material, which is reported to have an orthorhombic crystal structure at room temperature with lattice parameters of $a = 8.23$ Å, $b = 11.77$ Å, $c = 5.81$ Å [1]. The dielectric constant of PZ ceramic shows a sharp maximum at the phase transition from orthorhombic to cubic at the Curie point near 230°C [2]. Previous author reported that antiferroelectric to ferroelectric transition (under the application of a strong electric field to the ceramics in the antiferroelectric phase) leads to significant energy storage [3]. Then PZ is a candidate material for energy storage applications. PZ was also searched for its microwave dielectric properties because its dielectric relaxation is near microwave frequencies [3, 4]. The dielectric properties of PZ can be improved by incorporation of Ba ions into the Pb sites of PZ [5–8]. Therefore, the important modification of PZ becomes $(Pb_{1-x}Ba_x)$

ZrO_3 (PBZ). Many authors found that as the number of Ba ions in PBZ is increased, the Curie temperature of the PBZ is shifted to a lower temperature [5, 9]. Because of a large volume change in the phase transition, the PBZ is selected as a candidate material for energy conversion [8]. For the past decade, the electrical properties of PZ were widely studied, however, its mechanical properties have not been well researched. In this paper, the experimental results of the preparation of PZ by solid state reaction method are presented. Effect of sintering temperature on phase transition, electrical properties, and mechanical properties were also studied.

EXPERIMENT

In the present study, PZ powders were prepared by the mixed-oxide method. Reagent-grade of lead oxide (PbO) and zirconium dioxide (ZrO_2) powders were used as the starting materials. The starting powders were ball milling in ethanol for 24 h using zirconia balls as a grinding media. After mixing, the slurry were dried, the powder was then ground using an agate mortar and pestle into a fine powder. The mixed powder was calcined at various temperatures ranging from 500 to 900°C for 3 h with a heating rate of 5°C/min. To study the phase formation of the calcined powders, x-ray diffraction analysis (XRD) of the powders was performed using a diffractrometer with CuK_α radiation. To improve the powder compaction, 0.3 wt% of PVA binder was blended with the powder before pressing at 40 MPa into cylindrical pellets with 15 mm in diameter and 2 mm in thickness. The pellets were then sintered at 1100–1300°C for 2 h with a heating rate of 5°C/min. Density of the sintered samples was measured by Archimedes method with distilled water as the fluid medium. The phase of the sintered samples at various sintering temperatures was investigated by XRD. The microstructural evolution of the sintered samples was examined by scanning electron microscopy (SEM). For dielectric measurement, gold electrodes were sputtered on the samples and then subjected to an automated dielectric system measurement controlled by a computer. An impedance analyzer was also used to measure the dielectric constant and dissipation factor. The dielectric constant and dissipation factors were measured at 1 kHz, as the samples were heated in the range of 25–250°C at a rate of 3°C/min. Phase transition of the samples was studied by measuring the dielectric-temperature curve. The dielectric constants of the PZ at temperature above the phase transition may be expressed to an approximation by the Curie-Weiss law. The Curie temperature of the samples can be normally obtained from the plot of ε_r^{-1} as a function of temperature.

Effect of sintering temperatures on the mechanical properties of the ceramics was studied by Vickers and Knoop microhardness testers. Indentations were applied on the polished surfaces of PZ ceramics. Applied loads were in the range of 200–1000 g with an indentation period of 15 s. Indentation crack length (c) and indentation diagonal (d) was measured, and then used to calculate Vickers hardness, Knoop hardness and fracture toughness by the following equations:

$$H_V = 1854.4\left(\frac{P}{d_V^2}\right) \tag{1}$$

where H_V is a Vickers hardness (in GPa), d_V (in μm) and P is an applied load (in N).

$$H_K = 1.451\left(\frac{P}{d_K^2}\right) \tag{2}$$

where H_K is a Knoop hardness (in kg/mm^2), d_K is a longer diagonal length of a Knoop indentation (in mm) and P is an applied load (in N).

$$K_{IC} = \xi\left(\frac{E}{H_V}\right)^{1/2}\left(\frac{P}{c^{3/2}}\right) \tag{3}$$

where K_{IC} is a fracture toughness (in MPa·m$^{1/2}$), H_V is a Vickers hardness (in GPa), P is an applied load (in N), E is Young's modulus (in GPa) and c is the radial length measured from the centre of indentation impression (in m) [10, 11]. ξ is a material independent, dimensionless calibration constant which characterizes the geometry of the deformation filed. Studies on many ceramics led to an average value of $\xi = 0.016 \pm 0.004$ [12]. After indentation, the samples were etched by 10% HCl + 1 drop HF. Microstructure of the etched samples was again studied by SEM.

RESULTS AND DISCUSSION

Effect of calcination temperatures on the phase formation of the PZ powder was shown by XRD patterns in Fig. 1. At the calcination temperatures starting from 775°C, a single phase of PZ was detected. The phase analysis was carried out based on the Joint Committee on Powder Diffraction Standard (JCPDS) [1]. The density and Curie temperature of PZ ceramics were plotted as a function of sintering temperature are shown in Fig. 2. The value of density is in the range of 7.88–7.95 g/cm^3 or 97.68–98.48% of the PZ theoretical

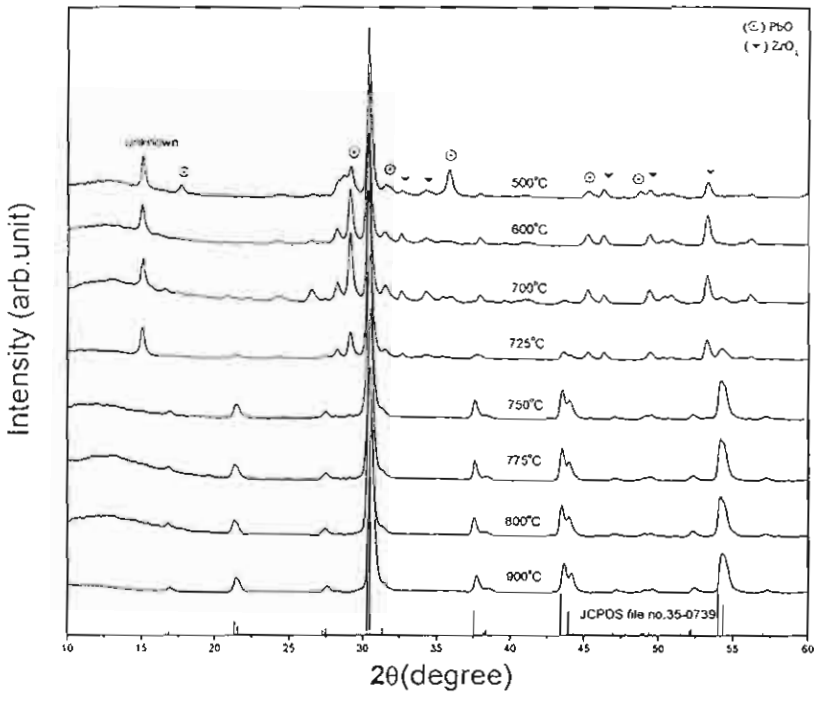

Figure 1. X-ray diffraction patterns of $PbZrO_3$ calcined at different temperatures.

density. The density increases with increasing the sintering temperature up to 1200°C and decreases with further increasing the sintering temperature. The maximum value of density is 98.48% of the theoretical density, observed in the ceramic sintered at 1200°C. Decreasing of the density is likely due to a vaporization of PbO at the temperatures above 1200°C [14]. Figure 3 shows the plot of grain size and porosity as a function of sintering temperature. Grain size of the samples is in the range of 0.9 to 1.5 μm and found to slightly increase with the increasing of the sintering temperature. Weight loss of the PZ ceramics as a function of sintering temperature is shown in Fig. 4. The weight loss increased with increasing the sintering temperature as expected.

The temperature dependences of dielectric constant and dissipation factor at various sintering temperatures were studied and as shown in Table I and plotted in Fig. 5. The measurement of dielectric constant at room temperature is in the range of 157 to 170, while the dissipation factor (tan δ) is in the range of 0.0042 to 0.0205. The highest dielectric constant at room

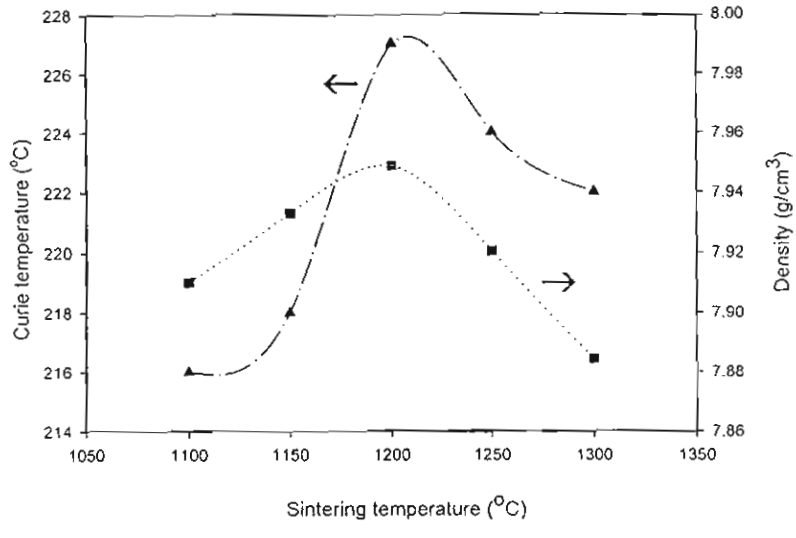

Figure 2. (▲) Curie temperature and (■) density of the sintered PZ ceramics with sintering temperature.

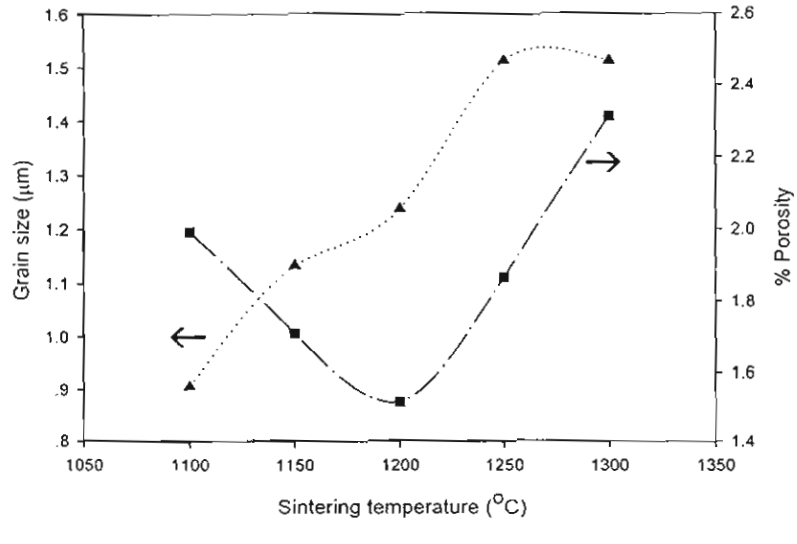

Figure 3. (▲) Grain size and (■) porosity as a function of sintering temperature.

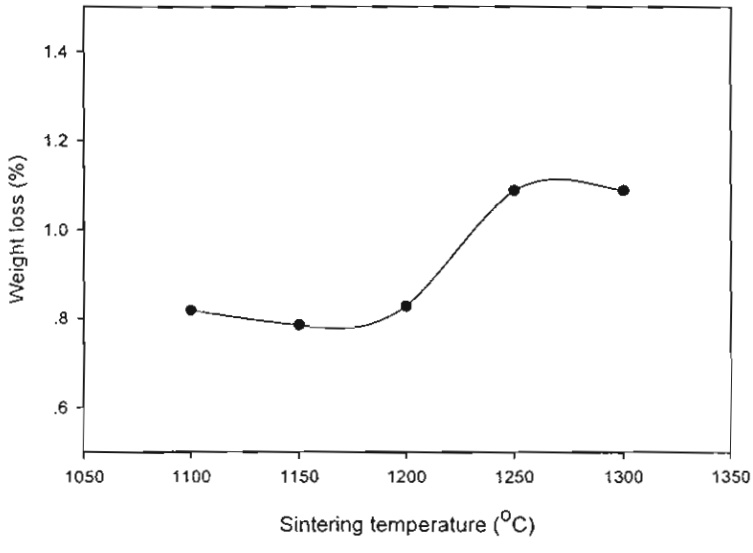

Figure 4. Weight loss of PZ ceramics at various sintering temperatures.

temperature is 170, observed in the PZ ceramic sintered at 1200°C with the grain size of 1 μm. Kong *et al.* prepared PZ ceramics from high-energy ball-milling method and found that the dielectric constant of their PZ ceramic decreases at the higher sintering which is caused by the loss of PbO [13]. The highest dielectric constant in their work is about 218 for the sample sintered at 1200°C with grain size of 8 μm. However, the highest value of the dielectric constant ($\varepsilon_r = 170$) at room temperature in our work for the ceramics with 1 μm grain size is close to the value found in their work.

TABLE I Dielectric properties of $PbZrO_3$ ceramics sintered at different temperatures

Sintering temperature (°C)	Dielectric constant at 27°C	Dissipation factor at 27°C	Curie temperature (°C)
1100	163	0.0042	227
1150	157	0.0147	228
1200	170	0.0205	232
1250	155	0.0230	231
1300	164	0.0229	230

The variation of Curie temperature as a function of the sintering temperature is also shown in Fig. 5. The maximum dielectric constants at the phase transition temperature are between 6750 and 7762, while Robert [9] and Shirane [5] reported the maximum values of dielectric constant at the phase

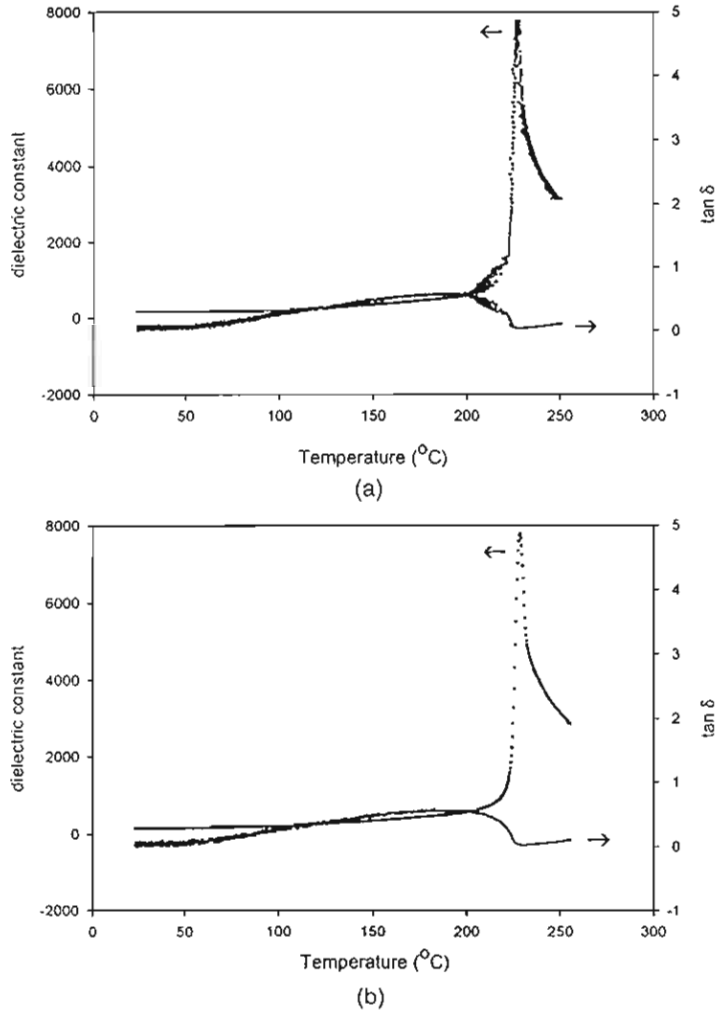

Figure 5. Temperature dependence of the dielectric constant and dissipation factor of PZ sintered at: (a) 1100°C, (b) 1150°C, (c) 1200°C, (d) 1250°C, and (e) 1300°C. *(Continued)*

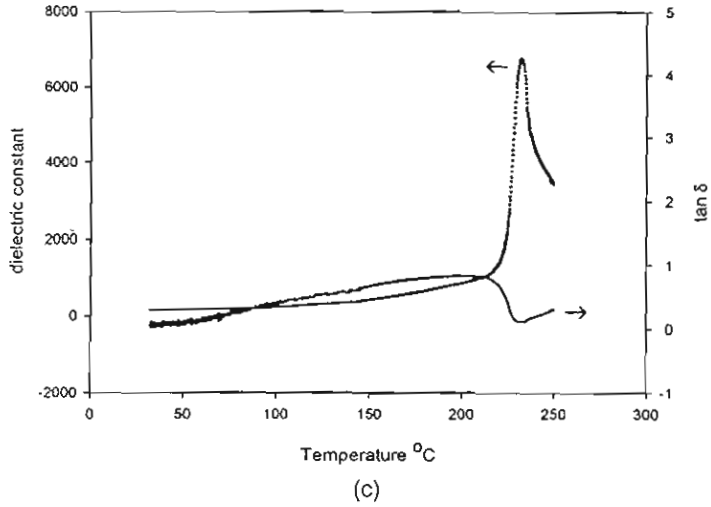

(c)

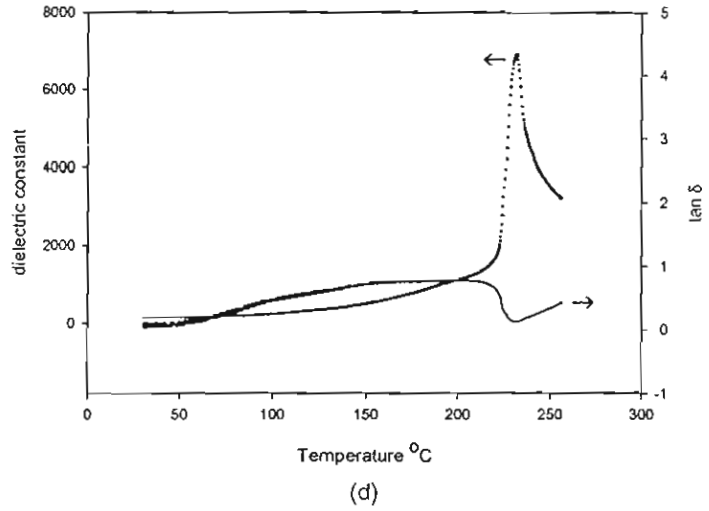

(d)

Figure 5. (Continued)

transition temperature are approximately 3260 and 2300, respectively. In the present work, the Curie temperature increases with the sintering temperature up to 1200°C and then decreases with further increasing the temperature. It can be noted that the Curie temperature results are well corresponded to the density results. This is well corresponded with the work done on a

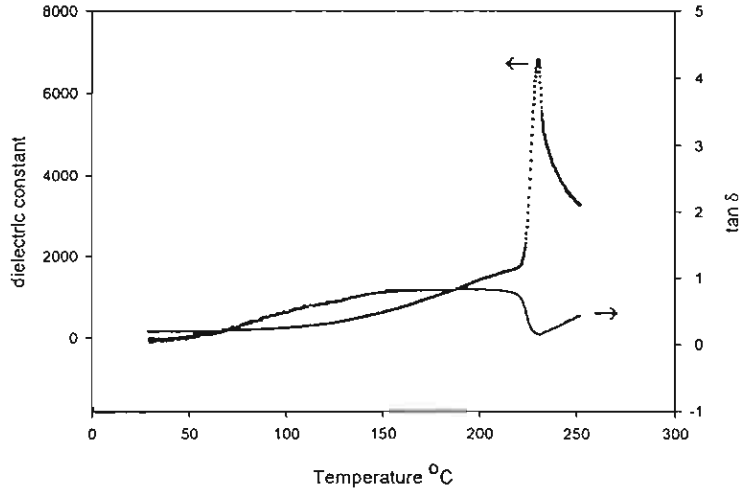

(e)

Figure 5. (Continued)

ferroelectric materials, i.e., $BaTiO_3$ by Fang *et al.*, where the Curie temperature increased with increasing the density of $BaTiO_3$ which is a ferroelectric materials [14].

The effect of sintering temperature on the mechanical properties of the samples was studied by using Vickers and Knoop microhardness testers. The values of Vickers hardness, Knoop hardness, and fracture toughness are listed in Table II, and the plot of these values as a function of sintering temperature are shown in Fig. 6. The hardness values trend to decrease as increasing the sintering temperatures. This result would be well corresponding

TABLE II Mechanical properties of $PbZrO_3$ ceramics sintered at different temperatures

Sintering temperature (°C)	Vickers hardness (GPa)	Knoop hardness (GPa)	Fracture toughness (MPa·m$^{1/2}$)
1100	5.37	4.42	1.38
1150	4.85	4.54	2.91
1200	4.77	4.49	2.91
1250	4.50	4.46	1.97
1300	4.65	3.94	1.12

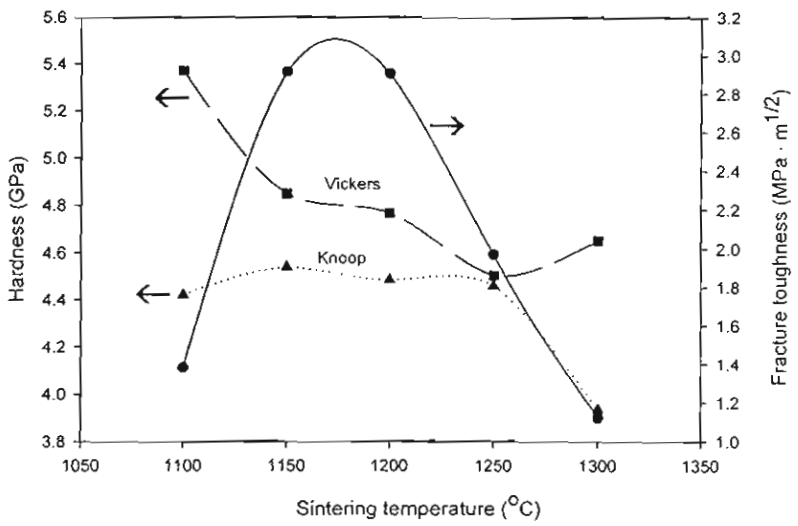

Figure 6. (▲,■) Hardness and (●) fracture toughness of the PZ ceramics plotted as a function of sintering temperatures.

with the density (Fig. 2.) and porosity (Fig. 3.) results, where they are significantly changed due to the loss of PbO at the temperature above 1200°C. For the fracture toughness values which were calculated mainly from the hardness and crack extension from the Vickers indentation impressions, seem to depend significantly on the density and porosity as well. The fracture toughness dramatically increases with the sintering temperature up to 1150°C and then decreases with further increasing the temperature. Figure 7(a) and (b) are SEM micrographs of Vickers and Knoop indentations performed on polished PZ samples sintered at 1200°C. The examples of crack characteristic extended from the Vickers indentation impressions are shown in Fig. 7(c) and 7(d). The cracks of PZ sintered at 1150°C are followed the grain boundaries, so called intergranular crack (Fig. 7(c)), while those cracks found in the sample sintered at 1300°C are rather straight through the grains indicating transgranular fracture (Fig. 7(d)). According to the Table II, the fracture toughness value of PZ sintered at 1150°C ($K_{IC} = 2.91$ MPa·m$^{1/2}$) is higher than that of PZ sintered at 1300°C ($K_{IC} = 1.12$ MPa·m$^{1/2}$). This result is well corresponding to the microstructure; the higher the fracture toughness, the harder the crack cut through the grains and vice versa. Generally, the

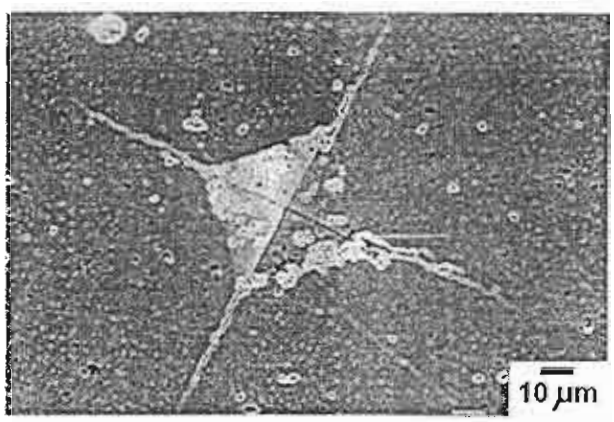

(a)

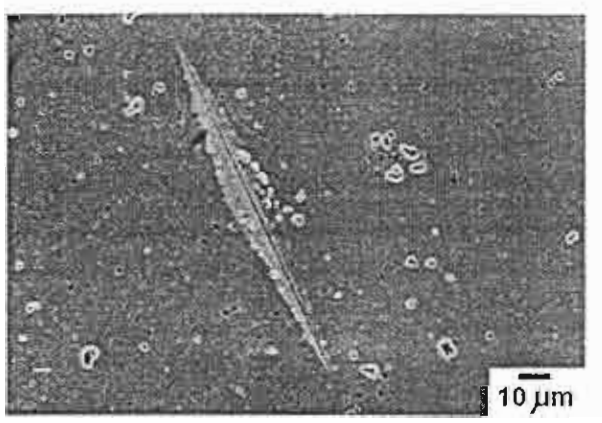

(b)

Figure 7. SEM micrographs of (a) Vickers indentation on surface of PZ sintered at 1200°C, (b) Knoop indentation on surface of PZ sintered at 1200°C, (c) indentation crack of PZ sintered at 1150°C, and (d) indentation crack of PZ sintered at 1300°C. *(Continued)*

hardness and fracture toughness of lead base ceramics depends on many factors such as grain size and porosity [15, 16]. In the present work, the reduction of hardness and fracture toughness at higher sintering temperature is likely to cause by the loss of PbO during sintering which form the lower density and imperfect ceramics [13].

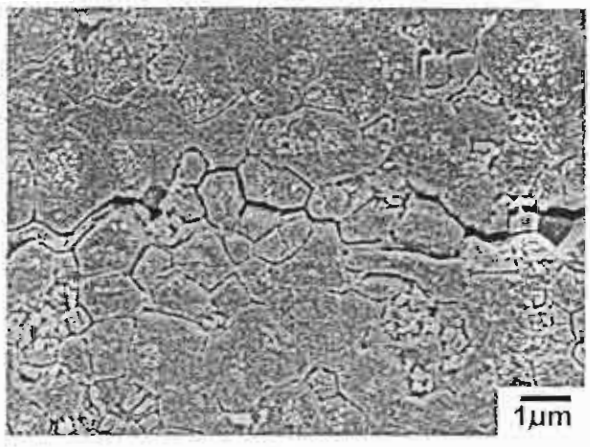

(c)

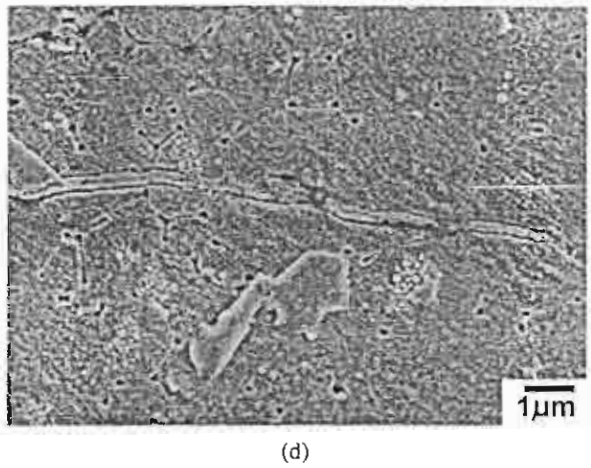

(d)

Figure 7. (Continued)

CONCLUSIONS

In the present work, the $PbZrO_3$ (PZ) was prepared via the mixed oxide method. The single phase of PZ was found in the powders calcined at the temperature $\geq$775°C. The sintering temperature has effects on phase transition behavior and mechanical properties of the PZ. Curie temperature and density of the PZ ceramics increased with increasing sintering temperature

up to 1200°C. However, they decreased for higher sintering temperature. The lower density is likely to cause by the loss of PbO during sintering above 1200°C which then result to the reduction of density, Curie temperature, hardness, and fracture toughness values.

ACKNOWLEDGMENTS

We would like to thank the Thailand Research Fund, Graduate School, Chiang Mai University, Faculty of Science Chiang Mai University, and Ministry of University Affairs for financial support throughout the project.

REFERENCES

[1] Powder Diffraction File, Card No. 35-0739. Joint Committee on Powder Diffraction Standards (JCPDS) PDF-4. Internation Centre for Diffraction Data (ICDD), 2000.
[2] B. Jaffe, W. R. Cook, and H. Jaffe, *Piezoelectric ceramics* (R.A.N. Publishers, 1971), pp.123–131.
[3] E. E. Oren, E. Taspinar, and A. C. Tas, *J. Am. Ceram. Soc.* **80**(10), 2714 (1997).
[4] M. T. Lanagan, J. H. Kim, S. Jang, and R. E. Newnham, *J. Am. Ceram. Soc.* **71**(4), 311 (1988).
[5] G. Shirane, *Phys. Rev.* 86(2), 219 (1952).
[6] B. P. Pokharel, M. K. Datta, and D. Pandey, *J. Mater. Sci.* **34**, 691 (1999).
[7] B. P. Pokharel and D. Pandey, *J. Appl. Phys.* **88**(9), 5364 (2000).
[8] K. H. Yoon, S. C. Hwang, and D. H. Kang, *J. Mater. Sci.* **32**, 17 (1997).
[9] S. Roberts, *J. Am. Ceram. Soc.* **33**(2), 63 (1950).
[10] D. B. Marshall and B. R. Lawn, *J. Mat. Sci.* **14**, 2001 (1979).
[11] B. R. Lawn, A. G. Evans, and D. B. Marshall, *J. Am. Ceram. Soc.* **63**, 574 (1980).
[12] G. R. Anstis, P. Chuntikul, B. R. Lawn, and D. B. Marshall, *J. Am. Ceram. Soc.* 64(9), 533 (1981).
[13] L. B. Kong, J. Ma, W. Zhu, and O. K. Tan, *Mater. Lett.* **49**, 96 (2001).
[14] T. Fang, H. Hsieh, and F. Shiau, *J. Am. Ceram. Soc.* **76**(5), 1205 (1993).
[15] K. Uchino, *Piezoelectric Actuators and Ultrasonic Motors* (Kluwer Academic Publishers, 1997), pp. 113–114.
[16] D. R. Biswas and R. M. Fulrath, *Trans. J. Brit. Cer. Soc.* **79**, 1 (1980).

เอกสารหมายเลข 1.9

ELSEVIER

Materials Science and Engineering B 108 (2004) 258–265

MATERIALS SCIENCE & ENGINEERING B

www.elsevier.com/locate/mseb

Influence of processing conditions on the phase transition and ferroelectric properties of $Pb(Zn_{1/3}Nb_{2/3})O_3$–$Pb(Zr_{1/2}Ti_{1/2})O_3$ ceramics

Naratip Vittayakorn [a,*], Gobwute Rujijanagul [a], Tawee Tunkasiri [a], Xiaoli Tan [b], David P. Cann [b]

[a] *Department of Physics, Faculty of Science, Chiang Mai University, Chiang Mai 50200, Thailand*
[b] *Materials Science and Engineering Department, Iowa State University, Ames, IA 50011 USA*

Received 23 July 2003; accepted 12 January 2004

Abstract

Ceramics solid solutions within the binary system of $xPb(Zn_{1/3}Nb_{2/3})O_3-(1-x)Pb(Zr_{1/2}Ti_{1/2})O_3$ with $x = 0.1$–0.5 were synthesized via the mixed oxide method and the columbite method. Phase development of calcined powders and the crystal structure of sintered ceramics were analyzed by X-ray diffraction. Ferroelectric properties were measured to elucidate the phase transformation and identify the impact of the processing conditions. It is shown that there was no significant difference in P_r across the composition range. However, the coercive field E_c was shown to exhibit a strong compositional dependence. Compared with ceramics prepared by the columbite method, ceramics prepared by the mixed oxide method showed a lower remanent polarization P_r and a higher coercive field E_c. In addition, both X-ray diffraction and ferroelectric measurements indicated a phase transformation from a tetragonal to a pseudo-cubic rhombohedral phase when the fraction of $Pb(Zn_{1/3}Nb_{2/3})O_3$ (PZN) was increased. The morphotropic phase boundary (MPB) is located between $x = 0.2$ and 0.3 according to observations made on ceramics prepared with the columbite method. However, this transformation was obscured in the ceramics prepared with the mixed oxide method. It is proposed that compositional heterogeneities were responsible for these experimental investigations.

Keywords: Phase transition; Ferroelectric properties; Ceramics

1. Introduction

Ferroelectric materials are widely used for various devices, including multilayer capacitors, sensors, and actuators. By the 1950s, the piezoelectric solid solution $Pb(Zr_{1-x}Ti_x)O_3$ (PZT) was found to host exceptionally high dielectric and piezoelectric properties for compositions close to the morphotropic phase boundary (MPB). This MPB is located around $PbTiO_3$:$PbZrO_3$ ~1:1 and separates the Ti-rich tetragonal phase from the Zr-rich rhombohedral phase [1]. Most commercial PZT ceramics are thus designed in the vicinity of the MPB with various dopings in order to achieve high properties.

$Pb(Zn_{1/3}Nb_{2/3})O_3$ (PZN) is an important relaxor ferroelectric material with the rhombohedral structure at room temperature. A diffuse phase transition from the paraelectric state to a ferroelectric polar state occurs at 140 °C [2]. Extensive research has been carried on PZN single crystals because of their excellent dielectric, electrostrictive, and optical properties [2,3]. Although single crystals of PZN can routinely be grown by the flux method, [4] it is known that perovskite PZN ceramics cannot be synthesized by the conventional mixed-oxide method without doping. This is because PZN has a low tolerance factor and small electronegativity difference between the cations and the pyrochlore phase appears to be more thermodynamically stable than the perovskite phase [5]. Attempts to synthesize perovskite PZN ceramics invariably results in the formation of pyrochlore phase with inferior dielectric and piezoelectric properties. The columbite method, as suggested by Schwartz and Shrout [6] for the prepa-

* Corresponding author. Tel.: +1-515-294-3801; fax: +1-515-294-5444.
E-mail address: naratip@iastate.edu (N. Vittayakorn).

0921-5107/$ – see front matter © 2004 Elsevier B.V. All rights reserved.
doi:10.1016/j.mseb.2004.01.006

ration of perovskite $Pb(Mg_{1/3}Nb_{2/3})O_3$ (PMN) ceramic, is not effective in suppressing pyrochlore phase formation in PZN ceramics [5]. Hot isostatic pressing was reported to be able to produce phase-pure perovskite PZN ceramics [7]. However, relatively poor piezoelectric properties were measured in the as-pressed ceramic. Various chemical additives, such as $Ba(Zn_{1/3}Nb_{2/3})O_3$, $BaTiO_3$, and $SrTiO_3$ have thus been explored in an attempt to stabilize the perovskite PZN ceramic and retain the excellent piezoelectric properties. Halliyal et al. [8] prepared $BaTiO_3$-stabilized PZN ceramics using $BaCO_3$, PbO, ZnO, Nb_2O_5, and TiO_2 as the starting materials. Villlegas et al. [9] incorporated $BaTiO_3$ and $Pb(Zr_{0.4}Ti_{0.6})O_3$ into PZN to produce the ternary system with the perovskite structure from $ZnNb_2O_6$ powder. However, a trade-off was made with these additives which yielded reduced dielectric constants and piezoelectric coefficients. Therefore, there is significant interest in finding a method to stabilize the perovskite phase in PZN without sacrificing the excellent dielectric and piezoelectric properties.

Since both PZT and PZN have perovskite structure and are known to have excellent dielectric and piezoelectric properties, it is suggested to alloy PZN with PZT to stabilize and optimize the PZN ceramics. Recent work by Fan and Kim [10] has shown promise in producing phase-pure perovskite PZN–PZT ceramics with the conventional mixed-oxide method. The present work aims to provide a comprehensive study on the process-property relationships in the binary system of PZN–PZT with a wide composition range. Both the conventional mixed-oxide method and the columbite precursor method have been used in synthesizing the PZN–PZT ceramics. The conventional method utilized a one-step reaction with all of starting materials whereas the columbite method was used an initial step of preparing columbite precursor ($ZnNb_2O_6$) and wolframite precursor ($ZrTiO_4$) followed by a reaction with PbO to form the PZN–PZT ceramics. Finally, a comparison of the important ferroelectric properties was made to identify the optimum processing conditions.

2. Experimental procedure

For the conventional method, regent grade oxides of PbO, ZnO, ZrO_2, TiO_2 and Nb_2O_5 were mixed in the required stoichiometric ratios for the general composition xPZN–$(1-x)$PZT where x = 0.1, 0.2, 0.3, 0.4, and 0.5. After ball milling for 24 h and drying at 120 °C, the mixture was calcined at temperatures between 750 and 950 °C for 4 h in a double crucible configuration [11]. A heating rate of 20 °C/min was selected for all of the compositions in this system [11]. For the columbite method, the columbite precursor $ZnNb_2O_6$ was prepared from the reaction between ZnO (99.9%) and Nb_2O_5 (99.9%) at 975 °C for 4 h. The wolframite precursor $ZrTiO_4$ was formed by reacting ZrO_2 (99.9%) with TiO_2 (99.9%) at 1400 °C for 4 h. The precursors $ZnNb_2O_6$, $ZrTiO_4$ were then subsequently mixed with PbO (99.9%) (with 2 mol% excess PbO) [11] and milled, dried, and calcined under the same conditions as the powder prepared by conventional method. The calcined powders of both methods were cold isostatically pressed into pellets at a pressure of 150 MPa. Five sintering conditions were selected to be used with both methods ranging 1175, 1200, 1225, 1250, and 1275 °C dwell 2 h. To prevent PbO volatilization from the pellets, a PbO atmosphere was controlled with a bed of $PbZrO_3$ powder placed in the vicinity of the pellets. The calcined powder and sintered pellets were checked for perovskite phase formation by X-ray diffraction (XRD). Data collection was performed in the 2θ range of 20°–60° with a step scan with a step size of 0.02° and counting time of 2 s per step. For profile fitting, a step scan

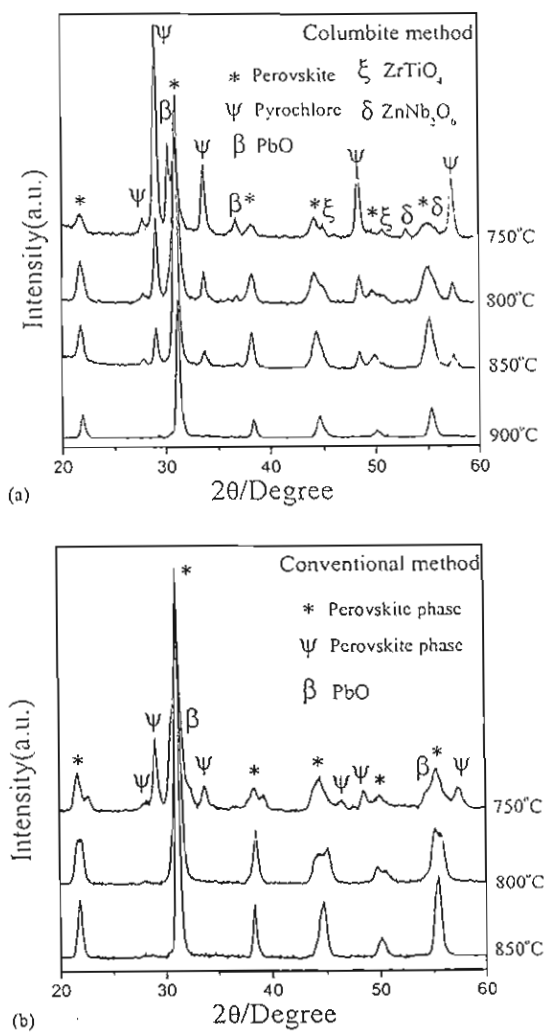

Fig. 1. XRD patterns for 0.3PZN–0.7PZT ceramics calcined at varies temperature for 4 h. (a) Columbite method; (b) conventional method.

with step size of 0.004° was used with a counting time of 5 s per step and peak deconvolution was done with JADE v.6.

The relative amounts of perovskite and pyrochlore phases were approximated by calculating the ratio of the major XRD peak intensities of the perovskite and pyrochlore phase via the following equation:

$$\text{Perovskite intensity (\%)} = \left(\frac{I_{\text{perov}}}{I_{\text{perov}} + I_{\text{pyro}} + I_{\text{PbO}}}\right) \times 100$$

where I_{perov}, I_{pyro}, and I_{PbO} refer to the intensity of the (1 1 0) perovskite peak, (2 2 2) pyrochlore peak, and the intensity of the highest lead oxide peak, respectively.

To investigate the influence of post-sintering heat treatments, specimens from both methods which had been sintered at 1175 °C were annealed at 1250 °C for a dwell time of 6 h in a closed Al_2O_3 crucible with PbO-rich atmosphere. The specimens were polished and electroded via gold sputtering, over which a layer of air-dry silver paint was applied to enhance the electrical contact. The ferroelectric polarization versus electric field (P–E) measurements was made using an RT66A standard ferroelectric test system.

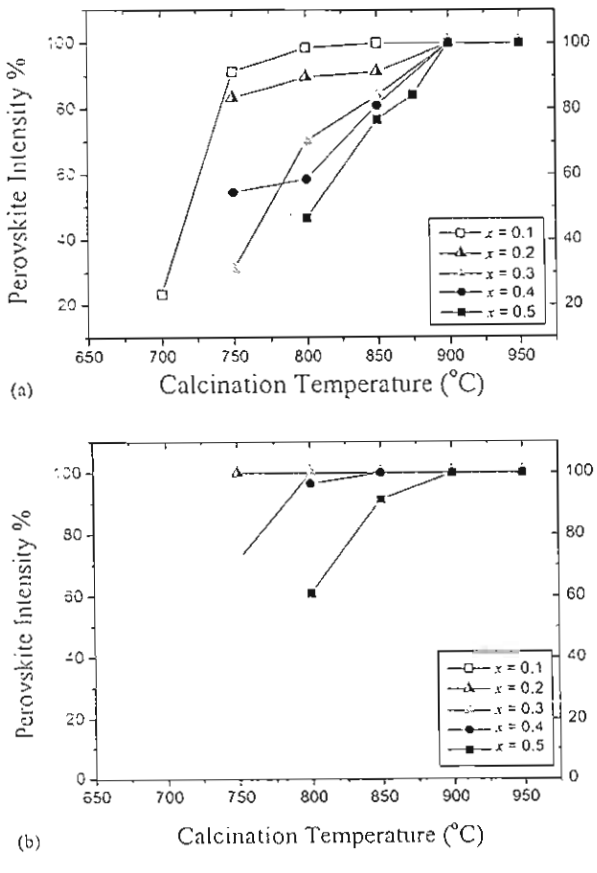

Fig. 2. Percentage of perovskite phase as a function of calcination temperature for xPZN–$(1-x)$PZT ceramics: (a) columbite method; (b) conventional method.

3. Results and discussion

3.1. Perovskite phase formation and the MPB

Powder XRD patterns of the calcined 0.3PZN–0.7PZT powders at different calcination temperatures for both methods are shown in Fig. 1(a) and (b). The XRD results show that the pyrochlore phase $Pb_{1.88}(Zn_{0.3}Nb_{1.25})O_{5.305}$ (JCPDS No. 25-0446) was dominant at calcination temperatures below 750 °C for all of the columbite-derived powders. The precursor phases PbO, $ZrTiO_4$, $ZnNb_2O_6$ were also detected by XRD at below 800 °C. No evidence of the precursor phase ZrO_2, TiO_2, Nb_2O_5 or ZnO was detected by XRD for conventional preparation. Moreover, the pyrochlore phase was only observed in the conventional method-derived powders for compositions with a high concentration of lead zinc niobate. It is assumed that the columbite phase $ZnNb_2O_6$

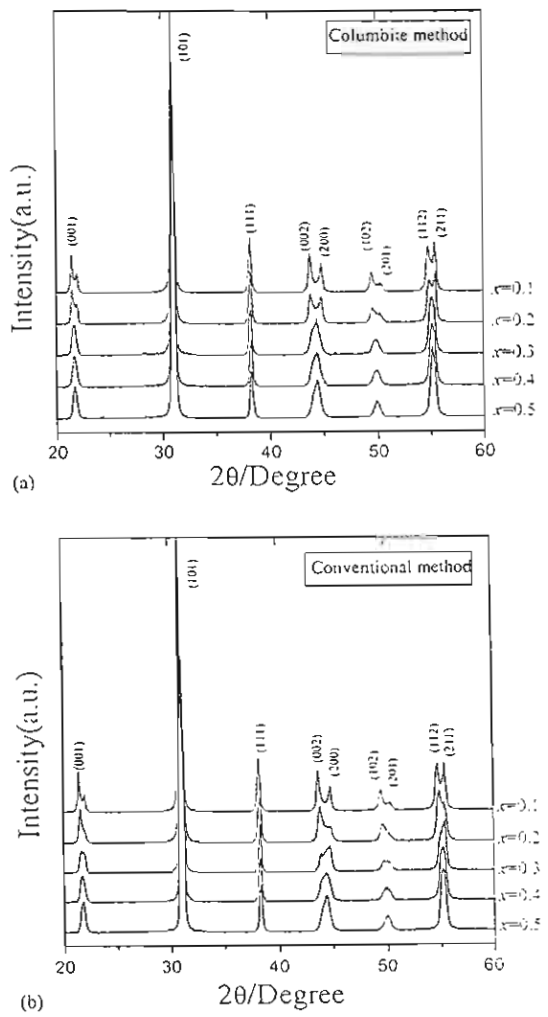

Fig. 3. XRD patterns for xPZN–$(1-x)$PZT ceramics sintered at 1250 °C for 2 h: (a) columbite method; (b) conventional method.

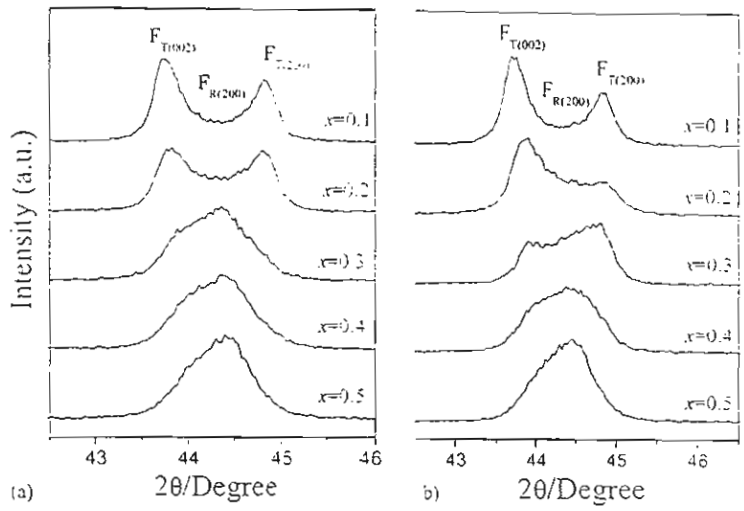

Fig. 4. Close examination of the (0 0 2) peaks shown in Fig. 2. (a) Columbite method; (b) conventional method.

decomposed via reaction with PbO at low temperatures to form the pyrochlore phase $Pb_{1.88}(Zn_{0.3}Nb_{1.25})O_{5.305}$. For the conventional method, $Pb_xNb_yO_z$ pyrochlore phases were found at calcination temperatures below 800 °C for $x > 0.3$. In the work by Chen et. al. [12] it was reported that in the lead-niobium pyrochlore system the cubic $Pb_3Nb_4O_{13}$, pyrochlore phase (JCPDS No. 25–443) forms first around 580 °C. At higher temperatures, it transforms to $Pb_2Nb_2O_7$, (JCPDS No. 40–828) and finally to $Pb_3Nb_2O_8$, (JCPDS No. 30–712) with increased calcination temperatures. At

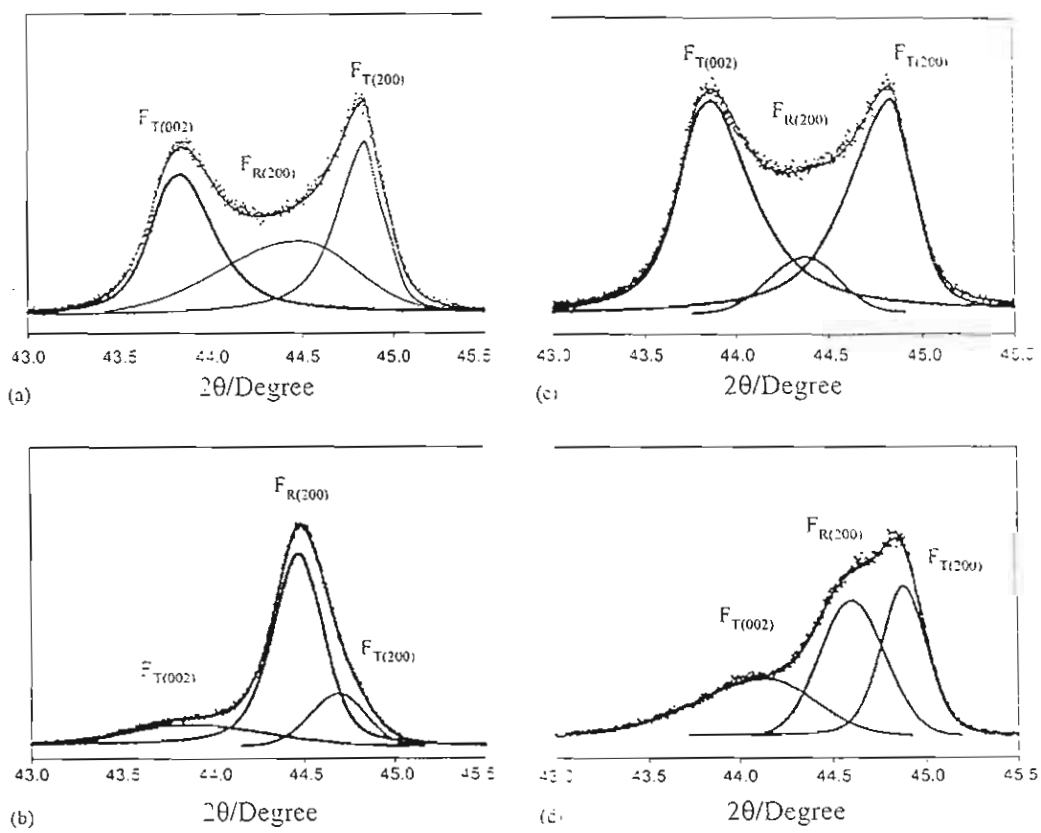

Fig. 5. Individual X-ray diffraction (0 0 2) peak for the tetragonal ($F_{T(002)}$, $F_{T(200)}$) and rhombohedral($F_{R(200)}$) phase for difference methods, (a) 0.2PZN–0.8PZT prepared by columbite method, (b) 0.3PZN–0.7PZT prepared by columbite method, (c) 0.2PZN–0.8PZT prepared by conventional method, (d) 0.3PZN–0.7PZT prepared by conventional method.

800 °C, the pyrochlore phase began to decrease and disappeared completely at 850 °C for powder prepared by conventional method and at 900 °C for the columbite method. The optimum calcination temperature for the formation of phase pure perovskite was found to be about 850 °C for the conventional method and 900 °C for the columbite method.

The perovskite phase formation for both processing methods at various calcination temperatures is shown in Fig. 2(a) and (b), respectively. All the compositions from both methods in the present work showed pyrochlore-free XRD scans at calcination temperatures at above 900 °C. These experiments indicate that for both methods as the concentration of the PZN phase increased the calcination temperature must be increased in order to obtain phase-pure perovskite. Most processing procedures for PZN-based ceramics make use of calcination temperatures in excess of 900 °C. The experiments in this study suggest that the conventional method helps to stabilize the perovskite phase compared with the columbite method. Moreover the perovskite formation temperature for the conventional method was significantly lower than that of the columbite method. The difference in the formation temperatures was presumably due to a different reaction path to the formation of the perovskite phase for the two methods.

Fig. 3 shows the XRD patterns of xPZN–$(1-x)$PZT ceramics sintered at 1200 °C for 2 h to illustrate the change in crystal structure as a function of composition for both processing methods. The results indicate that, for the same composition, different processing methods may develop a perovskite structure with different symmetries. Fig. 4 shows the evolution of the (2 0 0) peak as a function of composition and processing method. The $PbZrO_3$–$PbTiO_3$ phase diagram predicts that at room temperature $Pb(Zr_{1/2}Ti_{1/2})O_3$ falls within the tetragonal phase field near the MPB. The XRD patterns with low PZN concentration show strong (2 0 0) peak splitting which is indicative of the tetragonal phase. As the PZN concentration increased, for both processing methods the (2 0 0) transformed to a single peak which suggests rhombohedral symmetry.

Fig. 5(a–d) show the XRD patterns for both processing methods in the vicinity of the MPB at $x = 0.2$ and 0.3 over the range $2\theta = 43$–45.5. The data shows the appearance of a triplet peak due to the superposition of the tetragonal and rhombohedral (2 0 0) peaks. The columbite prepared samples show a relatively sharp transition between the tetragonal phase at $x = 0.2$ to the rhombohedral phase at $x = 0.3$. In the conventional prepared samples, while the $x = 0.2$ samples shows the presence of the tetragonal phase there is a strong co-existence of both phases for the $x = 0.3$ pattern.

While Fan and Kim report a phase boundary in the same PZN–PZT system at the composition $x = 0.5$, [13] there are no prior reports of the phase boundary observed in this work between $x = 0.2$ and 0.3.

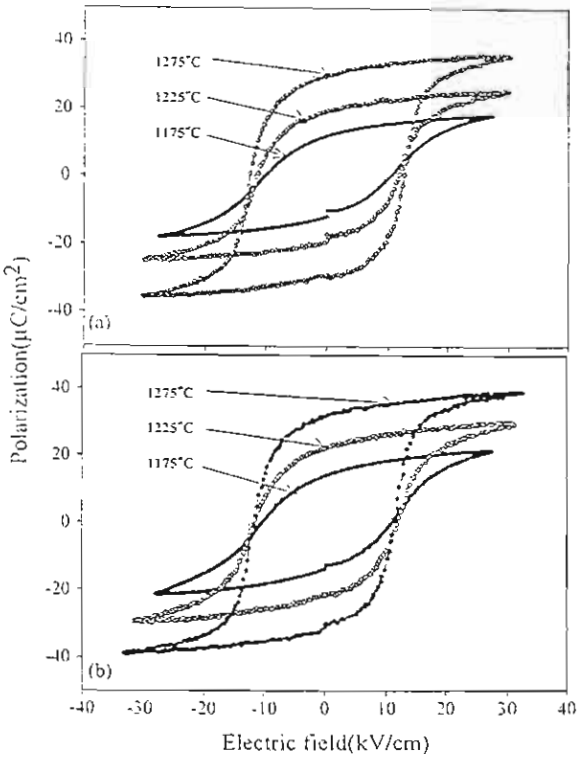

Fig. 6. Room temperature P–E hysteresis as a function of sintering temperature for 0.2PZN—0.8PZT: (a) columbite method; (b) conventional method.

3.2. Effect of sintering temperature and post-sinter annealing

The effect of sintering temperature on the properties was assessed by the polarization–field (P–E) measurements. Fig. 6 shows the results for the composition of $x = 0.2$ for both methods at different sintering temperatures. Ceramics from both methods showed normal ferroelectric behavior with a rectangular loop. The remanent polarization, P_r, was observed to increase with increasing sintering temperature. This is probably due to the smaller grain size at low sintering temperature. This may result in a smaller domain size, and furthermore domain wall motion in smaller grains is subject to stricter constraints [1]. Strong internal stresses are expected in fine-grained specimens and polarization switching is thus greatly suppressed. This was accompanied by the decrease in the coercive field with increasing sintering temperature [14].

For compositions with $x > 0.3$, the P_r decreased at high sintering temperatures. For the composition of $x = 0.1$, rectangular hysteresis loops were not observed even at a sintering temperature of 1250 °C, as shown in Fig. 7. It has been reported that post-sinter annealing is effective in improving the dielectric and ferroelectric properties of lead-based ceramics [15]. Specimens for each composition sintered at the lowest temperature (1175 °C) were annealed at 1250 °C for 6 h. Indeed, significant improvements of

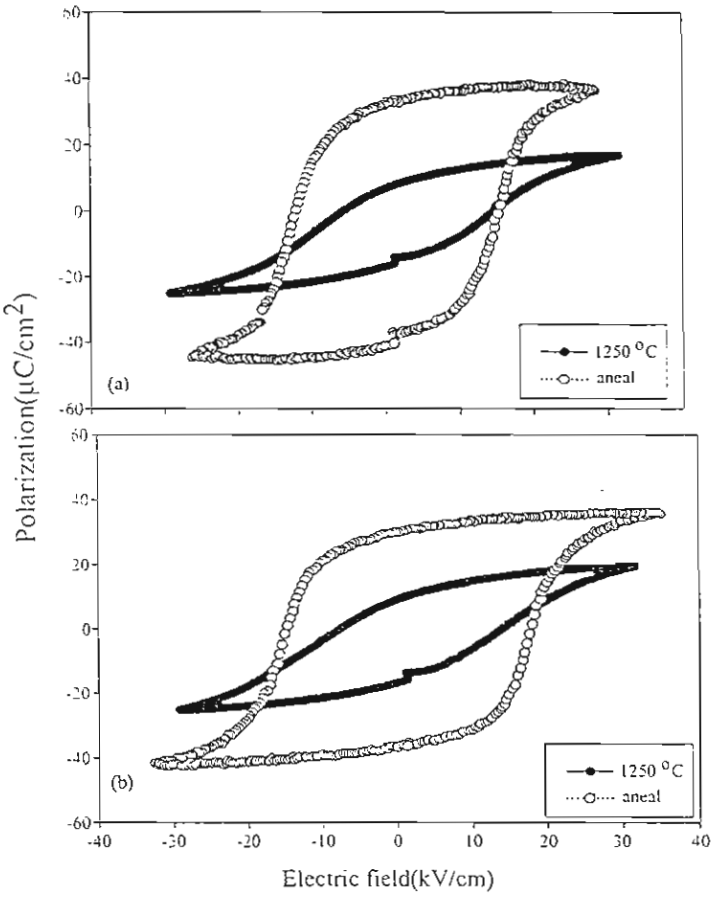

Fig. 7. Effect of post-sinter annealing on the P–E hysteresis for 0.1PZN–0.9PZT ceramics: (●) sintered at 1250 °C, (○) sintered at 1175 °C and annealed at 1250 °C for 6 h: (a) columbite method, (b) conventional method.

the ferroelectric properties were demonstrated (see Fig. 7 for the 0.1PZN–0.9PZT). The results on other compositions are listed Table 1. Very limited improvements were observed for the $x = 0.5$ composition because the higher PZN content required lower sintering temperatures, thus limiting the efficacy of the annealing step. It has been suggested that PZT ceramics should be sintered at temperatures above 1200 °C [8,9,16] and PZN-based ceramics should be sintered below this temperature [17] to achieve the best combination of density and properties. This explains the results in our present study where increasing molar fraction of PZN directly led to a lower sintering temperature. Therefore, post-sinter heat treatment is not necessary for ceramics with high PZN content.

Based on these ferroelectric measurements, the optimum sintering conditions for compositions of $x = 0.3$, 0.4, and

Table 1
Post-sinter annealing effects on the remanent polarization P_r and saturation polarization P_s in xPZN–$(1-x)$PZT ceramics sintered at 1175 °C for 2 h and annealed at 1250 °C for 6 h

x	xPZN–$(1-x)$PZT							
	Columbite method				Conventional method			
	P_r		P_s		P_r		P_s	
	Sintered	Annealed	Sintered	Annealed	Sintered	Annealed	Sintered	Annealed
0.1	7.6	37.1	15.8	42.9	9.4	34	19.0	39.2
0.2	14.6	36.1	20.6	38.9	13.8	31.5	21.4	35.0
0.3	31.9	30.4	37.2	33.5	23.8	20.0	27.9	23.2
0.4	32.3	30.6	35.8	34.5	30.5	23.2	35.0	28.7
0.5	35.6	36.4	40.4	42.1	29.4	29.5	34.5	34.9

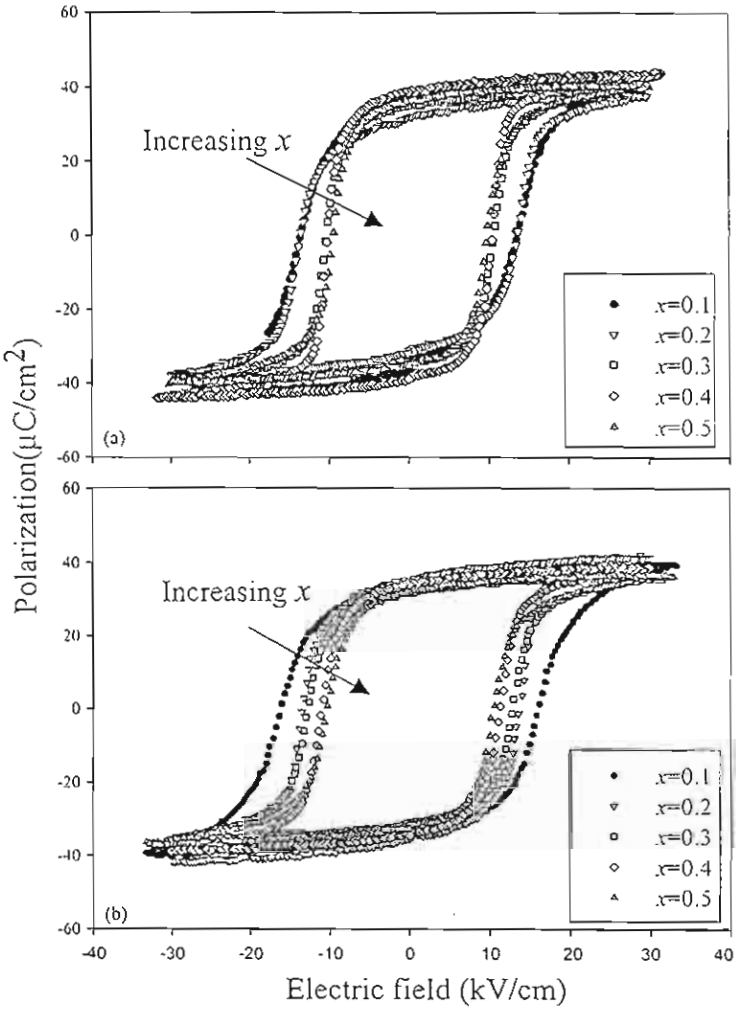

Fig. 8. Effect of composition (x) on the P–E hysteresis loops for xPZN–$(1-x)$PZT processed at the optimum processing conditions: (a) columbite method; (b) conventional method.

0.5 is 1200 °C for 2 h. The sintering process was not completed at these sintering conditions for compositions of $x = 0.1$ and 0.2 and therefore post-sinter annealing at 1250 °C for 6 h is necessary for improvement of ferroelectric properties. Further characterization techniques and comparisons, which are described in the following section, were made on these as-sintered specimens (for $x = 0.3$, 0.4, 0.5) and annealed specimens (for $x = 0.1$, 0.2) because they were found to have the optimum ferroelectric properties.

3.3. Effect of processing method on the phase transformation

The P–E ferroelectric property measurements for the specimens processed at optimum conditions are summarized in Fig. 8. It is shown that there is no significant difference in P_r across the composition range. However, the coercive field E_c is well dispersed over the compositions. This is further illustrated in Fig. 9. Compared to the conventional method, columbite method produces a slightly higher remanent polarization P_r as well as a lower coercive field E_c. Both methods show a considerable decrease in E_c with increasing molar fraction of PZN. However, the variation in ceramics prepared by conventional method is gradual and continuous, while an abrupt change in E_c occurs in ceramics processed by the columbite method, as indicated in Fig. 9(b). Combined with the XRD examination described in Section 3.1, the change in E_c clearly indicates a phase transformation over that compositional range. Therefore, an MPB separating the tetragonal phase (PZT-rich) from the pseudo-cubic rhombohedral phase (PZN-rich) exists between $x = 0.2$ and 0.3. Also consistent with the XRD data, the phase transformation in ceramics prepared by the conventional method is smeared out due probably to the chemical heterogeneities. These results lead to the conclusion that the columbite method produces ceramics with bet-

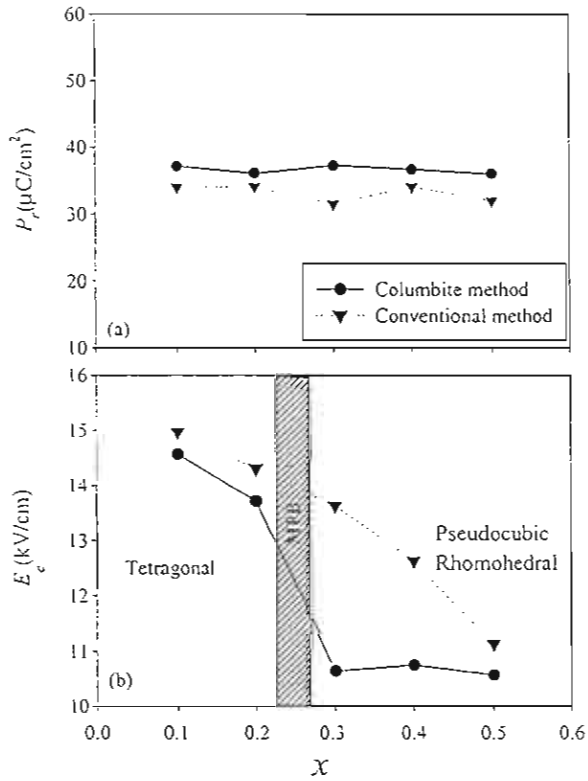

Fig. 9. Variation of remanent polarization P_r and coercive field E_c with composition for xPZN–(1 − x)PZT ceramics: (a) remanent polarization; (b) coercive field.

ter ferroelectric properties even though this method seems initially be prone to form pyrochlore phase. These results underscore the important role that B-site ordering plays in determining the thermodynamic stability and electrical properties of perovskite ferroelectrics.

4. Conclusion

A comparison between the conventional method and the columbite method was made in the preparation of ceramics within the solid solution of xPZN–(1 − x)PZT over a wide range in composition (x = 0.1–0.5). The optimum processing conditions for excellent ferroelectric properties were identified. Based on the X-ray structural analysis and ferroelectric property measurements, the following conclusions can be drawn:

1. Compared to the columbite method, the conventional method requires lower calcination temperature to eliminate the pyrochlore phase formation. Increasing in the molar fraction of PZN requires increased calcination temperatures in order to achieve phase-pure perovskite. At 900 °C, all the compositions for both methods can be converted to single-phase perovskite.
2. In ceramics sintered from columbite method prepared powders, a sharp transition from tetragonal to pseudo-cubic rhombohedral phase was evidenced by the XRD analysis. Thus, an MPB exists between x = 0.2 and 0.3. However, such a phase transformation is diffuse in ceramics prepared by the conventional method.
3. The results from XRD analysis are consistent with the ferroelectric property measurements. An abrupt change in coercive field, E_c, was observed in ceramics prepared by the columbite method at the same composition range of x = 0.2–0.3. In contrast, gradual change was found in ceramics prepared by the conventional method.
4. Lower sintering temperatures were required for compositions with an increasing molar fraction of PZN. For the x = 0.1 and 0.2 compositions, sintering at 1250 °C for 2 h was observed to produce inferior ferroelectric properties and post-sinter annealing was required to achieve excellent ferroelectric properties.
5. For both methods, no considerable variation of the remanent polarization with compositions was observed. However, the coercive field was observed to decrease with increasing amount of PZN. The columbite method was found to produce ceramics with better ferroelectric properties with higher remanent polarization and lower coercive field.

Acknowledgements

The authors are grateful to The Thailand Research Fund, Graduate School of Chiang Mai University, and the Ministry of University Affairs for financial support.

References

[1] A.J. Moulson, J.M. Herbert, Electroceramics: Materials, Properties, Applications, Chapman and Hall, New York, 1990.
[2] K. Uchino, Solid State Ionics 108 (1998) 43.
[3] K. Uchino, Ferroelectrics 151 (1994) 321.
[4] V.A. Bokov, I.E. Mylnikova, Sov. Phys-Solid state 2 (1960) 2428.
[5] T.R. Shrout, A. Halliyal, Am. Ceram. Soc. Bull. 66 (1987) 704–711.
[6] S.L. Swartz, T.R. Shrout, Mater. Res. Bull. 17 (1982) 1245–1250.
[7] Y. Matsuo, H. Sasaki, S. Hayakawa, F. Kanamaru, M. Koizumi, J. Am. Ceram. Soc. 52 (1969) 516–517.
[8] A. Halliyal, U. Kumar, R.E. Newham, L.E. Cross, Am. Ceram. Soc. Bull. 66 (1987) 671–676.
[9] M. Villegas, A.C. Caballero, C. Moure, R.E. Newham, J. Am. Ceram. Soc. 83 (2000) 141.
[10] H. Fan, H.-E. Kim, J. Mater. Res. 17 (2002) 180.
[11] N. Vittayakorn, G. Rujijanagul, T. Tunkasiri, X. Tan, D.P. Cann, J. Mater. Res. 18 (2003) 2882–2889.
[12] S.-Y. Chen, C.-M. Wang, S.-Y. Cheng, Mater. Chem. Phys. 49 (1997) 70–77.
[13] H. Fan, H.-E. Kim, J. Appl. Phys. 91 (2002) 317.
[14] U. Kenji, Ferroelectric Devices, Marcel Dekker Inc., 2000.
[15] F. Xia, X. Yao, J. Mater. Sci. 36 (2001) 247.
[16] J.R. Belsick, A. Halliyal, U. Kumar, R.E. Newnham, Am. Ceram. Soc. Bull. 66 (1987) 664.
[17] A. Halliyal, A. Safari, Ferroelectrics 158 (1994) 295–300.

เอกสารหมายเลข 1.10

ELSEVIER

Materials Science and Engineering B 108 (2004) 223–226

MATERIALS SCIENCE & ENGINEERING B

www.elsevier.com/locate/mseb

Effects of heat treatment on structural evolution and morphology of $BaTi_5O_{11}$ powder synthesized by the sol–gel method

S. Tangjuank, T. Tunkasiri*

Department of Physics, Faculty of Science, Chiang Mai University, Chiang Mai 50200, Thailand

Received 17 November 2003; accepted 26 November 2003

Abstract

$BaTi_5O_{11}$ powder was successfully prepared and characterized by the sol–gel method. The mechanisms of $BaTi_5O_{11}$ formation were studied by the fourier transform infrared spectroscopy (FTIR). The IR absorption peaks confirm the existence of a substitution reaction with the chelating reagent corresponding to different modes of vibration characteristic of the acetate group. The X-ray diffraction (XRD) results showed that the formation of single-phase monoclinic $BaTi_5O_{11}$ began at 700 °C and were stable up to 1100 °C in air. The particle sizes observed from scanning electron microscopy (SEM) are about 100 nm for a calcination temperature at 700 °C and 600 nm at 1100 °C.

Keywords: $BaTi_5O_{11}$ powder; Sol–gel method; FTIR; Calcination temperature

1. Introduction

Now a days, microwave communication systems have a great need for wireless communication such as personal communication, global positioning systems, etc. Dielectric resonator ceramics have been widely exploited in these systems because of their high dielectric constants, high quality factors, low dielectric loss, and near-zero temperature coefficients of resonant frequency [1]. $BaTi_5O_{11}$ has recently received much attention after Ritter et al. [2] used O'Bryan's et al's. [3] data to point out that single-phase $BaTi_5O_{11}$ ceramic might have superior properties suitable for microwave applications. A number of researchers tried to produce single-phase $BaTi_5O_{11}$ powder using several methods. O'Bryan and Thomson [4] prepared $BaTi_5O_{11}$ using solid state reaction but the technique could not yield single-phase material. Chemical processes were however successfully employed to obtain single-phase $BaTi_5O_{11}$. Fukui et al. [5] and Ritter et al. [2] reported that $BaTi_5O_{11}$ powder could be obtained by preparing via the alkoxide method at the calcination temperatures between 700 and 1100 °C. Other chemical preparation methods are still being searched in order to obtain single-phase and fine powder of $BaTi_5O_{11}$. Since these methods were successfully employed to prepare single-phase barium titanate ($BaTiO_3$) powder [6–8] and barium tetratitanate ($BaTi_4O_9$) powder [9]. Javadpour and Eror [10] prepared $BaTi_5O_{11}$ by liquid-mix technique of barium carbonate with tetraisopropyl titanate in an ethylene glycolcitric acid solution, while Lu et al. [7] used sol–gel process of barium granules with titanium ethoxide in nitric acid solution. Single-phase $BaTi_5O_{11}$ were obtained at 700–1100 °C in both cases. However, the reaction mechanisms, structural evolution and morphology of $BaTi_5O_{11}$ powder due to heat treatment are still not clearly understood. In this work, the sol–gel process was employed to prepare $BaTi_5O_{11}$ powder using barium oxide and titanium(IV) isopropoxide in acetic acid solution. Various techniques were used to characterize the synthesized powder.

2. Experimental

Barium oxide (BaO), titanium(IV) isopropoxide ($C_{12}H_{28}O_4Ti$), concentrated acetic acid ($C_2H_4O_2$), methanol (CH_3OH), and dried *n*-butanol ($CH_3(CH_2)_3OH$) were used as starting compounds. To form barium methoxide, BaO (0.1 mol) was dissolved in 30 cm^3 acetic acid and methanol (50 cm^3) was used as a solvent. Dried *n*-butanol (80 cm^3) was added to 50 cm^3 titanium(IV) isopropoxide to obtain a

* Corresponding author. Tel.: +66-53-943376; fax: +66-53-357512.
E-mail address: tawee@chiangmai.ac.th (T. Tunkasiri).

stable Ti-solution. The mixed solution of barium and titanium was heated at 80 °C on a hot plate with continuous stirring for 1 h. After that, 20 cm^3 of distilled water was added to the solution to form gel. The gel was dried in an oven at 110 °C for 24 h during which the white powder precursor was formed. The dried precursor was ground and heated in air at temperatures ranging from 500 to 1200 °C in steps of 100 °C. The annealing time at each temperature was 4 h to completely yield $BaTi_5O_{11}$ phase. The differential scanning calorimetry (DSC) and the thermogravimetic analysis (TGA) were used for the analysis of phase transformations of dried powders. In these analytical techniques, the samples were heated up to 1000 °C with a heating rate of 5 °C/min. Phase evolution of the calcined powders was carried out by X-ray diffraction (XRD). The morphology of the calcined powders was studied using scanning electron microscopy (SEM). The reaction mechanisms related to the calcination processes were studied using the fourier transform infrared spectroscopy (FTIR) at room temperature in the KBr plate method. [11].

3. Results and discussion

The DSC and TGA data are shown in Fig. 1. The results suggested that the decomposition occurred in three different weight loss steps. The first endothermic peak in the DSC curve was due to the vaporization of water at the temperatures below 100 °C and crystal water at below 300 °C, and

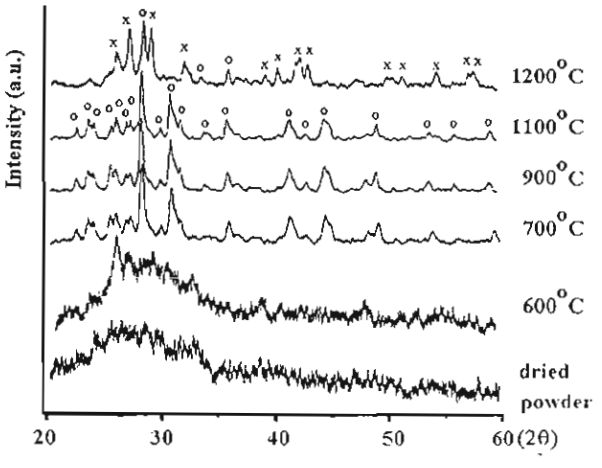

Fig. 2. XRD powder patterns of the dried precursor of $BaTi_5O_{11}$ calcined at various temperatures for 4 h (o: $BaTi_5O_{11}$ and x: $Ba_2Ti_9O_{20}$).

corresponded to 12% weight loss in the TGA curve. The second peak, corresponding to an endothermic peak accompanied by weight loss of 20.5%, was observed from 250 to 600 °C. This is related to the decomposition of the acetate groups and organic derivatives into carbonate which barium carbonate took place. Finally, the exothermic peak between 600 and 750 °C was probably due to the beginning of $BaTi_5O_{11}$ formation which can occur by the decomposition of the intermediate carbonate phase without any weight change. X-ray diffraction analysis (Fig. 2) showed that the dried powder and powders heated below 700 °C

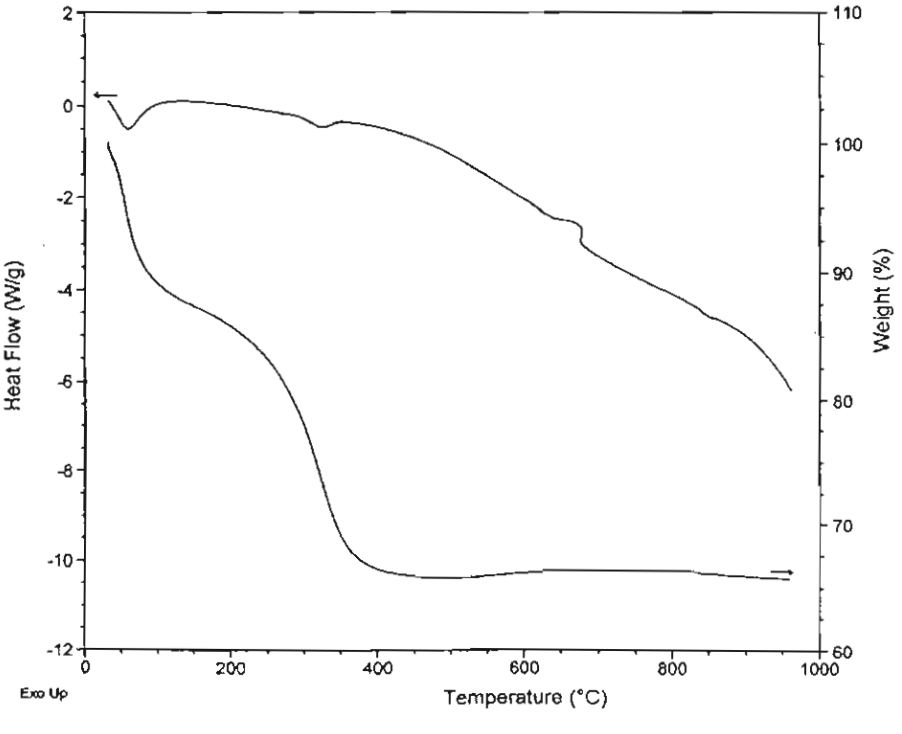

Fig. 1. DSC and TGA thermograms of the dried precursor of $BaTi_5O_{11}$.

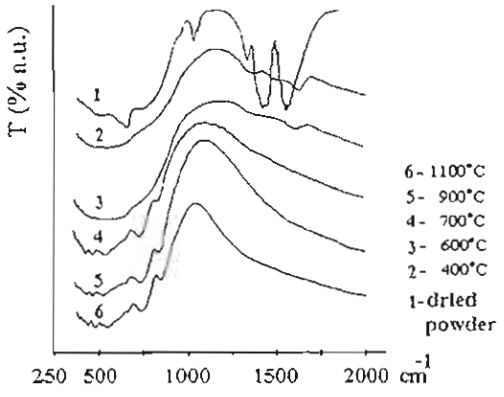

Fig. 3. FTIR spectra of the dried precursor of $BaTi_5O_{11}$ calcined at different temperatures: 110 °C (spectrum 1); 400 °C (spectrum 2); 600 °C (spectrum 3); 700 °C (spectrum 4). 900 °C (spectrum 5); 1100 °C (spectrum 6).

were amorphous. This amorphous phase was converted to single-phase crystalline $BaTi_5O_{11}$ only after heat treatment at 700 °C until 1100 °C. The phase analysis was based on the available data from joint committee on powders diffraction standard (JCPDS), card no. 35-0805. Heat treatment at 1200 °C for 4 h resulted in the crystallization of $BaTi_5O_{11}$ and $Ba_2Ti_9O_{20}$ phases. The results agree with those obtained by Lu et al. [7] and Javadpour and Eror [10]. However, the samples calcined at 1200 °C, Javadpour and Eror [10] obtained $BaTi_5O_{11}$ and $BaTi_4O_9$ (Table 1). Some FTIR spectra of the $BaTi_5O_{11}$ powders calcined at various temperatures are shown in Fig. 3. The absorption peaks located at 1552, 1414, 1323, 1020, and 645 cm^{-1} for the dried precursor (110 °C) corresponded to the vibration modes of the acetate group [12]. This agrees well with the reports of Woei-Kwo and Yong-Chien [13] and Xionghui et al. [14] for $BaTiO_3$ and $PbTiO_3$, respectively. Both groups employed acetate route. At 400–600 °C, the similar spectra showed up at 1342 and 1610 cm^{-1} whereas the peaks at 1552, 1414, 1323, 1020, and 645 cm^{-1} disappeared. This may be due to decomposition of the acetate group and can be attributed to the vibration modes of the ionic carbonate [12]. At 700–1100 °C, the peaks of 1342 and 1610 cm^{-1} disappeared and the infrared (IR) peaks were found at 835 and 729 cm^{-1}. This indicates that the carbonate group decomposed and the reaction occurred between barium carbonate and titanium oxide to form $BaTi_5O_{11}$ powder. The results are confirmed by DSC, TGA, and XRD characterizations as described earlier. Fig. 4 shows the particle morphology of $BaTi_5O_{11}$ powder after calcination at 800 and 1100 °C. The calcined powders

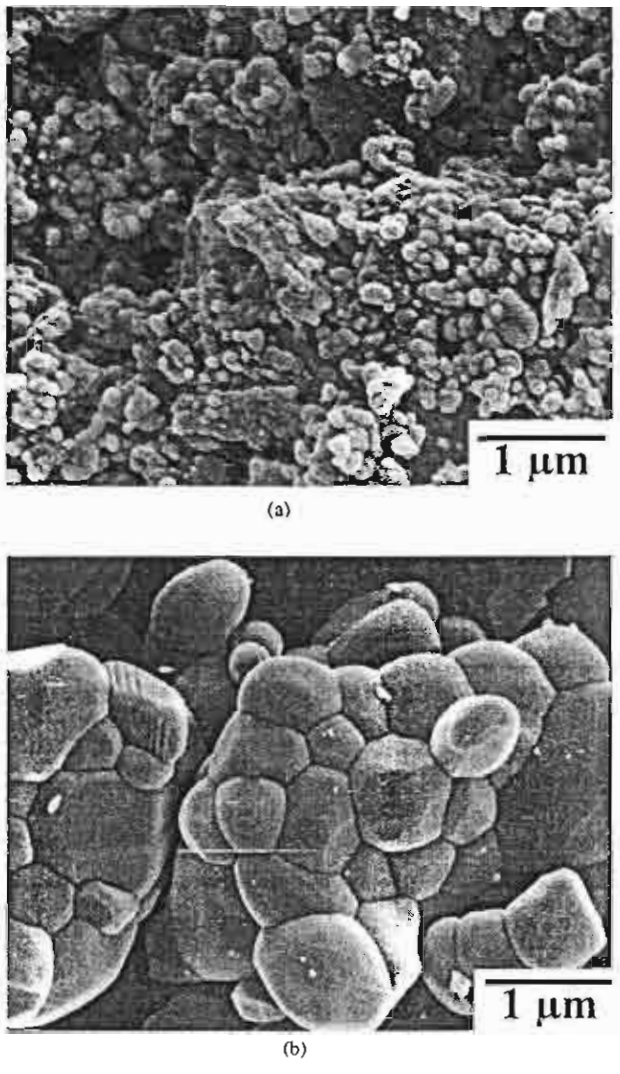

Fig. 4. The scanning electron micrographs of $BaTi_5O_{11}$ powders calcined at (a) 800 °C and (b) 1100 °C.

Table 1
Results of phases analysis of Ba:Ti = 1:5 at various calcination temperatures

Calcination temperature (°C)	Phases present		
	This work	Lu et al. [7]	Javadpour and Eror [10]
700	$BaTi_5O_{11}$	$BaTi_5O_{11}$	$BaTi_5O_{11}$
800	$BaTi_5O_{11}$	–	–
850	–	$BaTi_5O_{11}$	$BaTi_5O_{11}$
900	$BaTi_5O_{11}$	–	–
1000	$BaTi_5O_{11}$	$BaTi_5O_{11}$	$BaTi_5O_{11}$
1100	$BaTi_5O_{11}$	$BaTi_5O_{11}$	$BaTi_5O_{11}$
1200	$BaTi_5O_{11}$ + $Ba_2Ti_9O_{20}$	$BaTi_5O_{11}$ + $Ba_2Ti_9O_{20}$	$BaTi_5O_{11}$ + $BaTi_4O_9$

consisted of fine particles and the agglomerates were almost round in shape and were slightly bigger for higher calcination temperatures. With increasing the calcination temperature, the amount of agglomeration also increased. The occurring of aggregated particles during heat treatment resulted from a dense and rigid resin intermediate of acetic acid. The particle sizes were estimated to be in the range of 100–600 nm for the calcination temperatures from 700 to 1100 °C.

4. Conclusion

$BaTi_5O_{11}$ powder could be synthesized using the sol–gel method. Analysis by DSC, TGA, and XRD confirmed that the stable single-phase of $BaTi_5O_{11}$ occurred at the calcination temperatures ranging from 700 to 1100 °C, whereas at 1200 °C, the $BaTi_5O_{11}$ phase converted into a mixture of $BaTi_5O_{11}$ and $Ba_2Ti_9O_{20}$. The IR absorption peaks confirmed the existence of a substitution reaction with the chelating reagent, corresponding to different modes of vibration characteristic of the acetate group. The morphology of the $BaTi_5O_{11}$ powder indicated hard aggregates of fine particles which were almost round in shape. The particle sizes were estimated to be in the range of 100–600 nm and was found to increase with increasing calcination temperature.

Acknowledgements

The authors would like to express their sincere thanks to the Thailand Research Fund for the financial support.

References

[1] K. Plourde, C.L. Ren, IEEE Trans. Microwave Theory Tech. 29 (1981) 754.
[2] J.J. Ritter, R.S. Roth, J.E. Blendell, J. Am. Ceram. Soc. 69 (1986) 155.
[3] H.M. O'Bryan, J.K. Plourde, J. Thomson, D.F. Linn, J. Am. Ceram. Soc. 57 (1974) 450.
[4] H.M. O'Bryan, J. Thomson, J. Am. Ceram. Soc. 58 (1975) 454.
[5] T. Fukui, C. Sakurai, M. Okuyama, J. Mater. Res. 7 (1992) 192.
[6] T. Tunkasiri, G. Rujijanagul, J. Mater. Sci. Lett. 13 (1994) 165.
[7] H.C. Lu, L.E. Burkhart, G.L. Schrader, J. Am. Ceram. Soc. 76 (1991) 968.
[8] H.S. Potdar, S.B. Deshpade, A.S. Deshpande, Y.B. Khollam, A.J. Patil, S.D. Pradhan, S.K. Date, Int. J. Inorg. Mater. 3 (2001) 613.
[9] A. Cuneyt Tas, J. Am. Ceram. Soc. 82 (1999) 1582.
[10] J. Javadpour, N.G. Eror, J. Am. Ceram. Soc. 71 (1988) 206.
[11] K. William, Organic Spectroscopy, second ed., Macmillam Education Ltd., London, 1980, p. 38.
[12] K. Nakamoto, Infrared and Raman Spectra of Inorganic and Coordination Compounds, fifth ed., Wiley, New York, 1997, p. 75.
[13] K. Woei-Kwo, L. Yong-Chien, J. Mater. Lett. 29 (1994) 5625.
[14] Z. Xionghui, L. Yayan, W. Xiugan, Y. Wenchun, W. Lan, G. Hongxia, Mater. Chem. Phys. 77 (2002) 209.

เอกสารหมายเลข 1.11

JOURNAL OF MATERIALS SCIENCE 39 (2004) 1831–1835

Microstructures and positive temperature coefficient resistivity (PTCR) characteristics of high silicon addition barium-strontium titanate ceramics

P. BOMLAI, N. SIRIKULRAT, T. TUNKASIRI
Department of Physics, Faculty of Science, Chiang Mai University 50200, Thailand
E-mail: scphi003@chiangmai.ac.th

Ferroelectric barium titanate ($BaTiO_3$) shows a high intrinsic resistivity of more than 10^{10} Ω-cm when prepared in an oxidizing atmosphere [1, 2]. When polycrystalline $BaTiO_3$ ceramics are doped with higher valence cations such as La^{3+}, Y^{3+}, Nb^{5+} or Ta^{5+}, semiconducting properties and the positive temperature coefficient of resistivity (PTCR) effect can be obtained [1–5]. These effects involve a nonlinear change in the resistivity with temperature occurring around 120–130 °C which is known as the Curie temperature (T_C) [6, 7]. The T_C of $BaTiO_3$ can be shifted to lower temperatures by substituting barium with strontium [8–10]. The solid solution of $(Ba,Sr)TiO_3$ materials has, therefore, been widely used for fabrication of positive temperature coefficient (PTC) thermistors with various Curie temperatures [8]. The most acceptable model to explain the temperature dependent conduction mechanism in the PTCR barium titanate ceramics was proposed by Heywang and Jonker [7, 8, 11–13]. Above the Curie temperature, Heywang suggested that the formation of a Schottky barrier is caused by the presence of electron traps. Below the Curie temperature, Jonker proposed that the highly conductive semiconductor results from the charge compensation due to the polarized charges at the grain boundaries [11, 13].

In recent PTCR processing, excess titanium and silicon are commonly used to create a liquid phase and reduce the sintering temperature [14]. The eutectic temperature resulting from excess titanium is around 1320 °C. After addition of silicon, this temperature decreases to approximately 1260 °C [15]. Cheng *et al.* [11] prepared $Ba_{0.8}Sr_{0.2}TiO_3$ ceramics by adding 12.5 mole percent aluminum, silicon, and titanium (so called AST) with a ratio of 4:9:3. After sintering at 1350 °C for 1.5 h, a uniformly small granular structure was obtained with an increase in resistivity of 5 orders of magnitude (from 10^3 to 10^8 Ω-cm) at the Curie temperature. Many investigations have been

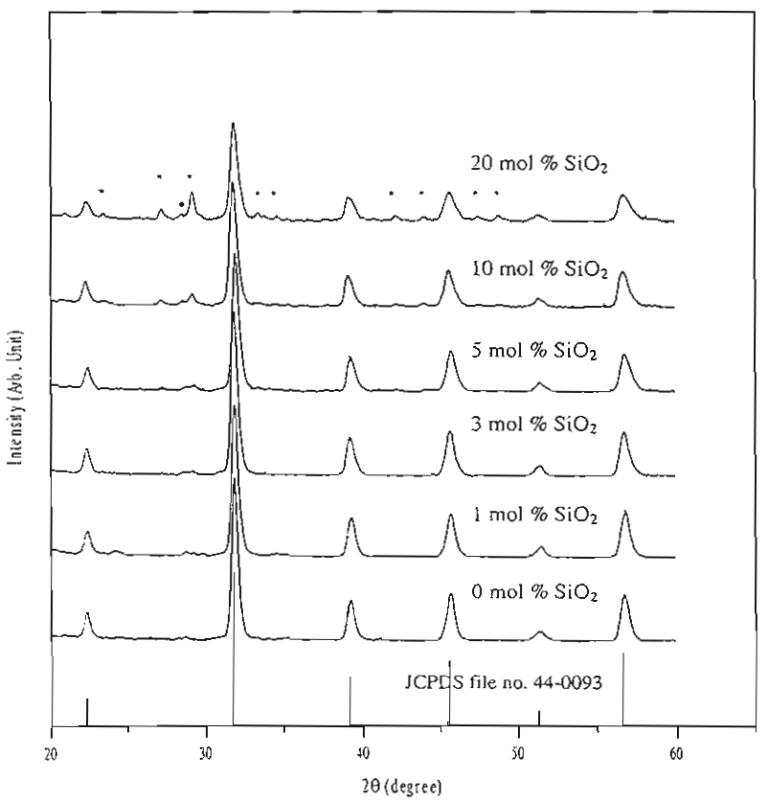

Figure 1 X-ray diffractograms of powders with various silicon content when calcined at 1100 °C. * = $Ba_2TiSi_2O_8$; · = $Ba_6Ti_{17}O_{40}$.

0022–2461

undertaken to study the effects of silicon additions to the PTCR ceramics [2, 14, 16]. However, the microstructures were found to be inhomogeneous due to the considerable difference in the densities of barium titanate and silicon [16]. Most of the investigations were performed with small (1–4 mol%) silicon additions [2, 14, 16]. The microstructural evolution might be significantly different when the liquid phase is incorporated in a larger proportion. The aim of the present investigation is, therefore, focused on studying the sintering behavior, microstructures and PTCR characteristics of antimony-doped $Ba_{0.8}Sr_{0.2}TiO_3$ materials with high levels of silicon addition.

Ceramic specimens in this work were prepared by the conventional mixed oxide process. The starting materials ($BaCO_3$, TiO_2, $SrCO_3$, Sb_2O_3, SiO_2, Aldrich Chemical Company, Inc.) were weighed according to the composition $Ba_{0.8}Sr_{0.2}TiO_3 + 0.15$ mol% $Sb_2O_3 + 1$ mol% $TiO_2 + xSiO_2$ where x varied from 0 to 20 mole percent. Antimony was used in order to form an n-type semiconductor and the amount of 0.15 mole percent was found to be optimum in these experiments. The excess of TiO_2 (1 mole percent) was added as a sintering aid to create a liquid phase during sintering so as to reduce the sintering temperature. The mixed powders were ball milled for 24 h and calcined at 1100 °C for 2 h in an alumina crucible using heating and cooling rates of 10 °C/min. In order to obtain compact pellets, the calcined powder was mixed with a small amount of polyvinyl alcohol (PVA) before being pressed into pellets and the specimens were sintered in air at 1275, 1285, 1300, 1350, 1400 and 1450 °C, for 2 h using heating and cooling rates of 5 °C/min. X-ray diffraction (Siemens D500) was employed to characterize the samples. The microstructures of the as-sintered surface were observed by scanning electron microscopy (Jeol JSM-840A). The resistivity change of the specimens as a function of temperature from room temperature to about 285 °C was measured using a digital multimeter (Agilent 34401A) and a D.C. power supply, after both sides of specimens were painted with silver paste.

Fig. 1 shows the X-ray diffractograms of the specimens with various silicon contents. Traces of fresnoite ($Ba_2TiSi_2O_8$) and $Ba_6Ti_{17}O_{40}$ are found, in addition to the major tetragonal barium-strontium titanate ($Ba_{0.77}Sr_{0.23}TiO_3$) phase. Peaks were identified on the basis of Joint Committee on Powder Diffraction Standards (JCPDS) data (card number 44-0093, 84-0924, 35-0817). Furthermore, it was found that the amount of the $Ba_2TiSi_2O_8$ increased with increasing silicon content. The presence of $Ba_2TiSi_2O_8$ and $Ba_6Ti_{17}O_{40}$ in these results is in agreement with those obtained by Abicht *et al.* [16] and Felgner *et al.* [17].

The developments of the microstructures of the specimens with various amounts of silicon are shown in Figs 2 and 3. It is obvious that the specimens show an abnormal grain growth and the size of the abnormally growing grains decreases with increasing sintering temperature as shown in Fig. 2. The grain structures of all the specimens when sintered above 1300 °C become rather uniform with sizes of 3–12 μm. The grain structures in the specimens with various amounts of silicon are shown in Fig. 3. It can be concluded that the grain size tends to decrease with increasing silicon contents, although the grain size of the sample with 5 mole percent of silicon (Fig. 2c) is slightly larger than that of the sample with 3 mole percent of silicon (Fig. 3b). In the specimen without silicon, the grains are irregularly sized and roughly equiaxed. However, in the specimens with higher silicon content (up to 20 mole percent) they

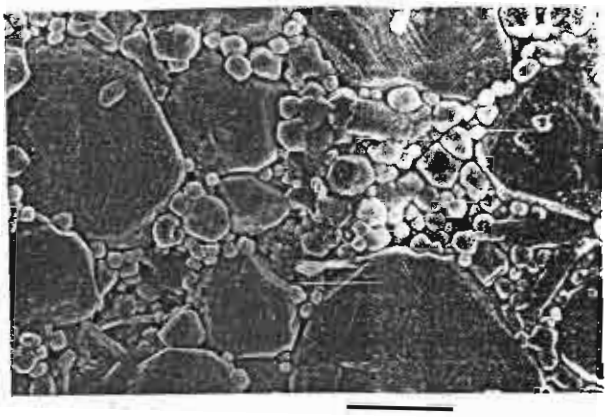

(a)

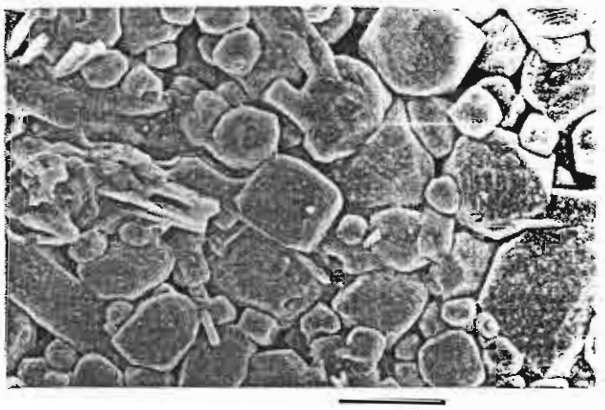

(b)

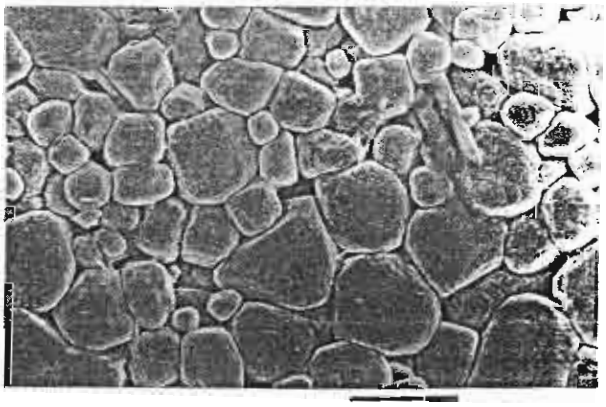

(c)

Figure 2 Microstructures of the specimens containing 5 mole percent of SiO_2 after sintering at various temperatures: (a) 1285 °C, (b) 1300 °C, and (c) 1350 °C.

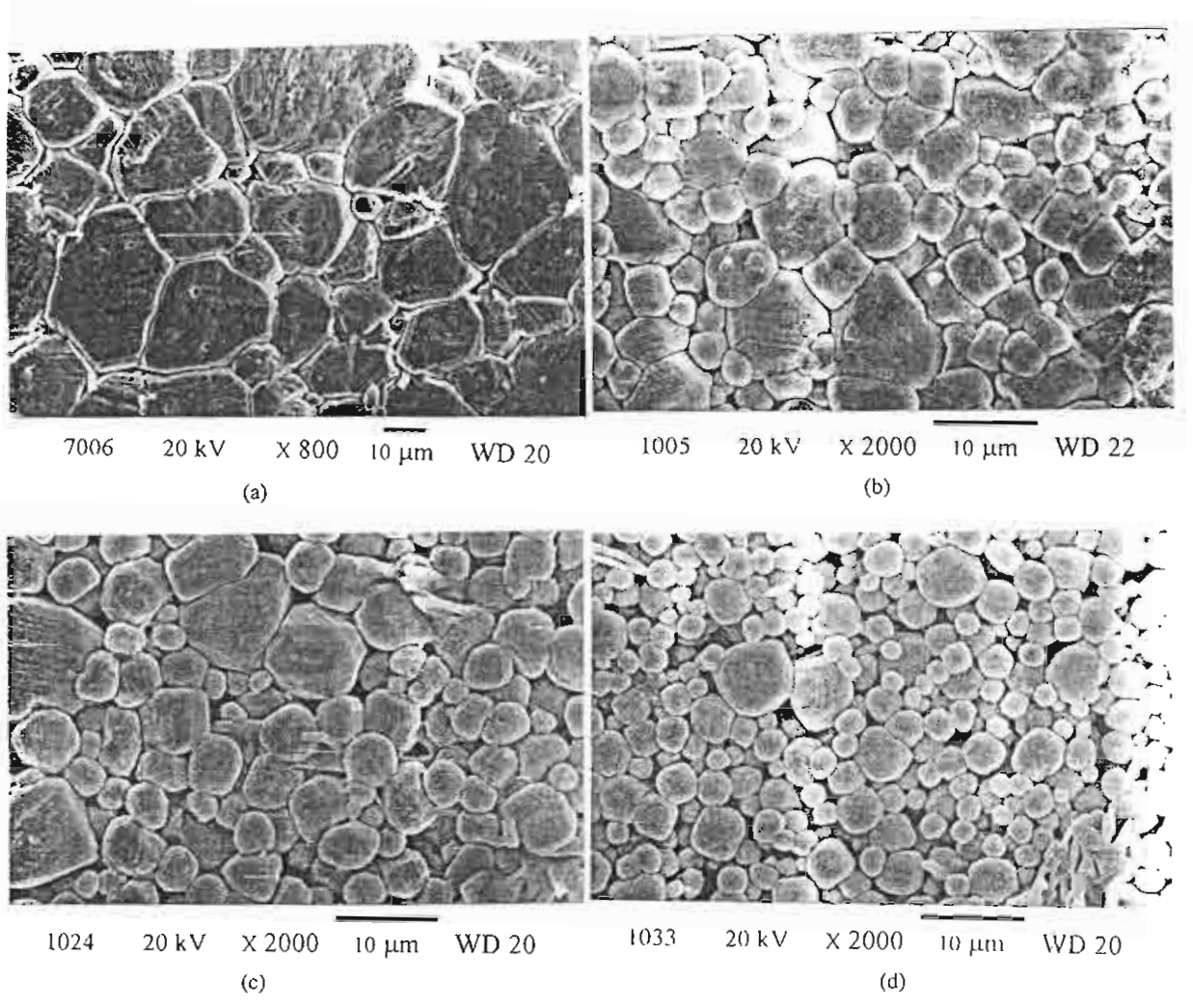

Figure 3 Microstructures of the specimens with various SiO_2 contents sintered at 1350 °C: (a) 0 mole percent SiO_2, (b) 3 mole percent SiO_2, (c) 10 mole percent SiO_2, and (d) 20 mole percent SiO_2.

become rounder and smaller with a grain size of about 2–5 μm as shown in Fig. 3d. The decrease in grain size with increasing silicon content is most probably caused by the large amount of liquid phase formed during sintering. Subsequently, the solid grains dissolve and become rounder in shape and smaller.

Porosity of the samples was also measured. It is found that porosity increases with decreasing sintering temperature but increases with increasing silicon content (Tables I and II).

The resistivity-temperature characteristics of the specimens prepared at various sintering temperatures and silicon contents are shown in Fig. 4. The Curie temperatures of these specimens are around 60 °C. It is also found that the room temperature resistivity (ρ_{RT}) varies as a function of silicon content and sintering temperature. The specimens without silicon cannot be sintered at temperatures lower than 1350 °C. The specimens sintered at 1350 °C show high resistivity. According to Liu and Roseman [14], however, low resistivity can be achieved by the addition of silicon to $Ba_{0.8}Sr_{0.2}TiO_3$. The resistivity at room temperature decreases to 10^1–10^4 Ω-cm in the specimens containing 1–20 mole percent silicon. The lowest room-temperature resistivity of about 25 Ω-cm can be obtained in the specimens containing 3 mole percent silicon when sintered at 1300 °C (see Fig. 5). The change in ρ_{RT} to higher values with decreasing sintering temperature is due to the coexistence of very large and very fine grains, as seen in Fig. 2a, As the silicon content increases so does the amount of $Ba_2TiSi_2O_8$ second phase (see Fig. 1). Consequently ρ_{RT} increases and there is a decrease in the magnitude of the PTCR characteristics (see Fig. 4d). Abicht *et al.* [16] found that the silicon containing second phases affect the electrical properties in an indirect manner. The resistivity changed over five orders of magnitude for the samples with 8–13% porosity (samples with 5–10 mole percent of silicon content, sintered at 1300 °C). Change of resistivity reduced to 2–3 orders

TABLE I Porosity, grain size and magnitude of PTCR effect in the specimens containing 5 mole percent SiO_2 sintered at various temperatures

Sintering temperature (°C)	% Porosity	Grain size (μm)	Order of magnitude of change in resistivity
1285	10.3	3.0–29.0	2.8
1300	8.6	3.5–12.0	4.7
1350	7.6	4.0–11.0	4.5

TABLE II Porosity, grain size and magnitude of PTCR effect in the specimens with various SiO_2 contents sintered at 1300 and 1350 °C

SiO_2 contents (mole %)	% Porosity		Grain size (μm)		Order of magnitude change in resistivity	
	1300 °C	1350 °C	1300 °C	1350 °C	1300 °C	1350 °C
0	–	5.2	–	10.0–30.0	–	–
3	8.4	5.8	3.0–11.0	3.1–10.0	3.8	3.3
10	13.2	11.1	3.2–10.0	3.6–7.0	5.0	3.1
20	20.8	16.9	2.7–5.5	2.3–5.5	3.2	2.0

if the porosity was less than 8%. It can be noted that the appropriate silicon addition brought a considerable enhancement of the PTCR characteristics. However, grain size, sintering temperature, porosity, and other second phases still affect the PTCR properties.

In conclusion, antimony-doped $Ba_{0.8}Sr_{0.2}TiO_3$ positive temperature coefficient resistors can be prepared below 1300-°C by the conventional mixed oxide process using silicon addition. The grains of the specimens sintered with a large addition of SiO_2 become rounder and smaller. However, $Ba_2TiSi_2O_8$ appeared as a second phase resulting in a decline in the electrical properties. The lowest room temperature resistivity of about 25 Ω-cm was obtained in the specimens containing 3 mole percent silicon, sintered at 1300 °C and the highest magnitude change in PTCR characteristics of

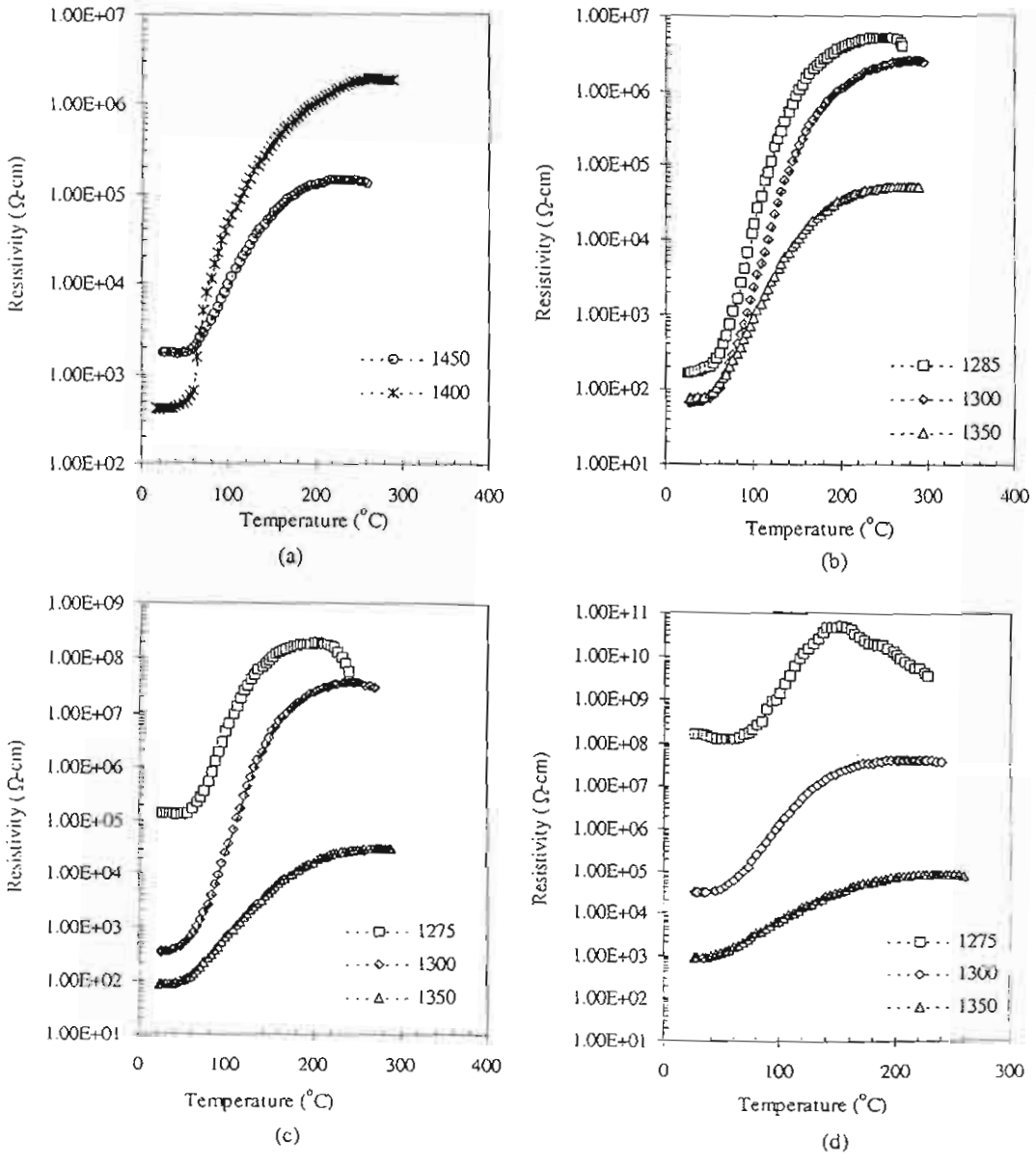

Figure 4 The resistivity-temperature (ρ-T) characteristics of the specimens with various sintering temperatures and SiO_2 contents: (a) 0 mole percent SiO_2, (b) 5 mole percent SiO_2, (c) 10 mole percent SiO_2, and (d) 20 mole percent SiO_2.

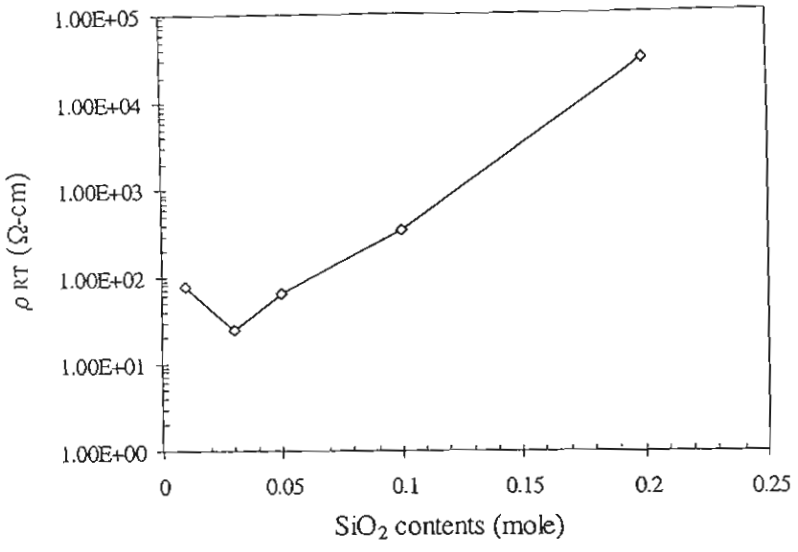

Figure 5 The room temperature resistivity of specimens with various amounts of SiO_2 sintered 1300 °C.

about 5 orders of magnitude was found in the specimens containing 5–10 mole percent silicon.

Acknowledgments

The authors would like to express their sincere thanks to the Thailand Research Fund, the National Metal and Materials Technology Center (MTEC) and the scholarship under the Ministry Staff Development Project of the Ministry of University Affairs, Thailand for the financial support. The authors would also like to thank Dr. L.D. Yu for his useful comments and correction on the manuscript.

References

1. R. D. ROSEMAN, J. KIM and R. C. BUCHANAN, in Proceeding of the 8th IEEE International Symposium on Application of Ferroelectrics (ISAF-92), 1992, edited by B. M. Kulwiki, A. Amin and A. Safari (IEEE, Piscataway, NJ, 1992) p. 185.
2. H. F. CHENG, *J. Appl. Phys.* **66** (1989) 1382.
3. B. HUYBRECHTS, K. ISHIZAKI and M. TAKATA, *J. Mater. Sci.* **30** (1995) 2643.
4. J. QI, Z. GUI, Y. WANG, Q. ZHU, Y. WU and L. LI, *Ceram. Intern.* **28** (2002) 141.
5. J. G. KIM, W. S. CHO and K. PARK, *Mater. Sci. Eng.* B **83** (2001) 123.
6. D. C. HILL and H. L. TULLER, in "Ceramic Materials for Electronics," edited by R. C. BUCHANAN (Marcel Dekker, New York, 1991) p. 249.
7. A. J. MOULSON and J. M. HERBERT, in "Electroceramics: Materials, Properties and Application" (Chapman & Hall, London, 1995) p. 147.
8. J. ZHAO, L. LI and Z. GUI, *Sens. Actuators* A **95** (2001) 46.
9. M. VIVIANI, P. NANNI, M. T. BUSCAGLIA, M. LEONI and V. BUSCAGLIA, *J. Eur. Ceram. Soc.* **19** (1999) 781.
10. D. KOLAR, M. TRONTELJ and Z. STADLER, *J. Amer. Ceram. Soc.* **65** (1982) 470.
11. H. F. CHENG, T. F. LIN, C. T. HU and I. N. LIN, *ibid.* **76** (1993) 827.
12. B. HUYBRECHTS, K. ISHIZAKI and M. TAKATA, *ibid.* **75** (1992) 722.
13. *Idem.*, *ibid.* **77** (1994) 286.
14. G. LIU and R. D. ROSEMAN, *J. Mater. Sci.* **34** (1999) 4439.
15. H. M. AL-ALLAK, T. V. PARRY, G. J. RUSSELL and J. WOODS, *ibid.* **23** (1988) 1083.
16. H. P. ABICHT, H. T. LANGGHAMMER and K. H. FELGNER, *ibid.* 26 (1991) 2337.
17. K. H. FELGNER, T. MÜLLER, H. T. LANGHAMMER and H. P. ABICHT, *J. Eur. Ceram. Soc.* **21** (2001) 1657.

Received 15 May
and accepted 1 October 2003

เอกสารหมายเลข 1.12

Ferroelectric Letters, 31:79–85, 2004

ISSN: 0731-5171 print / 1543-5288 online
DOI: 10.1080/07315170490480975

Taylor & Francis
Taylor & Francis Group

Analysis of X-Ray Diffraction Line Profiles of Lead Zirconate Titanate Using the Fourier Method

W. THAMJAREE, W. NHUAPENG, and T. TUNKASIRI

Department of Physics, Faculty of Science, Chiangmai University, Chiangmai 50200, Thailand

Communicated by Dr. George W. Taylor

(Received November 3, 2003)

Lead zirconate titanate (PZT) powder was prepared by a solid state reaction. The X-ray line broadening produced in PZT powder was analyzed by the Fourier method to estimate particle size and microstrain. It was found that an increase of the annealing temperature caused the microstrain to decrease owing to an increase in particle size. The Scherrer formula used to calculate the particle size yielded considerably smaller values.

Keywords: PZT; particle; Fourier method

INTRODUCTION

In the world of modern electronic ceramics, lead zirconate titanate (PZT) ceramics have become most widely employed as transducer materials. This is due to its high electromechanical coupling coefficients, enabling them to yield a high degree of mechano-electrical conversion [1]. As a result, PZT ceramics are being widely employed in hydrophones [2], ignitors, actuators for fine movement control [3] and many other applications.

Properties of fine ceramics such as PZT or barium titanate ($BaTiO_3$) depend greatly on the particle size of the starting materials [4]. Various techniques have been employed to measure the particle size of the starting powder prior to sintering, such as sedimentation, laser diffraction techniques [5], or scanning electron microscopy (SEM) [6].

X-ray diffraction profiles are also widely used to estimate the particle size and microstrain of materials. Uchino et al. [7], and Tornoda et al. [8] used the Scherrer formula to estimate the particle sizes of $BaTiO_3$ and lead

titanate (PT) powders, respectively. Tunkasiri and Rujijanagul [9] employed the integral breadth method of Halder and Wagner [10] to estimate the particle size and microstrain of $BaTiO_3$ powders. X-ray line broadening can also be analyzed employing the Fourier method of Warren and Averbach [11]. According to Lewis and Northwood [12], the particle sizes of filed lithium fluoride estimated by the Fourier method as well as by electron microscopy were of the same order of magnitude. The main purpose of this paper is the estimation of the particle size and the microstrain of PZT powder using both the Fourier method and the Scherrer formula.

EXPERIMENTAL PROCEDURE

PZT powder was prepared by the mixed oxides route. Lead oxide (PbO), zirconium oxide (ZrO_2) and titanium oxide (TiO_2), (mole ratio of 1:0.52:0.48), were mixed and milled in a zirconia pot with zirconia balls for 24 hours. The product was heated for 1 hour at temperatures ranging from 400°C to 1300°C in steps of 100°C. X-ray diffractometry was employed to study the sample obtained from each annealing step.

The X-ray diffraction profiles were scanned using a Jeol diffractometer with Ni filtered CuK_α radiation, at the speed of 1/8 degree per minute in 2θ. The (111) interplanar spacing was selected to estimate the particle size and microstrain. Rachinger's method [13] was used to resolve the $K_{\alpha 1}$ and $K_{\alpha 2}$ lines. Indexing of the samples was carried out according to the Joint Committee on Powder Diffraction Standards [14]. The measured line profiles were corrected for the instrumental broadening by the deconvolution of Fourier method of Stokes [15]. The sample annealed at 1300°C was used as the standard to estimate the contribution of the instrument broadening. The Fourier coefficients were determined using a computer programme, and analyzed by the procedure of Warren and Averbach [11]. For comparison, Scherrer's formula was also employed to estimate the particle sizes of the samples at each annealing step. The Scherrer method was performed in the way described by Klug and Alexander [16]. Both correction and without correction for instrumental broadening on the line profiles were carried out in the particle size estimation. Correction of the instrumental response was done according to the method described by Li and Shih [17].

RESULTS AND DISCUSSION

Figure 1 shows the variation of the Fourier coefficients (A_n) of some samples as a function of the harmonic number n, where n is the particular Fourier

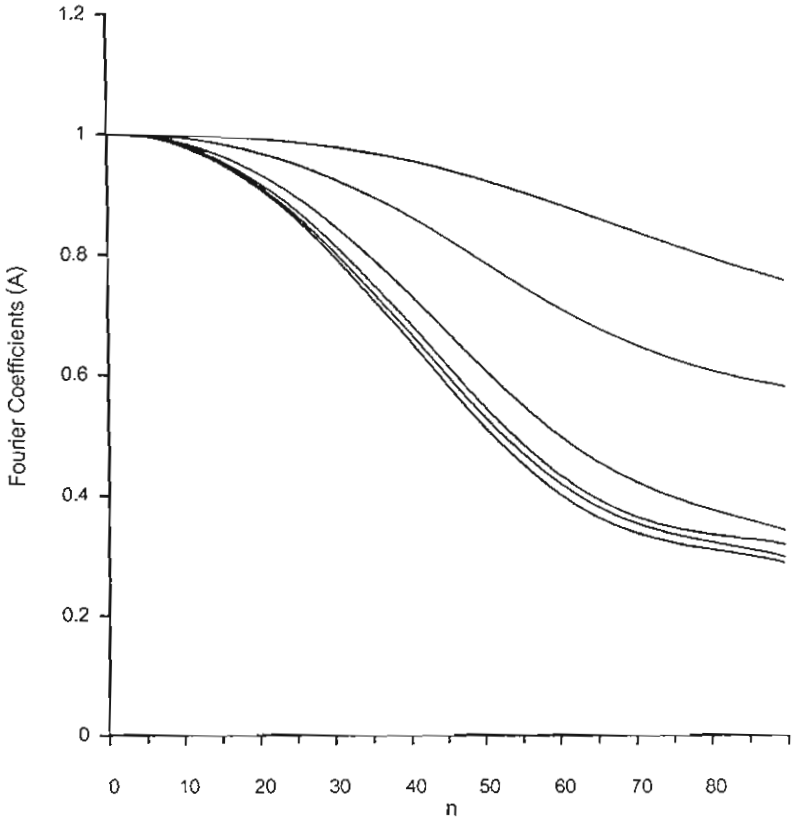

Figure 1. Variation of the Fourier coefficients A_n with n. From the bottom: ball milled sample at 25°C, and samples annealed at 500, 700, 900, 1000 and 1100°C, respectively.

series under consideration. The particle sizes and microstrains were calculated for each annealing step and plotted in Fig. 2. The microstrain decreased slowly with temperature up to about 900°C with little increase in particle size. At annealing temperatures above 900°C, the microstrain showed rapid decrease while the particle size increased by a factor of four. Beyond an annealing temperature of 1100°C both the change in microstrain and particle size slowed down. In Fig. 2 the particle sizes obtained from Scherrer's formula are presented together with other results from the literature [6, 18, 19]. The particle size obtained by Wu et al. [18] is rather close to those reported here, though their samples were prepared by the solgel technique and the average

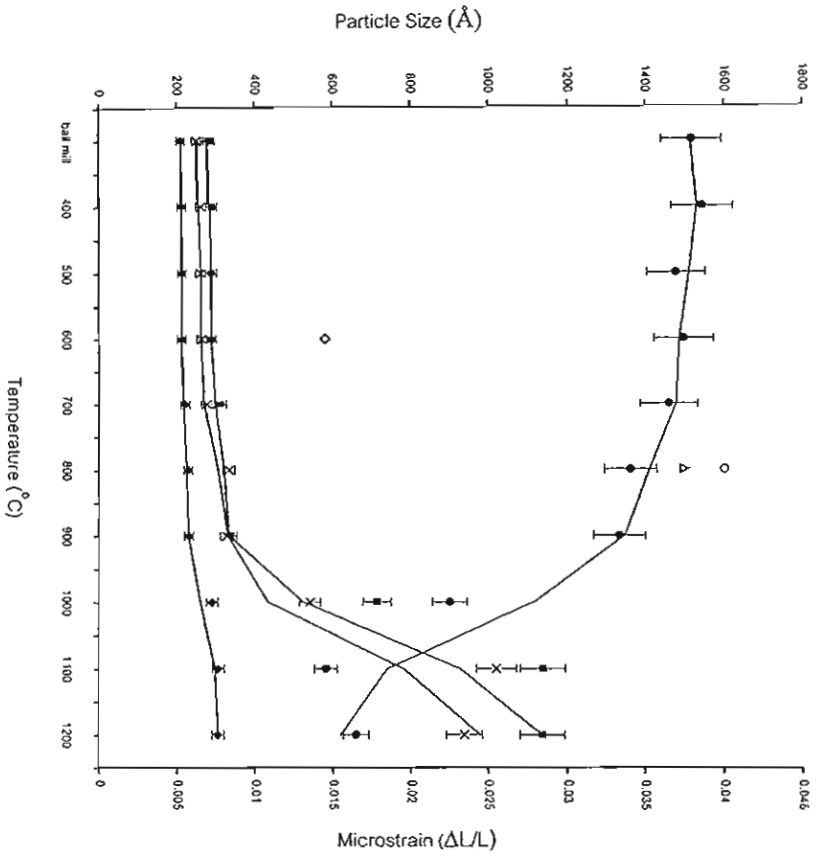

Figure 2. Particle size (Å) and microstrain of PZT powders as a function of the annealing temperature. Our data: × Fourier method [11]; ■ Scherrer formula with correction for instrument broadening [17]; υ Scherrer formula with out correction for instrument broadening [16]; ● Microstrain [11]. Reference data: ○ Chakrabarti and Maiti [19]; ◇ Wu et al. [18]; △ Yamamura et al. [6].

particle size were estimated using scanning electron micrographs. On the other hand, the results presented by Yamamura et al. [6] and Chakrabarti and Maiti [19] show much larger particle sizes. This may be due to the method of preparation and estimation since Yamamura et al. [6] Chakrabarti and Maiti [19] prepared the samples by co-precipitation and auto-combustion of citratenitrate gel methods, and particle size estimation were carried out from scanning electron micrographs and selected surface area respectively.

X-ray diffractograms indicated that the sample consist of PZT with trace of PbO. The line splitting of (100) and (001) PZT peaks showed that the tetragonal phase appear between 1100°C–1200°C, whereas the cubic phase exists at lower temperatures. Annealing at 1100, 1125, 1150, 1175 and 1200°C were carried out and the samples were re-examined. Some of the diffractograms are shown in Fig. 3. It may be concluded that transformation

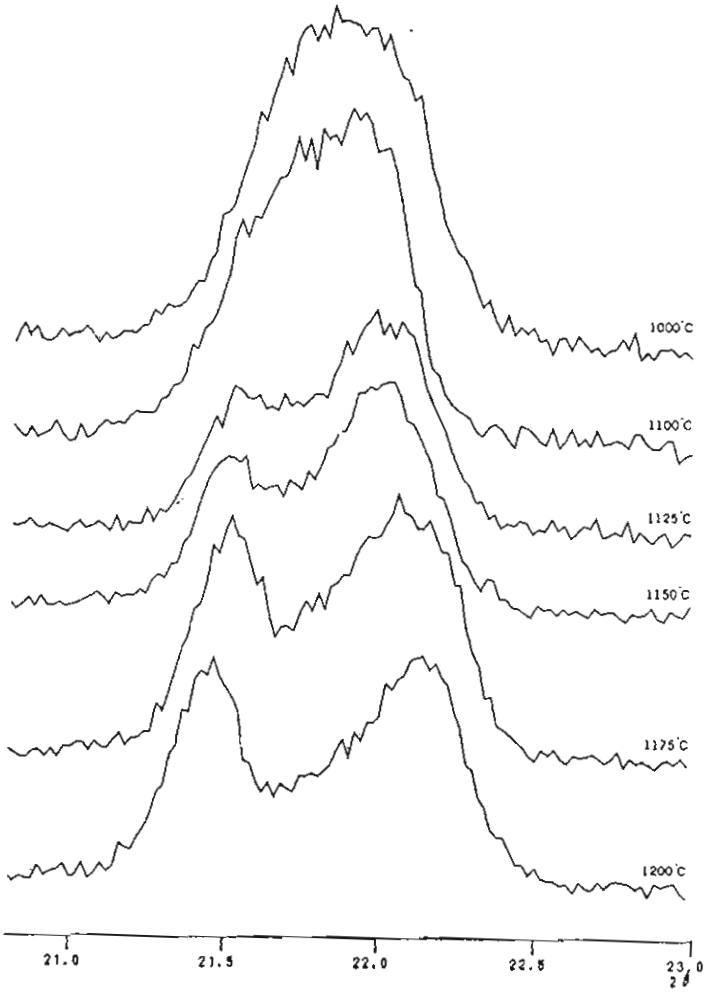

Figure 3. XRD pattern of the (100) and (001) peaks of PZT powder annealed at different temperatures.

of the cubic to the tetragonal phase starts at 1125°C, and is essentially completed at 1200°C. Tetragonality (c/a) was also calculated using Cohen's method [20] to be 1.011, 1.012, 1.013 and 1.015 for annealing temperatures of 1125, 1150, 1175, and 1200°C, respectively.

CONCLUSIONS

In conclusion, X-ray line broadening produced in PZT powder by ball milling is mainly due to the decrease in particle size. The Fourier analysis of Warren and Averbach can be used as a suitable method to analyze the microstructural changes introduced into the powder as a result of annealing. As the annealing temperature increases, an increase in particle size and a subsequent decrease in the intra-particle microstrain are observed. X-ray diffraction technique confirmed that the cubic to tetragonal phase started at 1125°C and was essentially completed at 1200°C.

ACKNOWLEDGEMENTS

The authors express their grateful thanks to the Thailand Research Fund (TRF) and the National Metal and Materials Technology Center (MTEC) of Thailand for the funding of this project. Thanks are aslso extened to Prof. Dr. Robert B. Heimann, Freiberg University of Mining and Technology, Germany for his fruitful and productive comments.

REFERENCES

[1] R. C. Buchanan, *Ceramic Materials for Electronics, Processing, Properties and Applications* (Marcel Dekker, New York, 1986), p. 164.
[2] Y. Kurihara, K. Mizumusa, and H. Ohashi, *Japan. J. Appl. Phys.* **31**, 3067 (1992).
[3] J. Randeraat and R. E. Setterington, *Piezoelectric Ceramics* (Mullard, London, 1974) p. 23.
[4] K. Kinorhita and A. Yamaji, *J. Appl. Phys.* **47**, 371 (1976).
[5] J. S. Reed, *Introduction to the Principles of Ceramic Processing* (John Wiley & Sons Inc., New York, 1988), p. 87.
[6] H. Yamamura, S. Kuramoto, H. Haneda, A. Watanbe, and S. Shirasaki, *Yogyo-Kyokai-Shi (Japan)* **94**, 545 (1986).
[7] K. Uchino, E. Sadanga, and T. Hirose, *J. Am. Ceram. Soc.* **72**, 1555 (1989).
[8] W. Tornoda, N. Okada. K. Yoshikawa, E. Anno, and K.Ishikawa, *Bull. Res. Inst. Electron. Shizuoka Univ. (Japan)* **23**, 11 (1988).
[9] T. Tunkasiri and G. Rujijanagul, *J. Mats. Sci. Lett.* **13**, 165 (1994).

[10] N. C. Halder and C. N. J. Wagner, *Acta Crystallogr.* **20**, 312 (1966).
[11] B. E. Warren and B. L. Averbach, *J. Appl. Phys.* **21**, 595 (1950).
[12] D. Lewis and D. A. Northwood, *Brit J. Appl. Phys.* **2**, 21 (1969).
[13] W. A. Rachinger, *J. Sci. Inst.* **25**, 254 (1948).
[14] Powder Diffraction File, Card No. 33-784, Joint Committee on Powder iffraction Standards, Swarthmore, PA.
[15] A. R. Stokes, *Proc. Phys. Soc.* **61**, 382 (1948).
[16] H. P. Klug and L. E. Alexander, X-ray diffraction procedures for polycrystalline and amorphous materials (Wiley, New York, 1974), p. 618.
[17] X. Li and W. Shih, *J. Am. Ceram. Soc.* 80, 2844 (1997).
[18] A. Wu, I. M. M. Salvado, P. M. Vilarinho, and J. L. Baptista, *J. Am. Ceram. Soc.* 81, 2640 (1998).
[19] N. Chakrabarti and H. S. Maiti, *Mater. Lett. (Netherlands)* 30, 169 (1997).
[20] B. D. Cullity, *Elements of X-ray diffraction* (Addison-Wesley, Reading, MA, 1987), p. 102.

เอกสารหมายเลข 1.13

2004 14th IEEE International Symposium on Applications of Ferroelectrics--ISAF-04

Influence of Processing Conditions on the Morphotropic Phase Boundaries and Ferroelectric Properties of $Pb(Zn_{1/3}Nb_{2/3})O_3$-$Pb(Ni_{1/3}Nb_{2/3})O_3$-$Pb(Zr_{1/2}Ti_{1/2})O_3$ Solid Solutions

David P. Cann, Xiaoli Tan
Materials Science and Engineering
Iowa State University
Ames, IA 50011 USA
$BaTiO_3$@iastate.edu

Naratip Vittayakorn, Gobwute Rujijanagul, and Tawee Tunkasiri
Department of Physics, Faculty of Science
Chiang Mai University
Chiang Mai, 50200 Thailand

Abstract— Ceramic solid solutions within the ternary system of $Pb(Zn_{1/3}Nb_{2/3})O_3$ - $Pb(Ni_{1/3}Nb_{2/3})O_3$ - $Pb(Zr_{1/2}Ti_{1/2})O_3$ (PZN-PNN-PZT) were synthesized via two methods: the mixed oxide method and the columbite method. Phase development of the calcined powders and the crystal structure of sintered ceramics were analyzed by x-ray diffraction. The ferroelectric properties of the ceramics were characterized by a combination of dielectric and hysteresis measurements. It was observed that for the binary systems PZN-PZT and PNN-PZT, the change in the transition temperature (T_m) is nearly linear with respect to the PZT content. Ferroelectric properties were analyzed to elucidate the nature of the phase transformation and identify the impact of the processing conditions. With these data, ferroelectric phase diagrams were derived showing the transition between the pseudo-cubic relaxor behavior of PZN and PNN to the tetragonal normal ferroelectric behavior of PZT. This transition was also correlated to changes in the diffuseness parameter δ_γ. When comparing ceramics prepared by the columbite method and the mixed oxide route, ceramics prepared by the mixed oxide method showed a lower remanent polarization P_r and a higher coercive field E_c. Additionally, ceramics prepared by the columbite method displayed sharp transitions in ferroelectric properties across the MPB composition, whereas these transitions were obscured in ceramics prepared by the mixed oxide method. It is proposed that the different reaction paths influenced the degree of compositional heterogeneity in these complex perovskite solid solutions, which was clearly reflected in the nature of the phase transition.

Keywords: morpotropic phase boundary, columbite method, perovskite, phase transition

I. INTRODUCTION

Ferroelectric materials based on Pb-perovskites have found use in countless applications including piezoelectric sensors and actuators, capacitors, pyroelectric and electro-optic devices, and ferroelectric memories [1,2]. In many instances, compositions near a morphotropic phase boundary (MPB) between ferroelectric phases of different symmetry have advantageous dielectric and piezoelectric performance characteristics [1,3]. There have been a number of MPB's identified in Pb-based systems including the most widely exploited system $PbZrO_3$-$PbTiO_3$ (PZT) [3]. Other MPB systems include $Pb(Mg_{1/3}Nb_{2/3})O_3$-$PbTiO_3$ (PMN-PT) [4], $Pb(Zn_{1/3}Nb_{2/3})O_3$-$PbTiO_3$ (PZN-PT) [5], $Pb(Sc_{1/2}Nb_{1/2})O_3$-$PbTiO_3$ (PSN-PT) [6], and many others.

This work will focus on perovskite solid solutions in two quasi-binary systems within the overall ternary system $Pb(Zr_{1/2}Ti_{1/2})O_3$- $Pb(Zn_{1/3}Nb_{2/3})O_3$- $Pb(Ni_{1/3}Nb_{2/3})O_3$: specifically $Pb(Zn_{1/3}Nb_{2/3})O_3$-$Pb(Zr_{1/2}Ti_{1/2})O_3$ (PZN-PZT) and $Pb(Ni_{1/3}Nb_{2/3})O_3$-$Pb(Zr_{1/2}Ti_{1/2})O_3$ (PNN-PZT). Polycrystalline ceramics based on Pb-perovskites are typically synthesized through high temperature solid state processes. A number of processing methods have been proposed to ensure phase pure perovskite. In this work, two common processing methods will be contrasted with the aim of understanding the influence of processing conditions on the phase equilibria and ferroelectric properties. The conventional mixed oxide method involves simply reacting all of the binary oxides (e.g. PbO, TiO_2, ZrO_2, etc.) in a single calcination step to form the desired perovskite phase. In the columbite method, first proposed by Swartz and Shrout [7], the B-site oxides are first pre-reacted to form intermediate phases such as $ZnNb_2O_6$, $ZrTiO_4$, $NiNb_2O_6$, etc. These intermediate phases are then reacted with PbO to form the desired perovskite phase.

Given that the PZN-PNN-PZT phases are all perovskite solid solutions, it is likely that the different reaction paths may lead to distinct differences in the homogeneity of the B-cation distributions. In this study, a combination of x-ray diffraction (XRD), dielectric measurements, and Raman spectroscopy will be employed to probe the influence of the different processing methods on such parameters as the perovskite phase distributions, remanent polarization (P_r), coercive field (E_C), diffuseness parameter (δ_γ), and others. With this information, it will be possible to optimize the processing conditions for solid solutions near MPBs.

0-7803-8410-5/04/$20.00 (c)2004 IEEE.

II. EXPERIMENTAL

The columbite precursors $ZnNb_2O_6$ and $NiNb_2O_6$ were prepared from the reaction between ZnO (99.9%) and Nb_2O_5 (99.9%) at 975°C for 4h and between NiO (99.9%) and Nb_2O_5 (99.9%) for 4h at 1100°C, respectively. The wolframite phase $ZrTiO_4$ was formed by reacting ZrO_2 (99.9%) with TiO_2(99.9%) at 1400°C for 4h. The powders of $ZnNb_2O_6$, $NiNb_2O_6$, and $ZrTiO_4$ were mixed in the required stoichiometric amounts with PbO (99.9%) with an excess of 2 mol% of PbO added. The milling process was carried out for 24 hours in isopropyl alcohol. The powders were calcined at 900°C-950°C for 4 h in a double crucible configuration with a heating rate of 20°C/min. After grinding and sieving, 5 wt% of polyvinyl alcohol (PVA) binder was added. Discs with a diameter of 12.5 mm were prepared by cold uniaxial pressing at a pressure of 150MPa. Binder burnout occurred by slow heating to 500°C and holding for 2h. The discs were sintered in a sealed alumina crucible at temperatures ranging from 950°C-1250°C using a heating rate of 5°C/min and a dwell time of 2 h. To prevent PbO volatilization from the discs, a PbO atmosphere was maintained by placing a bed of $PbZrO_3$ powder in the crucible.

Phase formation and crystal structure of the calcined powders and sintered discs were examined by x-ray diffraction (XRD). The pellets were polished and electroded via gold sputtering, over which a layer of air-dried silver paint was applied. The relative permittivity (ε') and dissipation factor (tan δ) of the pellets sample were measured at various temperatures over the frequency range between 100 and 100KHz using an LCR meter (HP 4284A). The remanent polarization P_r was determined from a P-E hysteresis loop measurements using a Sawyer-Tower circuit at temperatures between -66°C and 60°C.

III. RESULTS

Single phase perovskite was obtained for the pseudo-binary systems over the composition ranges *(1-x)*PZN-*x*PZT at $0.5 \leq x \leq 0.9$ and for *(1-x)*PNN-*x*PZT at $0.4 \leq x \leq 0.9$. For the 0.6PZN-0.4PZT composition a small amount of pyrochlore phase was noted. The results of the XRD, dielectric, and Raman measurements and the influence that can be attributed to processing conditions are summarized for each pseudo-binary system in the following sections.

A. PZN-PZT System

In the PZN-PZT system, phase pure perovskite was obtained at lower calcination temperatures using the conventional method compared to the columbite method. As shown in Fig. 1, the columbite method required calcination temperatures as much as 150°C higher for some PZN-PZT compositions. This effect was especially prevalent at high mole fractions of PZT. In analyzing the phase evolution at low temperatures, a high volume fraction of a pyrochlore phase was observed in the XRD data for the columbite derived powders. In the conventionally prepared powders the perovskite phase was the dominant phase even at 750°C. This suggests that each processing route followed a different reaction path in eventually forming the perovskite phase.

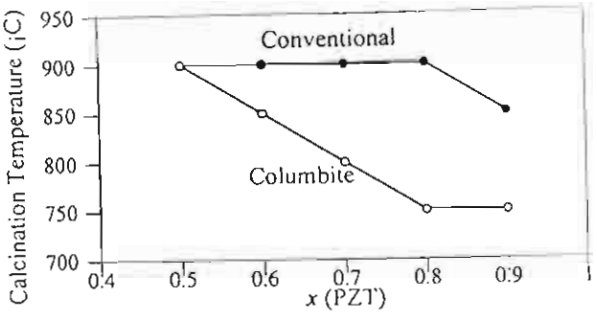

Figure 1. Calcination temperature at which phase pure perovskite is obtained for both the conventional and columbite methods.

The symmetry of the resultant perovskite phases obtained through XRD allows a pseudo-binary phase diagram to be derived (Fig. 2). Compositions close to PZT are tetragonal at room temperature, with a transition to rhombohedral symmetry for compositions at $x \leq 0.7$. Inspection of the XRD patterns of compositions close to the MPB at $x \approx 0.7$ revealed that the processing method had an influence on the phase distribution (Fig. 3). In columbite derived powders, only the rhombohedral perovskite phase was observed. However, in conventionally prepared powders a mixture of the rhombohedral and tetragonal phases were observed. This is strong evidence that the conventional method produces non-uniform mixing of the B-site cations as compared to the columbite method.

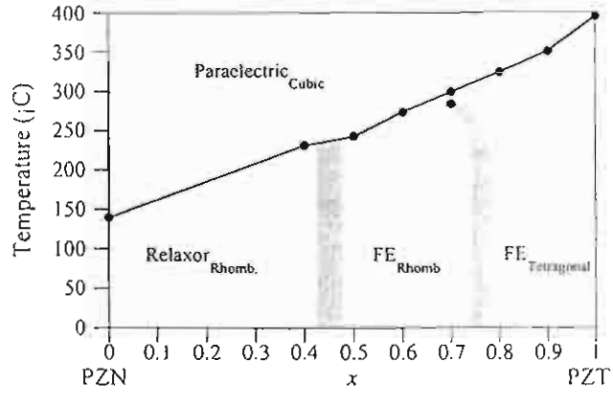

Figure 2. PZN-PZT phase diagram obtained through room temperature XRD and dielectric measurements.

Further evidence is seen in the dielectric data presented in Fig. 4. For compositions near the MPB at $x = 0.7$, a phase transition was clearly seen in the columbite derived ceramics at 284°C. As indicated in the phase diagram (Fig. 2), this corresponds to a transition from rhombohedral to tetragonal symmetry. The conventionally prepared ceramics at $x = 0.7$ did not show any anomalies within that temperature range.

Comparisons of the dielectric data for PZN-PZT ceramics prepared by the two methods are presented in Table I. These data show that ceramics prepared via the columbite method exhibit a significantly higher room temperature permittivity, higher permittivity at T_{max}, and a higher remanent polarization (P_r) determined from hysteresis measurements.

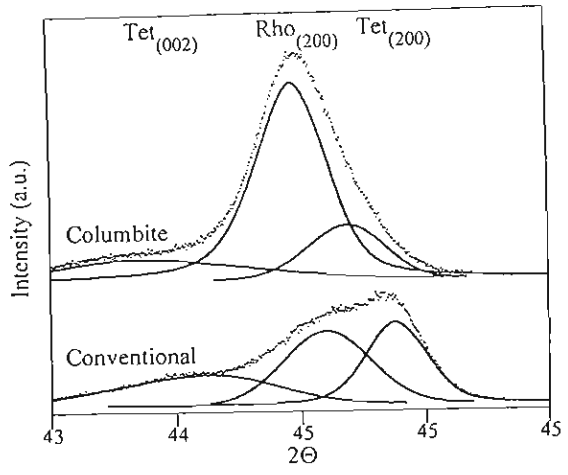

Figure 3. XRD patterns for the (002) peak for conventional and columbite prepared ceramics. Deconvolution of the data shows that relative proportions of the rhombohedral and tetragonal phases.

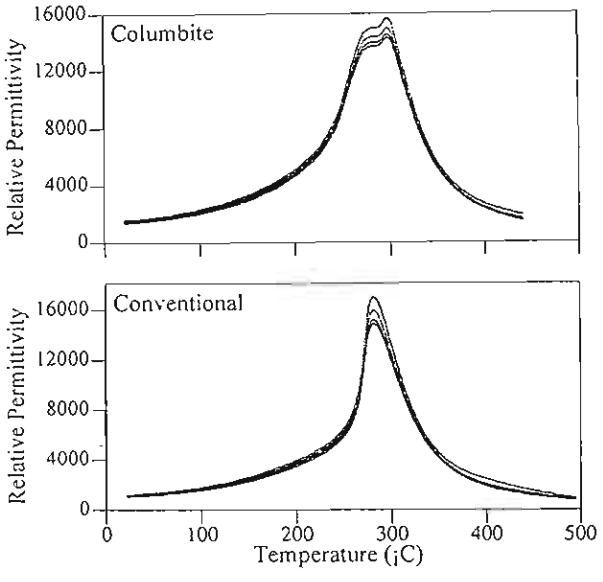

Figure 4. Relative permittivity versus temperature for a 0.3PZN-0.7PZT ceramic at measurement frequencies of 0.1, 1, 10, and 100 KHz.

It is important to note that there were no significant differences in the density or grain size when comparing the two processing methods. All samples in this study were of high density ($\rho_{Theoretical}$ > 96%) with grain sizes close to 5 μm. Therefore, it is possible to exclude the influence of density or grain size effects from these results.

In Fig. 5, the coercive field (E_C) as a function of x exhibits very different trends comparing the conventional and columbite prepared ceramics. The columbite ceramics exhibited a sharp transition in E_C at the MPB, whereas the conventionally prepared ceramic displayed a gradual transition.

TABLE I. PZN-PZT DIELECTRIC DATA

x	K at 25°C		K at T_{max}		P_r	
	Conv.	Col.	Conv.	Col.	Conv.	Col.
0.4	1,230	1,440	11,400	13,200		
0.5	1,220	1,430	20,800	21,200	29.5	36.4
0.6	1,230	1,440	17,000	20,800	23.2	30.6
0.7	980	1,580	14,300	15,700	20.0	30.4
0.8	1,230	1,550	25,000	25,800	31.5	36.1
0.9	810	1,590	13,300	21,200	34.0	37.1

Taking all of these results into account, PZN-PZT ceramics prepared by the columbite method exhibited more clearly defined phase transitions and MPBs compared to conventionally processed ceramics. Rhombohedral distortions in perovskites are linked to the geometric tolerance factor (t). In the PZN-PZT system, the magnitude of t is determined by the average B-cation radius. In the conventionally prepared ceramics, the coexistence of the tetragonal and rhombohedral phases near the MPB are indicative of a significant degree of variation in the composition of the B-site. Regions which were rich in smaller cations would favor tetragonal distortions, whereas regions rich in larger cations would favor rhombohedral distortions. The formation of columbite oxides prior to perovskite formation assures intimate mixing of the B-site cations. This ultimately leads to a more homogeneous distribution of B-site cations.

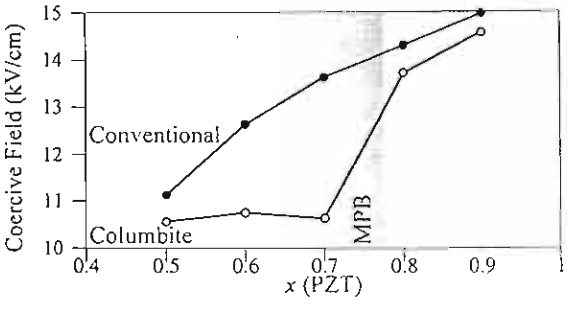

Figure 5. Coercive field as a function of composition x for columbite and conventionally prepared ceramics.

B. PNN-PZT System

In the PNN-PZT system, the columbite method was utilized to prepare phase-pure perovskite ceramics. Based on room temperature XRD and measurements of the relative permittivity versus temperature a phase diagram for PNN-PZT was derived (Fig. 6). At x = 0.8, an MPB region separates a tetragonal normal ferroelectric phase field from a rhombohedral relaxor ferroelectric phase field. XRD data within the MPB region featured splitting of both (200) and (111) peaks. This is indicative of the coexistence of both rhombohedral and tetragonal phases. Alternatively, as has been demonstrated in PZT the multiple peak splitting could be indicative of another lower symmetry phase (e.g. monoclinic) [8].

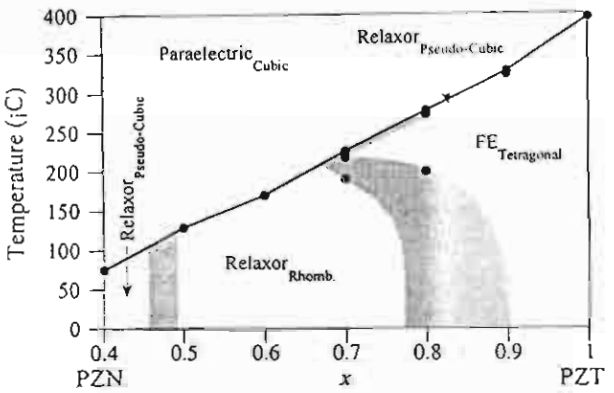

Figure 6. PNN-PZT phase diagram obtained through room temperature XRD and dielectric measurements.

Table II summarizes the results of the dielectric measurements on the PNN-PZT ceramics. As expected, the relative permittivity peaked at the MPB composition (x = 0.8) at a value of 36,000. A general transition from normal ferroelectric to relaxor ferroelectric behavior was observed as the mole fraction of PNN increased. Fig. 7 illustrates the relative permittivity versus temperature for $0.4 \le x \le 0.9$. The transition from normal ferroelectric behavior to relaxor ferroelectric behavior was clearly observed from the dispersion in the vicinity of T_{max}.

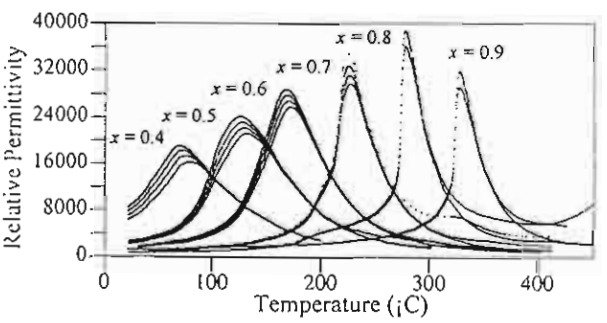

Figure 7. Relative permittivity versus temperature for *(1-x)*PNN-*x*PZT ceramics.

TABLE II. PNN-PZT DIELECTRIC DATA

x	T_{max} (°C)	K at 25°C	tan δ at 25°C	K at T_{max}	δ_γ
0.4	75.4	7,500	0.062	17,500	29.5
0.5	128.9	2,500	0.042	22,000	24.4
0.6	169.7	1,600	0.042	27,000	22.4
0.7	225.5	1,060	0.029	31,200	14.0
0.8	277.4	835	0.011	36,000	10.2
0.9	326.7	950	0.005	32,000	8.6

The parameter δ_γ can be used to quantify the diffuseness of the ferroelectric transition through the equation [9]:

$$\frac{K_{max}}{K(f,T)} = 1 + \frac{\left[T - T_{max}(f)\right]^{\gamma}}{2\delta_{\gamma}^{2}} \qquad (1)$$

where $\gamma = 1$ for Curie-Weiss behavior and $\gamma = 2$ for pure relaxor character. As shown in Table II, the δ_γ parameter increased linearly with increased PNN content.

IV. CONCLUSIONS

In this work, the ferroelectric phases within the pseudo-binary systems PZN-PZT and PNN-PZT were characterized. For the PZN-PZT compositions, MPBs were noted at $x \approx 0.75$ and $x \approx 0.45$. It was observed pre-reacting the B-site cations via the columbite method had significant effects on the perovskite phase stability and dielectric properties. These effects were most pronounced in the vicinity of the MPB, located near $x \approx 0.75$. It is likely that the columbite method produced a more homogeneous distribution of the B-site cations compared to the mixed oxide prepared ceramics. These compositional variations could be inferred from the observation of multiple phases near the MPB and poorly defined phase transitions.

In the PNN-PZT compositions, two MPBs were noted at $x \approx 0.8$ and $x \approx 0.45$. Even with columbite prepared ceramics, rhombohedral and tetragonal phases were found to coexist at the MPB at $x \approx 0.8$. It is interesting to note that in PNN the transition from the tetragonal PZT phase to the relaxor rhombohedral phase is more gradual than in PZN. This is likely due to the much closer B-cation radii match between $Zr_{0.5}Ti_{0.5}$ (0.803 Å) and $Ni_{1/3}Nb_{2/3}$ (0.797 Å), as compared to $Zn_{1/3}Nb_{2/3}$ (0.813 Å).

ACKNOWLEDGMENT

The authors are grateful to the Thailand Research Fund, Graduate School at Chiang Mai University and Ministry of University Affairs in Thailand for financial support.

REFERENCES

[1] A. J. Moulson and J. M. Herbert, Electroceramics: Materials, Properties, Applications. New York: Chapman and Hall, 1990.

[2] K. Uchino, Ferroelectric Devices. New York: Marcel Dekker, Inc., 2000.

[3] B. Jaffe and W. R. Cook, Piezoelectric ceramics. R.A.N., 1971

[4] S. W. Choi, T. R. Shrout, S. J. Jang, and A. S. Bhalla, "Dielectric and pyroelectric properties in the $Pb(Mg_{1/3}Nb_{2/3})O_3$-$PbTiO_3$ system," Ferroelectrics, vol. 100, 1989.

[5] J.Kuwata, K.Uchino, and S.Nomura, "Dielectric and piezoelectric properties of $0.91Pn(Zn_{1/3}Nb_{2/3})O_3$-$0.09PbTiO_3$ single crystals.," Jpn. J. Appl. Phys., vol. 21, pp. 1298-1302, 1982.

[6] V. J. Tennery, K. W. Hang, and R.E.Novak, "Ferroelectric and structure properties of $Pb(Sc_{1/2}Nb_{1/2})_{1-x}Ti_xO_3$ system," J. Am. Ceram. Soc., vol. 51, pp. 671-674, 1968.

[7] S. L. Swartz and T. R. Shrout, "Fabrication of perovskite lead magnesium niobate," Mater. Res Bull., vol. 17, pp. 1245, 1982.

[8] B. Noheda, D.E. Cox, G. Shirane, J.A. Gonzalo, L.E. Cross, and S-E. Park, "A monoclinic ferroelectric phase in the $Pb(Zr_{1-x}Ti_x)O_3$ solid solution," Appl. Phys. Lett. Vol. 74, pp. 2059 (1999).

[9] K.Uchino and S.Nomura, "Critical exponents of the dielectric constants in diffused phase transition crystals," Ferroelectrics Letters, vol. 44, pp. 55, 1982.

เอกสารหมายเลข 1.14

Appl. Phys. A (2004)
DOI: 10.1007/s00339-004-3136-6

Applied Physics A
Materials Science & Processing

W. THAMJAREE
W. NHUAPENG✉
A. CHAIPANICH
T. TUNKASIRI

Fabrication of combined 0–3 and 1–3 connectivities PZT/epoxy resin composites

Department of Physics, Faculty of Sciences, Chiang Mai University, Chiang Mai 50200, Thailand

Received: 20 October 2004/Accepted: 25 October 2004
Published online: 21 December 2004 • © Springer-Verlag 2004

ABSTRACT PZT/epoxy resin composites of combined 0–3 and 1–3 connectivities were fabricated, for the first time, using suction, dice and fill techniques. Two types of composites (PZT(m)/epoxy resin and PZT(sp)/epoxy resin) were produced using PZT powders prepared by mixed oxide and spray-drying methods. Physical, mechanical, dielectric and piezoelectric properties of the composites were examined. Generally, overall results between the two composites were found to be very similar (volumetric changes ~ 34%–37%, $d_{33} \sim 20.2$–25.3 pC/N, $K_p \sim 0.54$–0.61). Higher density was found in PZT(sp)/epoxy resin, however, due to better packing of particles. Moreover, both PZT/epoxy resin composites exhibited very low acoustic impedance ($Z \sim 4.12$–4.84 Mrayls), which is very close to that of human tissue and water. Therefore, these new composites may be suitable for use in medical applications.

PACS 81.05.Qk; 81.05.Zx; 77.87.-s

1 Introduction

Piezoelectric ceramics, such as lead zirconate titanate ($Pb(Zr_xTi_{1-x})O_3$ or PZT), have been employed as sensors, actuators and transducers due to their high piezoelectric coefficient (d_{33}) and dielectric constant (ε_r) [1, 2]. Nevertheless, their transverse charge coefficient (d_h), the hydrostatic voltage coefficient (g_h) and the hydrophone figure of merit ($d_h g_h$) are low. Furthermore, PZT ceramics are hard and brittle in nature and may not be flexible enough to suit a curved surface. They also exhibit high acoustic impedance, causing great acoustical mismatching between ceramics and the transmitting medium, like water or human tissue [3, 4]. In order to obtain low acoustic impedance for matching these media, piezocomposites which employed an active piezoelectric material in conjunction with an active or passive polymer phase have been suggested with different connectivity patterns [5].

Early reports revealed that the connectivity of 1–3 ceramic/polymer composites, which comprise an active piezoceramic rod embedded with a passive polymer, possessed excellent overall piezoelectric properties when used in hydrophone and medical-imaging applications [3, 6–8]. Schwarzer and Roosen [1] fabricated 1–3 PZT/polymer composites by dice and fill, tape-casting and injection-molding methods. These composites were found to exhibit good piezoelectric and dielectric properties ($d_{33} = 466$ pC/N and $\varepsilon_r = 1146$). Janas et al. [3] produced 1–3 piezocomposites by tape casting, honeycomb dicing and ceramic fiber weaving, obtaining $d_{33} = 370$ pC/N and $\varepsilon_r = 300$. Taunaumang et al. [7] also fabricated 1–3 piezocomposites by the dice and fill method; the obtained d_{33} and K_p for the composites were 746 pC/N and 0.64, respectively. Furthermore, other techniques which may be regarded as novel in producing 1–3 piezocomposites have been developed by weaving PZT fiber bundles through a honeycomb support [6], lost mold [8] and laser cutting [9].

On the other hand, the 0–3 connectivity of piezoceramic polymer is considered to be less complicated in terms of fabrication and appropriate to be molded to any designed surface due to its high flexibility. In this type of composite, the ceramic powder has no physical particle–particle contact while the polymer phase has a three-dimensional connection. One of the methods used to prepare the 0–3 ceramic/polymer was the centrifuge method by Nhuapeng and Tunkasiri [10]. However, the acoustic impedance (Z) obtained from their results was about 6 Mrayls (at a volumetric percentage of ceramic phase of 30%), which is still high in comparison to that of human tissue or water (1.6 Mrayls [11]). In order to obtain a reasonably low acoustic impedance compared to that of water and a considerably high piezoelectricity of piezocomposites, we have attempted to fabricate piezocomposites with a combination of 0–3 and 1–3 connectivities. In this work, the samples were fabricated based on the dice and fill techniques. The physical, mechanical and electrical properties of composite samples were investigated. The microstructure of piezocomposites was also studied with the use of scanning electron microscopy (SEM).

2 Experimental details

Combinations of 0–3 and 1–3 connectivities composites were produced based on the dice and fill method [7]. Firstly, PZT powders obtained from the mixed-oxide method (particle size ~ 4 μm) and the spray-drying technique (particle size ~ 1 μm) were used as active phase and epoxy resin (Epofix, Strurer) was employed as passive polymer phase.

✉ Fax: +66-5335-7512, E-mail: nhuapeng@yahoo.com

Thereafter, 0–3 PZT/epoxy resin composites were fabricated by the suction technique. Details of the suction technique are described in Fig. 1. PZT powders were put in a plastic syringe with a filter paper (Whatman) placed underneath. Epoxy resin was then poured into the syringe with PZT powders and the resin was plugged in a flask partly filled with water, as shown in Fig. 1; suction was carried out using an air pump for enhancing the flow of the resin through the PZT powders. A filter (no. 42) was used to prevent the powders flowing into the suction system. The samples were left for two days at room temperature, allowing them to settle. The sample in the syringe is now a 0–3 piezoceramic/epoxy resin composite, about 1-cm thick and 1.5 cm in diameter. The sample was then diced using a diamond saw (series 15HC Diamond, Buehler) into squares of $0.35 \times 0.35\ mm^2$ to create a 1–3 connectivity pattern. Epoxy resin was then poured in again to fill up the spaces. The samples were left for two days to settle. These new samples are now a combined 0–3 and 1–3 ceramic/epoxy resin composite where each column (0–3 ceramic/epoxy resin) formed a 1–3 connectivity with the resin in the spaces. The composite sample was then taken out from the syringe and cut into disks with a thickness of 1 mm (Fig. 1b). The density of the samples was measured by the conventional Archimedes' method.

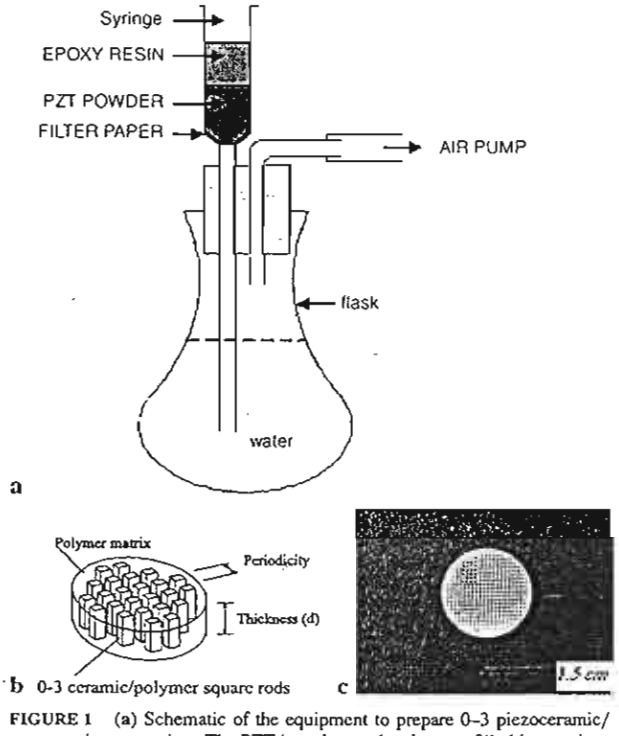

FIGURE 1 (a) Schematic of the equipment to prepare 0–3 piezoceramic/epoxy resin composites. The PZT/powders and resin were filled in a syringe with a filter underneath. The syringe was plugged in a flask partly filled with water. Suction was carried out through an air pump. (b) Schematic of photograph of (0–3) and (1–3) combined piezocomposite sample where polymer matrix = epoxy resin filled in the spaces to form the 1–3 connectivity with 0–3 ceramic/polymer rods (0.35×0.35 mm). Thickness (d) = 1 mm, periodicity = 0.7 mm. (picture based on [7]) (c) Top view photograph of the composite

Disks of the composite samples were electroded by silver paste (Electrodrag 1415M, Acheson) to the top and bottom surfaces and left to dry at room temperature. Dielectric properties were measured using a LCZ meter (model 4276, Hewlett-Packard). Poling was done in silicone oil at 80 °C with a poling field of 8 kV/mm for 30 min. The piezoelectric coefficient (d_{33}) of the samples was measured using a piezo d_{33} meter, while the echo-shift method [12] was used for the acoustic impedance measurements. Distributions of PZT powder phase in the composites were investigated using SEM.

3 Results and discussion

Figure 2 shows a typical SEM micrograph of the top view of the composite (combined 0–3 and 1–3 connectivities). Particles obtained from both preparation techniques were found to have similar morphology. The dark area belongs to the resin while the brighter squares belong to the 0–3 composites. Enlarged pictures of some squares are shown in Fig. 3. It can be concluded that the average size of the powders obtained from the mixed-oxide route is bigger ($\sim 4\ \mu m$) than that obtained from the spray-drying technique ($\sim 1\ \mu m$). This is confirmed by the cross-section micrographs (Fig. 4). However, in Fig. 3 the PZT phase shows agglomeration of the particles produced from the spray-drying technique. The composites fabricated by the suction, dice and fill method have a very low acoustic impedance (4–5 Mrayls).

Table 1 illustrates the volumetric percentage of density (ϱ) and acoustic impedance (Z) of the composites, compared with those obtained by others [10, 13–15].

PZT/epoxy produced from PZT powder of smaller particle size (PZT(sp)/epoxy resin) yields higher volumetric percentage (37%) and possesses higher ϱ ($2119.6\ kg/m^3$) and Z

composites	vol(%)	density (kg/m^3)	Z (Mrayls)
PZT(m)/epoxy resin	34	1878.6	4.12
PZT(sp)/epoxy resin	37	2119.6	4.84
Nhuapeng and Tunkasiri [10]	60	5026	11.41
Sripada et al. [13]	-	4225.4	13.94
Grewe et al. [14]	40	-	7.50
Slayton and Setty [15]	70	-	8.00

TABLE 1 Physical and mechanical properties of the PZT/polymer composites PZT(m), PZT(sp) = powders obtained from mixed oxide method and spray drying techniques, respectively

composites	d_{33} (pC/N)	K_p	ε_r	tanδ
PZT(m)/epoxy resin	25.3	0.61	14	0.026
PZT(sp)/epoxy resin	20.2	0.54	15	0.05
Schwarzer and Roosen [1]	466	0.58	1146	0.028
Janas et al. [3]	370	-	300	0.029
McNulty et al. [6]	230	-	130	-
Taunaumang et al. [7]	29.6	-	-	-
Nhuapeng and Tunkasiri [16]	26	-	84	0.0141
Sripada et al. [13]	-	0.4	-	-
Shrout et al. [16]	270	-	480	0.017
Ohara et al. [17]	274	-	536	-

TABLE 2 Dielectric and piezoelectric properties of the PZT/polymer composites compared with those of previous work

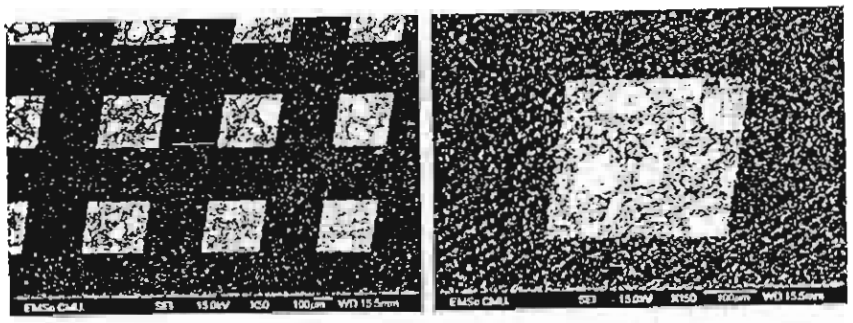

FIGURE 2 The typical SEM micrographs of top view of PZT/epoxy resin composites

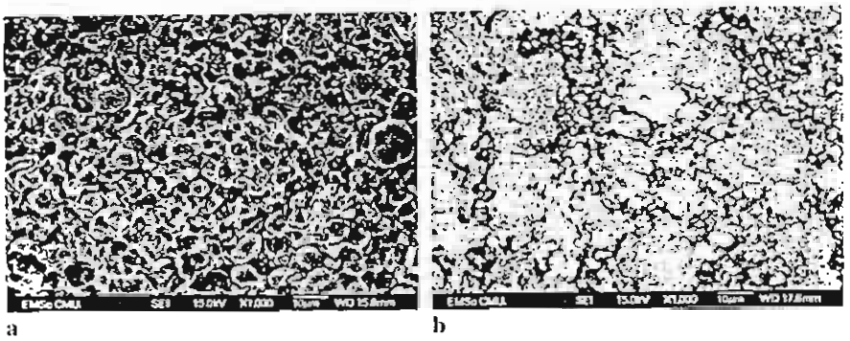

FIGURE 3 SEM micrographs of PZT/epoxy resin which PZT composites employing powders prepared from mixed oxide route (a) and spray dry techniques (b)

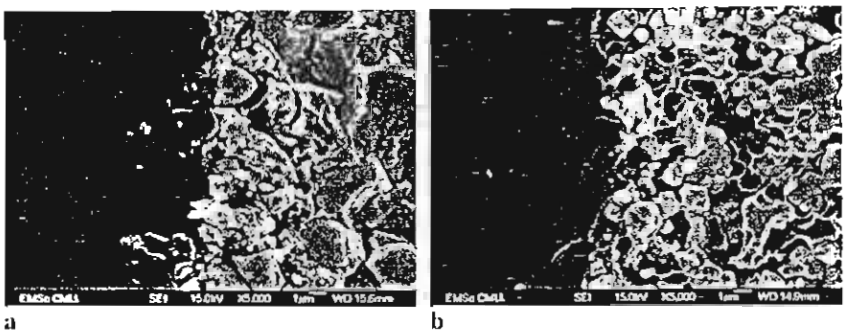

FIGURE 4 SEM micrographs of cross section of PZT/epoxy resin composites employing powders PZT powder prepared from mixed oxide route (a) and spray dry techniques (b). Dark and brighter areas correspond to the resin and the PZT powders, respectively

(4.84 Mrayls) values as compared to the PZT(m)/epoxy resin composite with corresponding values of 34%, 1878.6 kg/m^3 and 4.12 Mrayls, respectively. Both composites fabricated by our methods (combination of suction, dice and fill) were noted to have very low acoustic impedance (4.12 and 4.84 Mrayls). These values are lower than those previously reported by Nhuapeng and Tunkasiri [10], Sripada et al. [13], Grewe et al. [14] and Slayton and Setty [15]. This is due to the different fabrication routes and different volumetric percentages.

Furthermore, our Z values were found to be comparable to that of water (1.6 Mrayls). Therefore, this fabrication method could be seen as suitable in preparing low acoustic impedance PZT/epoxy resin composites for biomedical applications. Table 2 shows dielectric properties (ε_r and tanδ) and piezoelectric properties (d_{33} and K_p) of the composites, together with those of Schwarzer and Roosen [1], Janas et al. [3], McNulty et al. [6], Taunaumang et al. [7], Nhuapeng and Tunkasiri [10], Sripada et al. [13], Shrout et al. [16] and Ohara et al. [17].

The d_{33} and K_p values obtained from PZT(m)/epoxy composite are 25.3 pC/N and 0.61, respectively, while the d_{33} and K_p values of PZT(sp)/epoxy composite are 20.2 pC/N and 0.54, respectively. It can be seen that the d_{33} values for both composites are very close to the value reported by Nhuapeng and Tunkasiri [10], who fabricated the 0–3 PZT/polymer composites by the centrifuge method. The ε_r values obtained from this work are quite low (14–20), which may be due to the effect of quantity of PZT particles in the composites.

4 Conclusions

Through a combination of suction, dice and fill techniques, a new type of PZT/epoxy resin composites combining 0–3 and 1–3 connectivities was fabricated. The measured piezoelectric coefficient (d_{33}) and coupling factor (K_p) were 25.3 pC/N and 0.61 for PZT(m)/epoxy resin, respectively, while the values for PZT (sp)/epoxy resin were 20.2 pC/N (d_{33}) and 0.54 (K_p).

The most interesting finding in this investigation, however, is the very low acoustic impedance obtained for both PZT/epoxy resin composites (4.12 Mrayls for PZT(m)/epoxy resin and 4.84 Mrayls for PZT (sp)/epoxy resin). There is, therefore, a potential for these composites to be used

in biomedical applications since these acoustic impedance values are very close to those of human tissue and water.

Furthermore, from SEM, the particles from the spray-drying technique were shown to be better packed together, resulting in the composite being denser than the one prepared from the mixed-oxide method.

ACKNOWLEDGEMENTS The authors would like to express their sincere thanks to the Thailand Research Fund and the Graduate School of Chiang Mai University for financial support.

REFERENCES

1 S. Schwarzer, A. Roosen: J. Eur. Ceram. Soc. **19**, 1007 (1999)
2 S.T. Lau, K.W. Kwok, H.L.W. Chan, C.L. Choy: Sens. Actuators A **96**, 14 (2002)
3 V.F. Janas, T.F. McNulty, F.R. Walker, R.P. Schaeffer, A. Safari: J. Am. Ceram. Soc. **78**, 2425 (1995)
4 R.P. Tandon, D.R. Chaubey, R. Singh, N.C. Soni: J. Mater. Sci. Lett. **12**, 1182 (1993)
5 S.S. Livneh, F.V. Janas, A. Safari: J. Am. Ceram. Soc. **78**, 1900 (1995)
6 T.F. McNulty, V.F. Janas, A. Safari: J. Am. Ceram. Soc. **78**, 2913 (1995)
7 H. Taunaumang, I.L. Guy, H.L.W. Chan: J. Appl. Phys. **76**, 484 (1994)
8 R.K. Panda, V.F. Janas, A. Safari: in *Proc. 10th IEEE Int. Symp. Applications of Ferroelectrics, 1996*, Vol. 2, p. 551
9 K. Li, D.W. Zeng, K.C. Yung, H.L.W. Chan, C.L. Choy: Mater. Chem. Phys. **75**, 147 (2002)
10 W. Nhuapeng, T. Tunkasiri: J. Am. Ceram. Soc. **85**, 2 (2002)
11 T.R. Gururaja, W.A. Schulze, L.E. Cross, R.E. Newnham, B.A. Auld, Y.J. Wang: Trans. Son. Ultrason. **32**, 481 (1985)
12 T. Bui, H.L.W.C.J. Unsworth: J. Acoust. Soc. Am. **83**, 2416 (1988)
13 S. Sripada, J. Unsworth, M. Krishnamurty, Y.S. Ng: Mater. Res. Bull. **31**, 731 (1996)
14 M.G. Grewe, T.R. Gururaja, R.E. Newnham, T.R. Shrout: in *IEEE Ultrasonics Symp., 1989*, p. 713
15 M.H. Slayton, H.S.N. Setty: in *IEEE Int. Symp. Applications of Ferroelectrics, 1990*, p. 90
16 T.R. Shrout, L.J. Bowen, W.A. Schulze: Mater. Res. Bull. **15**, 1371 (1980)
17 Y. Ohara, M. Shiwa, H. Yanagida, T. Kishi: J. Ceram. Soc. Jpn. **102**, 368 (1994)